STUDY OF ROTATIONAL FRETTING OF QUENCHED AND TEMPERED 4340 STEEL

A Thesis
Presented to
The Academic Faculty
By

Paul Mathew

In Partial Fulfillment
Of the Requirements for the Degree
Master of Science in Mechanical Engineering

Georgia Institute of Technology
August 2013

STUDY OF ROTATIONAL FRETTING OF QUENCHED AND TEMPERED 4340 STEEL

Approved by:

Dr. Richard W. Neu, Woodruff
School of Mechanical Engineering
School of Materials Science and Engineering
Georgia Institute of Technology

Dr. Jeffrey L. Streator, Woodruff
School of Mechanical Engineering
School of Materials Science and Engineering
Georgia Institute of Technology

Dr. Shreyes N. Melkote, Woodruff
School of Mechanical Engineering
School of Materials Science and Engineering
Georgia Institute of Technology

Date Approved: June 28, 2013

ACKNOWLEDGEMENTS

I would first like to thank my advisor, Dr. Richard W. Neu for giving me the opportunity to carry out this thesis work under his guidance. His high level of patience and critical insights has resulted in the successful completion of this work.

I would like to thank my co-advisor Dr. Ramkumar Oruganti from GE, for his constant guidance and support in defining and shaping this work and for being a good mentor. His inputs at critical junctures helped me stay the course. I would also like to thank Dr. K Anand for motivating me, by opening an avenue to carry out this work at GE and for sharing his initial thoughts on this subject.

I would like to thank and acknowledge the experimental and characterization support received from Biju Dasan, T. Vishwanath and T. Shalini. Special thanks to Dr. Mallikarjun Karadge for carrying out the TEM characterization of specimens with limited resources. The results have enabled a new direction for future research in microstructural deformation of fretting.

I'm also thankful to the thesis committee members, Dr. Jeffrey L. Streator and Dr. Shreyes N. Melkote, for taking the time to review my work.

Special thanks to my family for their encouragement, patience and understanding.

Finally, thanks to God Almighty from whom all blessings flow, the very source of all inspiration and meaning in life.

TABLE OF CONTENTS

LIST OF TABLES

LIST OF FIGURES

LIST OF SYMBOLS

A	Fretting Loop Energy Ratio
CoF	Coefficient of Friction
CBN	Cubic Boron Nitride
D	Sliding Ratio
EDS	Energy Dispersive Spectroscopy
E*	Effective Elastic Moduli
Ft	Tangential force
FCC	Face Centered Cubic
FDP	Fretting Damage Parameter
FFPV	Fretting Fatigue Process Volume
GB	Grain Boundary
GSR	Gross Slip Regime
LCF	Low Cycle Fatigue
MSR	Mixed Slip Regime
MRFM	Material Response Fretting Map
RCFM	Running Condition Fretting Map
P_o	Max. Hertzian Contact Pressure
P	Load per unit Length
PSR	Partial Slip Regime
PSD	Power Spectral Density
R	Effective Radius of the cylinders
SEM	Scanning Electron Microscope
SS	Stainless Steel
TTS	Tribologically Transformed Structure
TEM	Transmission Electron Microscope
UTS	Ultimate Tensile Strength
Wd	Energy dissipated during fretting
Wt	Total Energy at the fretting contact
S	Slip Ratio
δ	Slip Index
ν_1	Poisson's Ratio

SUMMARY

Fretting phenomenon occurs when two bodies in contact undergo small repetitive relative motion such that the localized surface and subsurface material properties are altered leading to damage or failures. Fretting conditions are obtained by controlling externally applied parameters such as load, frequency of displacement, displacement amplitude. Material properties which influence fretting behavior include hardness, ductility, hardening behavior. External parameters like surface roughness, temperature also play a role in deciding the extent of damage.

Based on fretting conditions and specimen geometry, various fretting modes can be classified. Rotational fretting is one such damage mode, observed in industrial applications such as cable ropes under tension used for support in construction industry and variable stator vanes (VSVs) in compressors of turbines. In spite of industrial and engineering relevance, rotational fretting has received little attention.

In the present work, rotational fretting of self-mated AISI 4340 material pair was studied, with the objective of characterizing subsurface damage induced by fretting. AISI 4340 (EN 24) is a low alloy martensitic steel with an excellent combination of strength, ductility and toughness. It is widely used in high strength cyclic loading applications like gears, bearings, automobile pistons and aircraft landing gears as well as in low corrosion, high strength offshore applications. It can be readily machined and surface hardened which makes it useful for wear related applications. A novel rotational fretting test set up, capable of operating under various test loads, frequencies, displacement amplitudes and temperatures was used to perform experiments. Specimens were subjected to a combination of normal load and rotational displacement and caused to mutually contact on non-conformal curved surfaces which simulate a bearing or

bushing geometry. Fretting results were primarily determined by the frictional torque versus angular displacement plots. The running condition response was linked to the fretting material response regime.

Surface and subsurface characterization studies of fretted regions were conducted using Scanning Electron Microscopy (SEM) and Transmission Electron Microscopy (TEM). TEM studies revealed varying levels of fretting induced plastic deformation within the fretted contact zone. Good correlation with available literature relating to formation of dislocation cells and presence of high dislocation density in the fretting damaged regions was established. Although quantifying the dislocation density as a damage indicator is a challenge, it is proposed that a microstructural feature based approach has the potential to be developed into a useful tool for life assessment and life prediction studies.

CHAPTER 1

INTRODUCTION

1.1 Introduction

Fretting is defined as small amplitude oscillating motion between two bodies in contact under certain load. Fretting causes mechanical degradation of material integrity at the contacting surfaces. Parameters that influence fretting can be broadly divided into three categories namely a) Externally applied conditions and environments, b) contact surface related parameters which includes pre-contact as well as in-situ dynamic changes and c) material properties which dictate the extent of fretting damage. Such myriad factors make fretting a complex phenomenon to deal with [1]. A good understanding of a given fretting situation in terms of dominant fretting factors and material response is necessary to design for better fretting mitigation solutions and to predict fretting damage.

AISI 4340 (equivalent to EN 24) is a low alloy martensitic steel. It can be readily machined and surface hardened which makes it useful for many applications. Combination of heat treatment methods can be used to control the microstructure which in turn can control the strength, ductility and fracture toughness. Austenitizing at 1200°C followed by step quenching to 870°C provides a very high UTS of 2193 MPa. With 2% Silicon and tempering temperature of 300°C, very high fracture toughness values of 85 MPa$\sqrt{m}$ and UTS of 2050 MPa can be obtained [4].

Fretting fatigue of AISI 4340 steels has been primarily studied under quenched and tempered condition. AISI 4340 steel heat treated to 44HRC, showed significant reduction in

fatigue life due to early nucleation of fretting cracks and its propagation to failure [49]. In the same study, oxide layers 2-6microns thick were also observed on the fretted surface [50]. In another study, AISI 4340 hardened to 31HRC, showed increased surface roughness, microcracks, pits and oxide particles in the surface damaged region due to fretting fatigue. Patches of finely spaced parallel marks or striations were also seen on the fracture surface. Crack growth at 60^{o} angle to the surface, due to shear stress, with origin close to the boundaries of surface-damaged areas, was also observed in the subsurface [53]. To the author's knowledge, no past rotational fretting studies on AISI 4340 steel material are reported in literature.

1.2 Scope of Thesis

In general, limited data exists in literature on rotational fretting. The purpose of this research was to study subsurface damage due to rotational fretting. Effect of subsurface damage on reliability and performance of components is relevant to design and engineering of components. A novel experimental test set up was employed and the damaged surfaces characterized to understand the various aspects of rotational fretting. This study was carried out on self-mated AISI 4340 material. Self-mated bulk material is not a recommended fretting combination, due to identical surface material properties which cause the initiation of fatigue cracks that can be dangerous or adhesion and galling issues [1]. However, to develop a preliminary understanding of rotational fretting damage, a self-mated material pair was chosen. Additionally, it also provides an avenue to confirm damage characteristics on a given specimen, by identifying and characterizing identical regions on the counterpart, as required. The specimens were studied in high temperature tempered condition (having

low hardness of 57 HRA or 15 HRC) to capture if possible, even the weakest sign and features of fretting damage at the subsurface. The test included specimens that were subject to varying numbers of fretting cycles, to record damage trends. Microstructural tools like Scanning Electron Microscopy (SEM) and Transmission Electron Microscopy (TEM) were employed to develop an initial understanding of the damage progression and accumulation. An attempt to correlate observed damage with existing literature information on fretting damage forms was made.

1.3 Layout of Thesis

This thesis is divided into six chapters:

- Chapter 2 provides the background information for this thesis.

-Chapter 3 describes the experimental procedures followed

-Chapter 4 lists the experimental results

-Chapter 5 contains the microstructural results and related discussions

-Chapter 6 provides a summary of the work and recommendations for future work

CHAPTER 2

BACKGROUND

2.1 Fretting Details

Fretting is defined as small amplitude oscillating motion between two bodies in contact under certain load. The combination of relative displacement between the two bodies and the applied load often decides the damage mode at the contact surface. The contacting surfaces during fretting are subjected to cyclic displacement and hence undergo fatigue locally. Fretting is further influenced by external, contact and material related parameters. External factors include load, speed, temperature, environment, displacement amplitude. Contact factors include surface roughness, geometry of surfaces. Material factors include hardness, toughness, ductility, fracture toughness. Externally applied conditions and environments, can be used to categorize fretting.

2.1.1. Types of Fretting

Based on type of motion imposed on the surfaces, fretting can be categorized as Tangential, Radial, Rotational or Torsional fretting as shown in Fig 2.1

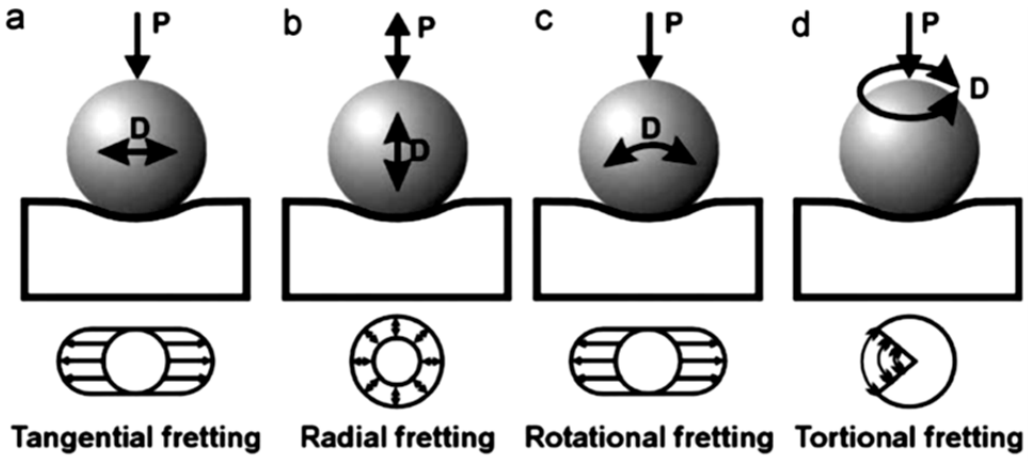

Fig 2.1 Schematic of fretting modes [5], ***By Permission of Elsevier Ltd., May-June, 2010***

Tangential fretting occurs when small amplitude oscillatory motion is imposed on flat surfaces, perpendicular to the direction of loading. Most work in literature pertains to tangential fretting which is the most common mode of fretting. Rotational fretting occurs when the relative oscillatory motion on curved surfaces is rotational. A torque is applied about the axis perpendicular to the direction of applied load. Radial fretting occurs when the relative oscillatory motion on curved surfaces is in the radial direction, parallel to the direction of applied load. Radial fretting is achieved by varying the normal force or by thermal cycling. The surfaces are always in contact and there is no impact. Cyclic deformation of the contacting surfaces allows the relative motion between the surfaces which can be considered as a form of fretting fatigue. Zhu et al. [6] [7] studied the radial fretting behavior of 52100 ball against coated and uncoated steel surfaces and studied the contact degradation. They observed adhesion for metals and material removal by delamination for coatings as the main damage process and the dependence of friction on the contacting surfaces. Radial fretting can also occur due to vibration in fitted assemblies and joints, especially when the motion is in the radial direction. In torsional fretting, the torque axis is parallel to the direction of loading [5].

External environments such as oxidizing or corrosive can also influence fretting behavior. Hard oxides get trapped in-between asperities which can either be lubricating or cause three-body abrasion [24]. Corrosive product formation or lack of formation inside fretted zone, can have a beneficial or detrimental synergistic effect. Fretting corrosion appears to be more prominent at lower amplitudes of slip and lower frequencies of oscillation since this allows sufficient time for the material to interact with the environment in-between each fretting pass [26][27] .

2.1.2 Rotational Fretting

Wire ropes in industrial applications like lifts, mines and bridges are faced with fretting issues due to tensile, torsional and bending stresses. The individual wires in a strand when subjected to tensile load changes the contact pressure which sets oscillatory motion between the contacting wires. The nature of the contact can be a line contact or point contact. In such situations, fretting fatigue cracks can form and propagate leading to failure of the wire rope [1] [2]. Literature reports the use of a "crossed cylinder" test configuration to study the fretting failure in ropes [3]. Cathodic protection using zinc galvanizing and use of lubricants like protective grease are few suggested solutions for the wire rope fretting problem [2].

Engineering components having curved and non-conformal contacts are more likely to undergo rotational fretting. This can be seen in case of valves which operate to guide fluid flow and in case of bushing assembly of inlet guide vanes (IGVs) which regulate air intake to compressor. Fretting related binding of the IGV shaft can lead to blade cracks [52]. Hence the frictional and fretting wear response of such components with rotational angular displacement amplitude needs to be studied. The general response of materials in rotational fretting is similar to that of tangential fretting [5], although more work needs to be done to enable a detailed comparison.

2.1.3 Definition and classification of Damage

The macro fretting behavior of materials is recorded in the form of hysteresis loops which capture the correlation between friction force and linear displacement or torque and angular displacement. The nature of the contact is manifest as - full stick, partial slip (implies partial stick) or gross slip (implies no stick). These would correspond to surface damage characteristics

such as low damage fretting, fretting cracks affecting fatigue life and fretting wear respectively [9]. This is also represented in the torque versus displacement loop characteristics.

Fig 2.2 illustrates full stick, partial slip and gross slip contact condition. In the full stick condition, the surface asperities maintain a continuous elastic contact. This elastic response is represented in the torque versus displacement plot by a linear line, passing through the origin [4]. Such a condition is only theoretical as in practice the tangential force and the displacement amplitude which although is very small continues to either cause microslip or deformation, at the contact edges due to singularity. With increase in the tangential force or displacement amplitude or both, the central contact zone remains in stick, while the surrounding peripheral slip annulus experiences microslip. This is known as partial slip and is expressed by the widening of the hysteresis loop. When the ratio of the tangential force to the normal force or the displacement amplitude exceeds a certain threshold limit, the entire contact experiences slip. This is known as gross slip. The dotted box indicates the transition from elastic to plastic shear in partial slip and the sudden drop in the tangential force, F_t , from static to kinetic friction in Gross Slip [29]. Such a drop in torque or friction in the gross slip regime is not commonly observed**.**

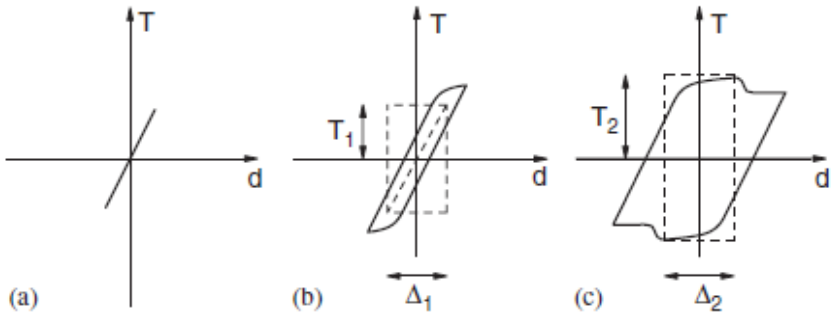

Fig 2.2 a) – Different fretting conditions a) full stick b) Partial Slip c) Gross Slip [9] ***By Permission of Elsevier Ltd., Sep 1, 1988***

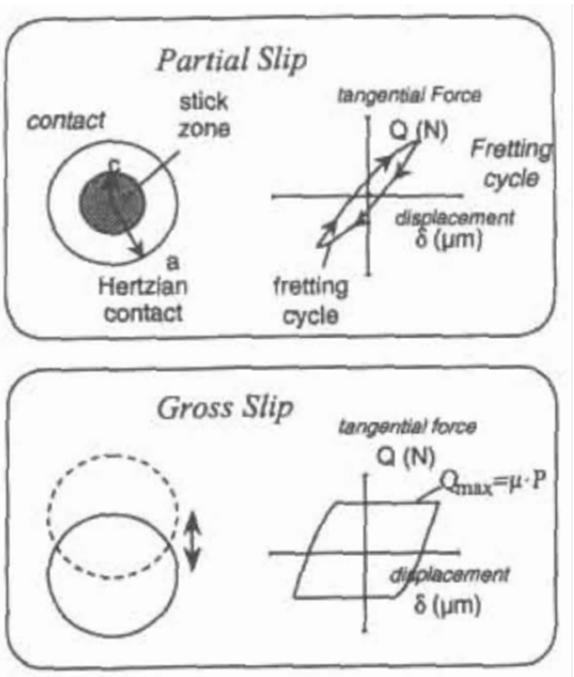

Fig 2.2 (b) – Greater detail of the Partial Slip and Gross Slip condition [12] ***Reprinted with permission, from STP 1367 Fretting Fatigue: Current Technology and Practices, copyright ASTM international, 100 Barr Harbor Drive, West Conshohocken, PA 19428***

Fretting maps in general describe the overall behavior of fretting, such as contact condition, fretting regime, wear mechanism, crack nucleation and propagation. Based on amplitude of motion, fretting damage was initially categorized into fretting or fretting wear. Vingsbo and Soderberg [9] characterized fretting on the basis of displacement amplitude only as shown in Fig 2.3. Fretting damage typically occurs when the slip amplitude is within 3 to 20 microns, measured / controlled remotely away from the actual contact. Maximum damage occurs at relative slip amplitudes within 10 to 20 microns. Literature also suggests that the range of displacements below 5 microns is thought to be absorbed by elastic deformation [11].

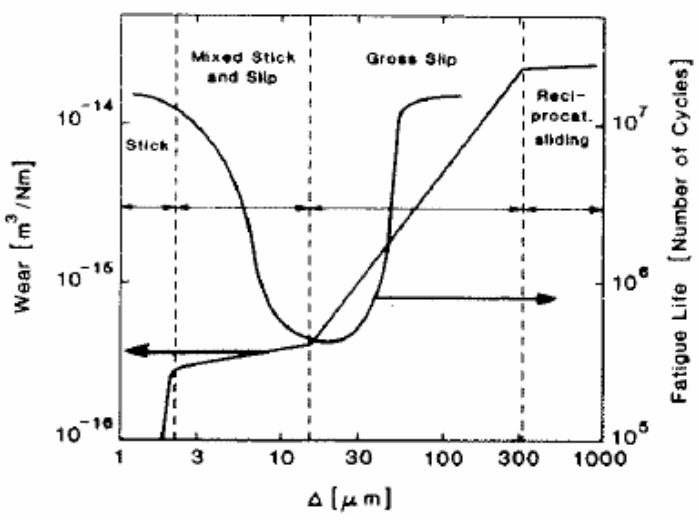

Fig 2.3 Schematic of fretting damage and life against displacement amplitude [9] ***By Permission of Elsevier Ltd., Sep 1, 1988***

Damage is characterized by surface and subsurface cracks that get generated inside the fretting zone which if superimposed with macroscopic cyclic loading, can lead to catastrophic failures. The combined action of fatigue on fretting damage is termed as fretting fatigue. Fretting is also associated with fatigue since the surfaces in contact are subject to cyclic displacements and fatigue occurs locally in the fretted surfaces. Fretting wear occurs when the amplitude of displacement is typically within 20-300 microns. Wear can occur either by oxide formation or progressively increased adhesion of contact asperities leading to cold welding and galling or delamination of material due to subsurface cracking and subsequent removal of plate–like material. Fretting amplitudes higher than 300microns result in reciprocating wear [9]. Classification based on amplitude is a challenge since it greatly depends on the accuracy of the measurements. Additionally, fretting classification in terms related to amplitude only may not be accurate since fretting is also dependent on friction and normal force.

Fig 2.4 depicts the Running Condition Fretting Map (RCFM) as well as the Material Response Fretting Map (MRFM).

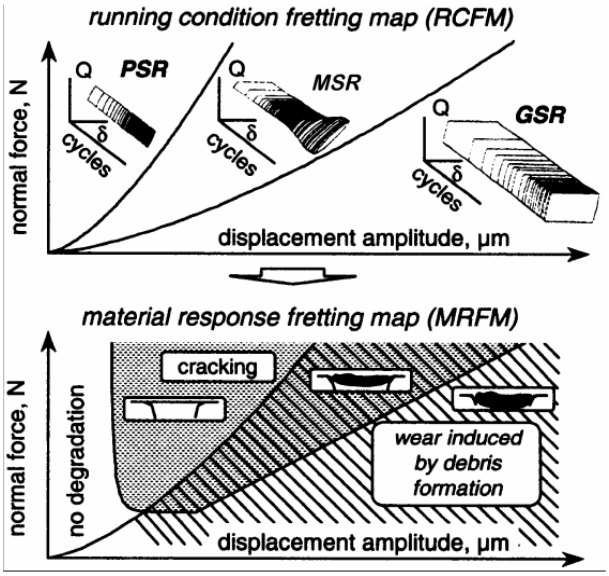

Fig 2.4 – Fretting maps RCFM and MRFM [12] ***Reprinted with permission, from STP 1367 Fretting Fatigue: Current Technology and Practices, copyright ASTM international, 100 Barr Harbor Drive, West Conshohocken, PA 19428***

The characteristics of the loop represent the mode of energy dissipated in each fretting cycle- recoverable (elastic) or non-recoverable (plastic). The area inside the hysteresis loop represents the level of energy dissipated due to interfacial shear work. Friction, along with displacement amplitude, characterizes the fretting contact behavior. Fretting contact is dynamic and the contact conditions change with number of cycles, often due to changes in coefficient of friction associated with changes in the surface of the bodies at the contact region. The running condition of the contact can be divided into three distinct regimes- Partial Slip regime (PSR), Mixed Slip Regime (MSR) and Gross Slip Regime (GSR). Partial Slip Regime is distinguished by partial slip contact condition for all cycles. This is characterized by narrow fretting loops. The mixed

slip regime (also known as mixed fretting regime) is characterized by gross slip initially followed by transition to partial slip with increase in number of fretting cycles, usually due to an increasing coefficient of friction caused by the fretting damage. In MSR, the fretting loop transitions from wide parallelepiped shaped loop to narrow elliptic loops. The gross slip regime (GSR) is characterized by gross slip condition for all cycles. The loops stay wide open in parallelepiped shape for all fretting cycles. From the Material Response Fretting Map (MRFM), it is clear that cracks develop during the Partial Slip Regime (PSR) at higher amplitudes at the stick – slip interface. In the Mixed Slip Regime (MSR), a combination of cracking and wear takes place. Transformational changes in subsurface microstructure as well as the formation of multiple cracks attributed to large plastic strains were observed uniquely in the MSR [50][51]. With higher slip amplitudes, wear is dominant in the gross slip regime, which reduces the risk of crack propagation significantly, since the material removal rate is faster than crack initiation and propagation process.

Fouvry et al. [10] proposed the criteria for transition from partial slip to gross slip in terms of energy ratio, A and sliding ratio, D. Energy Ratio, A is the ratio of the dissipated energy W_d to the total energy W_t. For a purely energy dispersing system, i.e. no elastic accommodation, the dissipated energy W_d will be equal to total energy W_t. The sliding ratio D, is the ratio of the "aperture" δo, to the maximum displacement amplitude δ^*. ("Aperture" as defined by the authors is the displacement recorded in the torque vs displacement loop, when the tangential force Q, is zero). It is easy to determine the Energy Ratio compared to the sliding ratio. For values of $A>0.2$ and $D>0.26$ fretting would transition from partial slip to gross slip regime. Varenberg et al. [13] defined Slip Index and Slip Ratio as dimensionless entities which help distinguish between Gross Slip, Partial Slip across different length scales - making it a universal

method of classification. Fig 2.5 is a schematic which provides the friction loop details. Slip index, δ, is defined as the ratio of Displacement amplitude, A_d ,times stiffness S_c , divided by the normal load N. Slip Ratio, *S*, is defined as the ratio of Slip amplitude, A_s to Displacement amplitude, A_d.

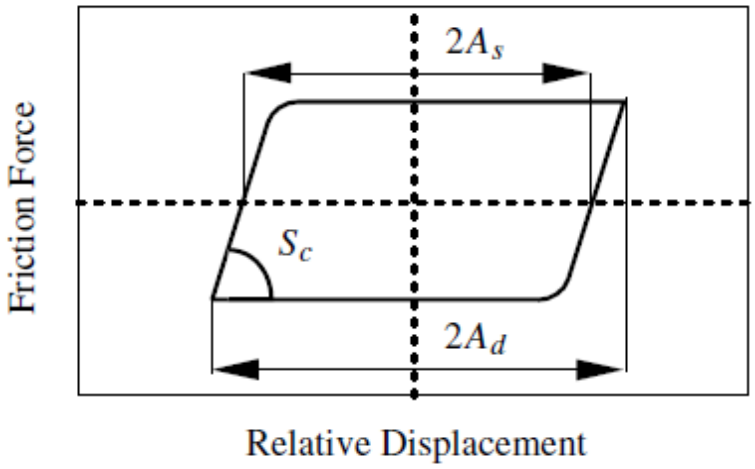

Fig 2.5– Friction Loop details [13] ***By Permission of Springer, October1, 2004***

The slip amplitude, A_s, is a function of all independent governing parameters, displacement amplitude, A_d, Normal Load, N and Elastic Slope of friction loop, S_c, which is the combined tangential stiffness of the contact interface and the machine support.

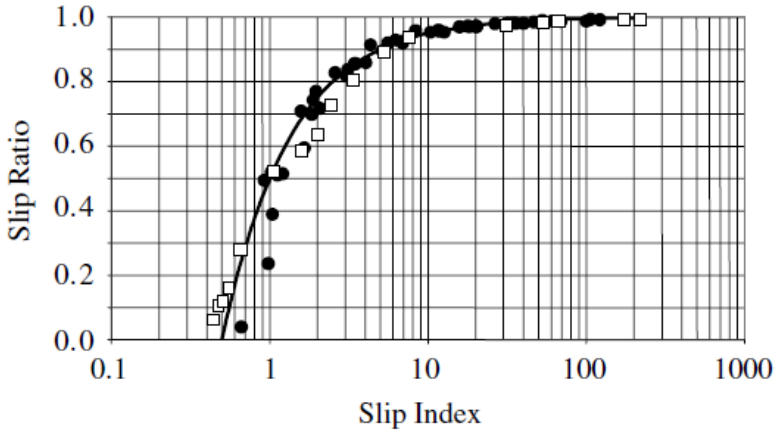

Fig 2.6 – Variation in Slip Ratio *S* **with Slip Index δ [13]** ***By Permission of Springer, October1, 2004***

Fig 2.6 shows the variation in slip ratio with slip index. A value of *S* close to zero, characterizes stick conditions. As the value of S increases, partial slip and then gross slip evolve. A value of *S* close to 1 characterizes reciprocal sliding conditions. The authors through dimensional analysis show that *S* is governed by δ and direct characterization in terms of δ is possible. For $\delta > 11$, reciprocal sliding occurs, and $\delta < 10$ pertains to fretting conditions. Gross Slip is characterized by $0.8 < \delta < 10$ and partial Slip by $0.5 < \delta < 0.6$. The regime corresponding to $0.6 < \delta < 0.8$ indicates the transition from partial slip to gross slip condition. The regime $\delta < 0.5$ had an experimentally very small slip ratio and probably corresponds to stick condition which needs more investigation [13].

Most of the current understanding is in tangential fretting. Similar to tangential fretting, rotational fretting running behavior also produces distinct wear regimes which can be controlled by angular displacement amplitude, as shown in Fig 2.7. However a notable difference from tangential fretting, is the presence of a projected area formed at the center of the contact interface (bulge) caused due to plastic deformation accumulation, specific to rotational SR for angular displacement of 0.5° Increase to a larger displacement of 1.5° caused a larger wear depth and disappearance of the projected area. Fig 2.8 shows the friction coefficient for the various regimes as a function of number of fretting cycles [5].

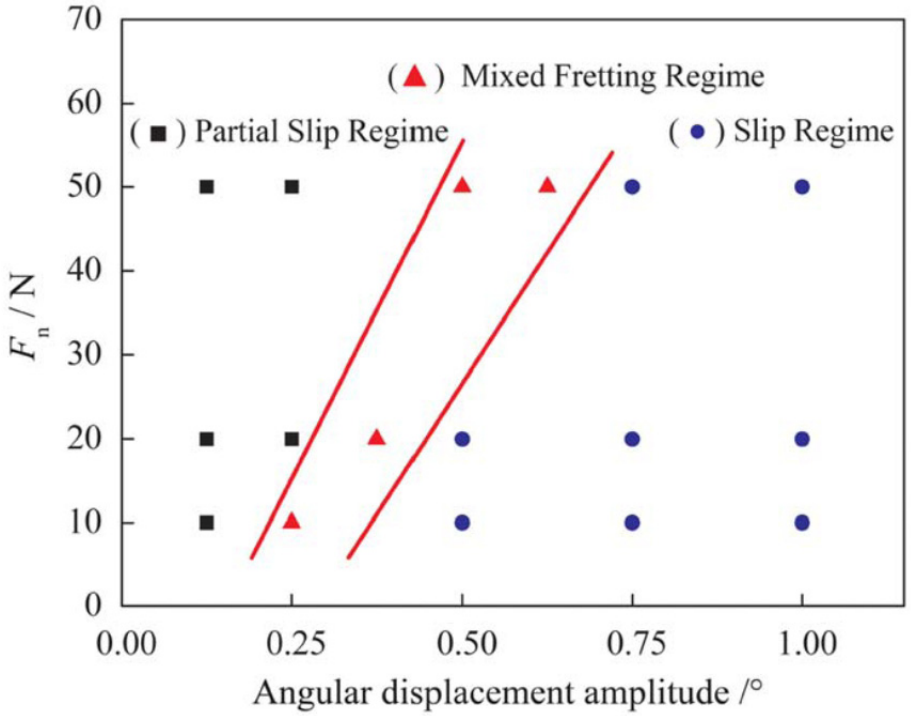

Fig 2.7 Running condition map for 7075 Aluminium alloy under rotational fretting [5] ***By Permission of Elsevier Ltd., May-June, 2010***

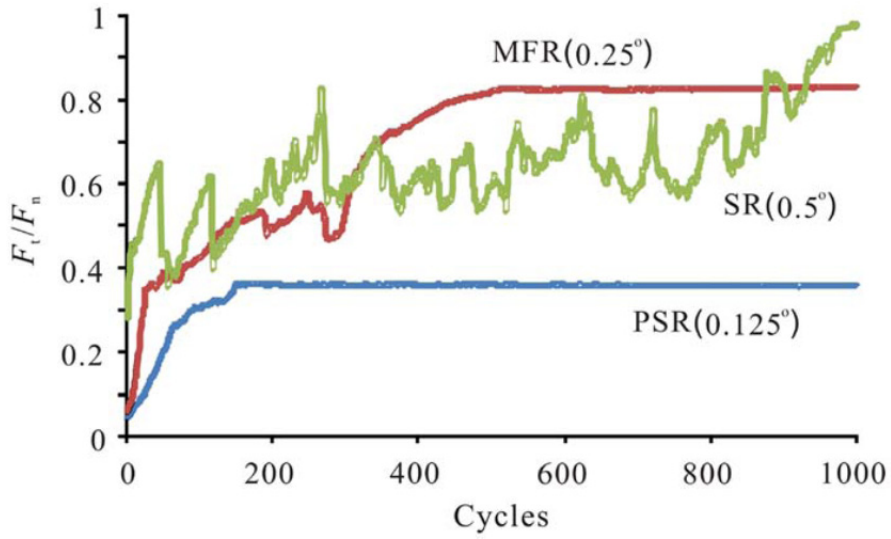

Fig 2.8 Ft/ Fn curves for varying angular displacements [5] ***By Permission of Elsevier Ltd., May-June, 2010***

Effect of number of cycles on the critical transition boundary between fretting fatigue and fretting wear was studied by Yan [11] using a crossed cylinder geometry test configuration. The tangential force required to make the transition is predominantly determined by the size of the stick zone and its junction strength, which can be achieved with increasing number of cycles under a specific set of fretting conditions, provided the contact zone has not reached a stable state. Three different combinations of material pair were studied in fretting: self-mated Cu pair, self-mated SS pair, Cu Vs SS pair. Varying degrees of the central stick and surrounding slip annulus across the three material combinations were found. For the self-mated cases, adhesion and welding of contact characterized the central stick region while the annulus slip region showed plastic deformation. This makes the specimen pair susceptible to cracking at the stick-slip interface. While for the Cu/SS pair which had a greatly varying hardness, there was no evidence of adhesion [11]. This is expected since similar materials have a great tendency to adhere to each other under a tangential force, which induces a shearing process that involves a very intimate contact of the surfaces.

The combination of fretting load and friction coefficient at the contact region determines if the material will undergo plastic straining. The mechanism for plastic strain accumulation due to cyclic loading at the contact can be divided into three regimes a) *Cyclic Plastic Straining*, in which material experiences steady, reversed cyclic plastic strains b) *Ratcheting* in which the plastic strain magnitude increases continually with each loading cycle c) *Shakedown* in which the plastic strains saturate after a few cycles and subsequent material response is entirely elastic [41]. The intrinsic plastic flow stress behavior of materials can be categorized into three categories 1) Elastic- Perfectly plastic 2) Kinematic Strain hardening 3) Isotropic Strain hardening, as depicted in Fig 2.9

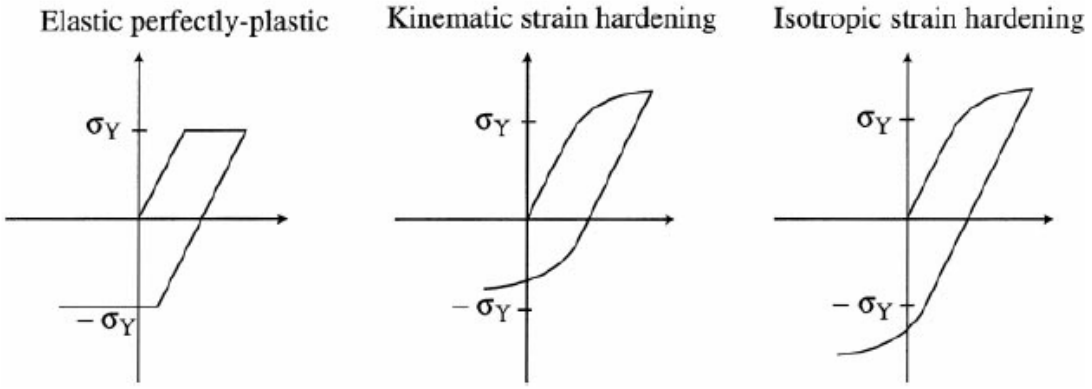

Fig 2.9 Categories of plastic flow behavior of materials [41] ***By Permission of Elsevier Ltd., November, 2000***

2.2 Damage features

In general, fretting damage is visibly manifested either as cracks which propagate and cause failure or as material which is removed periodically. In the fretted zone, the asperities from the stick region undergo weld due to load. The weld junctions are then subject to cyclic shear force which primarily results in elongation of the weld junction, with minimal rupture of weld junctions. In the slip region, there is a continuous interaction of surface asperities, resulting in material removal through various wear mechanism processes.

2.2.1 Fretting

The initial stage of any fretting damage is always associated with crack nucleation which occurs due to fretting conditions of Full Slip, Partial Slip and No-slip (Full Stick) [12] [47][50][51]. Cracks nucleate anywhere within the contact region in full slip due to reverse bending fatigue of asperities, at the stick slip boundary during partial slip due to cyclic movement of the stick/slip boundary and within the contact region of full stick potentially due to reciprocating subsurface stress associated with the reversing elastic deformation of contacting asperities [47]. All such

fretting cracks driven by surface shear stress propagate only to a certain depth inside the material and either get arrested or removed by material removal process. If fretting cracks do not grow outside the fretting fatigue process volume (FFPV), which is associated with crack formation, then failure would not occur. The drivers for fretting crack nucleation and crack growth cannot be isolated easily and their understanding is necessary to mitigate fretting damage [16].

However, when surface shear stress gets coupled with fatigue stress (due to externally applied bulk tensile forces applied on the body) the cracks propagate deeper into the material and are redirected perpendicular to the fretting surface and the direction of applied forces. This phenomenon is termed as Fretting Fatigue. This can lead to catastrophic failure of components. Kovalevskii et al. [23] noted that fretting fatigue is primarily influenced by localized weak regions that get generated due to low cycle fatigue (LCF). These weak regions contain a high concentration of defects and vacancies, which coagulate with dislocations and grain boundaries which eventually form submicrocracks and microcracks. They also indicate the formation of a dual slope in fretting fatigue curve which occurs when the stress is close to the critical fatigue stress and submicrocracks occur at the onset of stress cycling [23].

Literature lists various fatigue based models to characterize fretting damage in terms of crack initiation and prediction of useful life limits for fretting fatigue. Crack initiation is predicted by taking into account fatigue parameters like Fatemi- Socie (FS), Smith- Watson- Topper (SWT), Dang Van and Crossland's crack nucleation cracking risk. [14] [15]. Fouvry et al. [12] applied Dang Van's mesoscopic parameter and have shown an average size dimension of 5-6 microns edge cube representing a micro-volume required in low alloy steel (30NCD16) for predicting crack nucleation under fretting fatigue test condition. The Dang Van Criterion to predict crack nucleation for fretting fatigue condition is a function of the maximum local shear and the

hydrostatic pressure, as shown in Fig 2.10, while the Crossland criterion predicts crack nucleation through a combination of shear, hydrostatic pressure as well as the second invariant of the stress deviator J_2 [30][15].

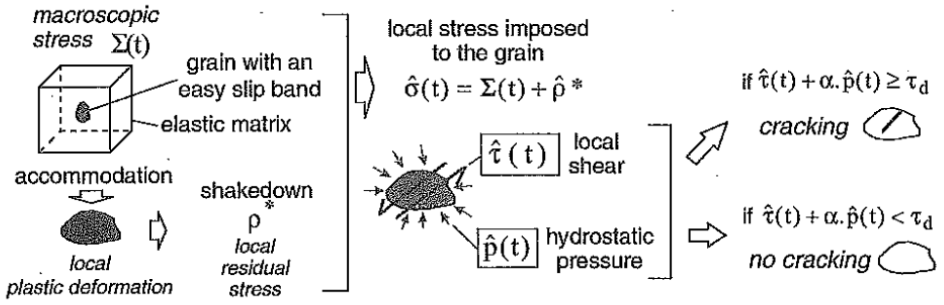

Fig 2.10 Wear progress condition and Energy Wear Coefficient [30] ***Reprinted with permission, from STP 1367 Fretting Fatigue: Current Technology and Practices, copyright ASTM international, 100 Barr Harbor Drive, West Conshohocken, PA 19428***

The FS parameter predicts the severity of fatigue damage using a combination of shear strain range and maximum normal stress on the same plane during a cycle, thereby indicating the orientation of the plane on which crack formation is most likely. Similarly, the SWT parameter predicts fatigue life using the maximum product value of normal strain amplitude and maximum stress on the same plane for all orientations [48]. It is of interest to note that all the listed parameters are directly based on a combination of shear and normal stress or strain and stress.

2.2.2 Fretting Wear

Fretting wear is primarily associated with gross slip condition. Sauger et al. [18] described wear induced by fretting (WIF) through formation of Tribologically Transformed Structure (TTS), which is one of the fretting wear mechanisms. TTS is created due to surface strain hardening which occurs due to adhesion and plastic deformation of the surface. TTS then breaks into small

fragments which forms wear debris, that gets oxidized later and form the fully oxidized third body. This provides an understanding of sequence of events leading to particle removal at a macro level and is shown schematically in Fig 2.11. Fig 2.12 also shows the TTS formed on the surface region.

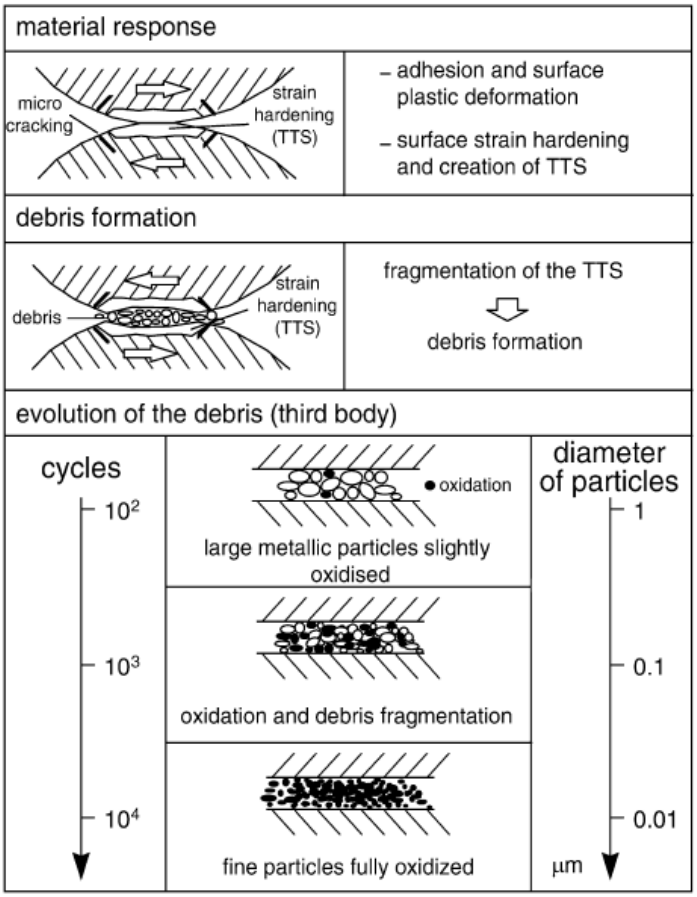

Fig 2.11 Debris creation and third body evolution at contact interface [18] ***By Permission of Elsevier Ltd., October, 2000***

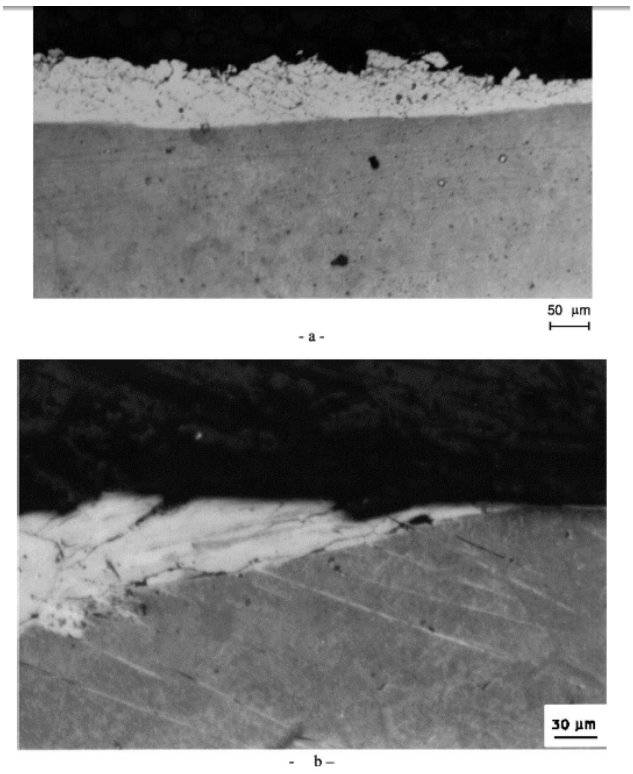

Fig 2.12 Tribologically Transformed Structure [18] ***By Permissions of Elsevier Ltd. October, 2000***

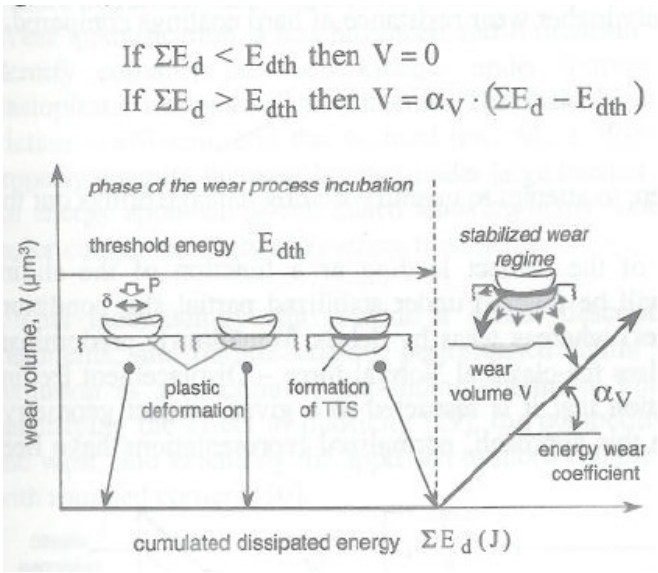

Fig 2.13 Wear progress condition and Energy Wear Coefficient [12] ***Reprinted with permission, from STP 1367 Fretting Fatigue: Current Technology and Practices, copyright ASTM international, 100 Barr Harbor Drive, West Conshohocken, PA 19428***

Fouvry et al. [12] suggested an energy based approach to quantify wear. Fig 2.13 provides a schematic of wear progress. Once the total cumulative dissipated energy $\sum E_{d,}$ indicated by the area under the hysteresis loop, exceeds the threshold energy, E_{dth}, wear begins to take place.

2.3 Martensitic Steel

The hardness of the AISI 4340 steel in the hardened and tempered condition is generally in the range of 37-56 HRC and its tensile strength lies between 930-1080MPa.

Table 2.1- Typical composition of 4340 steel:

C	Mn	P	S	Si	Cr	Ni	Mo
0.38-0.43	0.6-0.8	0.035 max	0.04 max	0.15-0.3	0.7-0.9	1.65-2.0	0.2-0.3

The general tempering temperature for this steel ranges from 100-650°C. Various microstructural changes that occur at different tempering temperatures and time are reported in literature. It is important to note that a widely used material like AISI 4340 steel is prone to temper embrittlement if tempered at 300°C [25]. This is caused due to the presence of interlath austenite which during tempering at 300°C decomposes to form carbide / cementite film which is susceptible to embrittlement. The mechanical behavior depends on the tempering temperature and hold time, the effect of the former is more significant than the latter.

2.3.1 Fretting of Steel

Literature reports fretting behavior of steels. Gaul et al. [24] studied the fretting corrosion behavior of 4130 steel and concluded that the rise in interface temperature followed the velocity pattern, with the fact that maximum temperature is closely associated with maximum velocity. Effect of material hardness on fretting is also reported by Gao et al. [31]. The harder materials

experienced a greater reduction in strength due to fretting fatigue at relative slip amplitudes of 45-55 microns, while softer materials experienced such effects only at relative slip amplitudes of 10-12 microns. This is explained by the fact that at lower amplitudes much less damage accumulation occurs in harder materials, while at higher amplitudes the nucleated cracks are worn away in soft materials, before causing further damage. Fretting fatigue failure of 4340 steel components by Chan et al. [53] revealed the presence of micro pits, cracks, increased surface roughness and oxide particles in the fretted regions. A major crack at 60^{o} angle to the surface was found very close to the boundary of the damaged and undamaged regions. Presence of reddish brown deposits on the regions having high surface roughness was indicative of surface oxidation. Pape et al. [51] studied the fretting damage evolution of PH 13-8Mo steel by exposing specimens to increasing number of interrupted fretting fatigue cycle test. Increase in subsurface fretting crack depth and subsurface hardness with higher number of cycles and the propagation of a major crack to failure were clearly evident from their studies. Adhesion between the fretting pad and specimen and the transformation of the damaged region was distinctly observed for PH13-8Mo material. Variation in the fretting scar damage morphology as a function of decreasing stress amplitude in the mixed fretting regime as well as the detection of crack by a sudden decrease in friction force amplitude that resulted from a change in the local compliance of the material was also highlighted [49].

Pape et al.[34][49] compared the fretting fatigue behavior of PH 13-8Mo with 4340 steel in quenched and tempered condition having Yield strength values of 1286 MPa and 1456 MPa, respectively. A greater reduction in fatigue life (post-fretting fatigue test) was observed for PH 13-8Mo compared to 4340 steel. The nucleation and propagation of a major crack close to the boundary of the hard damaged region and the undamaged region was observed for both these

steels and the presence of surface ripples and striations close to the crack are observations which are common with findings reported by Chan et al. [53]. TEM studies showed the presence of very fine grains, of orders of tens of nanometers within the microstructurally region of PH 13-8Mo steel [50]. Similar transformation was absent in 4340 steel. Local shear strain accumulation and local temperature rise are two likely mechanisms suggested for microstructural transformation. The thermal conductivity of 4340 steel is 40-50 W/ (m.K) at 100°C is 3X higher than 14W/ (m.K) at 100°C for PH 13-8Mo steel. This would lead to higher local temperature rise in PH 13-8Mo, for the same fretting conditions and a greater likelihood of microstructural transformation [34].

Bill et al. [54] studied the influence of fretting on the flexural fatigue of SS 304 and 1020 mild steel. Fretting caused a greater reduction in the flexural fatigue life of SS 304 in the 265- 334 MPa range compared to 1020 mild steel that was subjected to an alternating flexural stresses of 162-217MPa. This difference in behavior was primarily attributed to the compressive residual stress and plastic flow occurring in 1020 steel under combined contact and flexural stresses. Fretting beyond 50K cycles didn't have a significant effect on the fatigue life of SS 304 at stress level of 317MPa. Similarly, no effect of fretting was observed on fatigue life at a stress level of 359 MPa and higher. As per the authors, this is due to the inherently short unfretted fatigue life at such high stresses that do not allow the distinct manifestation of fretting on fatigue. They also observed that fretting below 30K cycles, are insufficient to initiate surface damage necessary to start a crack, which highlights the concept of fretting-fatigue damage threshold. Damage was caused due to a primary fretting crack that led to failure. The primary crack showed a rapid evidence of crack growth near the surface, which turned parallel to the bending axis with

increasing depth. Both the primary crack and secondary cracks originated in the slip region of contact.

2.4 Damage assessment techniques / parameters

Along with the surface and subsurface microstructural features obtained through SEM, analysis of subsurface using TEM is essential to understand damage mechanisms that correlate surface microstructural features with subsurface fretting damage and events. Sauger et al. [18] used Transmission Electron Microscopy (TEM) and Electron Energy-Loss Spectroscopy (EELS) to study Tribologically transformed structures (TTS) that formed at the subsurface during fretting. They also studied the role of alloying elements in the formation of TTS and did not observe any significant dependence. Swalla et al. [35] used Orientation Imaging Microscopy (OIM), to correlate low-angle misorientations of grains with fretting deformation substructure evolution due to plastic strain and crack formation. SEM, EDS, Profilometry (Power Spectral Density PSD and surface roughness), microhardness have all been used to characterize the differences in the stick and slip region of the fretted zone.

No parameters to quantify rotational fretting induced damage are reported in literature. Besides mechanical parameters, microscopy based parameters can also be used for assessment, although this would be qualitative in nature. Evolution of dislocation interaction, its arrangement and density as a function of strain can be a good indicator of damage accumulation leading to material degradation and failure. Conventionally, dislocation density is measured by measuring the number of intersections of the dislocations with a grid of lines in a TEM image. If L1 & L2 are the total length of the grid lines in two mutually perpendicular directions and N1 & N2 are the corresponding numbers of intersections with the dislocations respectively, then the dislocation density, ρ is provided by

$$\rho = \left(\frac{N1}{L1} + \frac{N2}{L2}\right)\frac{1}{t}$$

were t is the thickness of the material foil [39]. However when the dislocation density is very high, methods which involve resolving individual dislocations are cumbersome and inaccurate.

Few other indirect methods to measure dislocation density that have similar limitations are resistivity change, density change, X-ray line broadening. The release of stored internal energy, as a function of temperature through Differential Scanning Calorimetry (DSC) measurements can also be used to estimate the number of dislocations present within a material [39].

General literature provides information of dislocation pattern evolution and the strain dependence of the microstructure on activation energy for cross-slip of dislocation rather than independent parameters such as Stacking Fault Energy (SFE) or Shear Modulus. Influence of homologous temperature is also discussed [33].

2.5. Microstructure and Fretting Damage

The material under study AISI 4340, has a bainitic microstructure comprising of regions having feather-like lamellar structure of ferrite and cementite as well as the lens shaped carbide in ferrite matrix. At the subsurface level, investigations and predictions of fretting damage have been attempted. Mall et al. [21] studied the effects of fretting fatigue crack initiation in Ti-6Al-4V and found homogenous duplex microstructure more resistant to crack initiation compared to fully transformed heterogeneous lamellar texture which is contrary to the conventional short and long crack behavior. This may be explained based on the finding of Hines et al. [22] which reported differences in growth of microcracks and macrocracks for Ti-6Al-4V material subjected to plain fatigue. They explained that the crack nucleation is influenced by two factors- intrinsic resistance of the lattice to deformation and the dislocation slip length. The former is a function of the yield

stress of the material. Microcracks develop surface roughness ahead of the crack front once it reaches 100microns in size. The crack front of the microcrack must interact with an increasing number of microstructural features as the crack grows, until it reaches a point when the localized interaction effects can be averaged out. Owing to these factors, the microcrack grows faster in the fully lamellar microstructure and the macrocrack grows faster in the bi-modal microstructure [22].

Investigators have reported submicron scale damage evolution of steels subjected to deformation modes other than fretting. For example, Cuddy et al. [43] observed the formation of dislocation cell structure as a result of deformation by slip during pull test of annealed 4340 steel. The tendency for cell structure formation is strongly controlled by the mobility of dislocations which is influenced by Stacking Fault Energy (SFE), temperature, strain and alloy content. They reported the evolution of the substructure microstructure, through various stages, as a function of increasing strain in annealed AISI 4340 steel. The unstrained baseline microstructure consisted of low density dislocation substructure, Fig 2.14a. At strain ε=0.12, the microstructure contained numerous individual dislocations and tangles, shown in Fig 2.14b. As strain increased to the range of 0.15-0.18, fully developed dislocation cell structures were observed, Fig 2.14c. These cell structures consisted of dislocation tangles that enclosed regions of low dislocation density. With further increase in strain, the cells undergo refinement and exhibit more regular cell boundaries. As strain increased to the range of 0.3-0.4, cell formation was observed exclusively in the pearlitic ferrite regions of the pearlite microstructure, Fig 2.14 d. The initial size of these cells corresponded to the spacing between cementite platelets. With further increase in strain, these cells were equal or lesser in size compared to cells found in the free ferritic region of the matrix. The differences in dislocation mobility for a given strain between the ductile ferrite

grains of the matrix and the constrained ferrite in pearlite, was responsible for the delayed cell formation in pearlite. As stated by the authors, this difference in dislocation mobility is caused by the much lesser local stresses present in the ferrite regions compared to the stresses present in pearlite, which is caused due to the differences in elastic moduli and yield strengths of the composite pearlite constituents- ferrite and cementite. This leads to the understanding that dislocation activity in the ferrite grains or in interlamellar ferrite region, appears to control the work hardening behavior of this alloy [43].

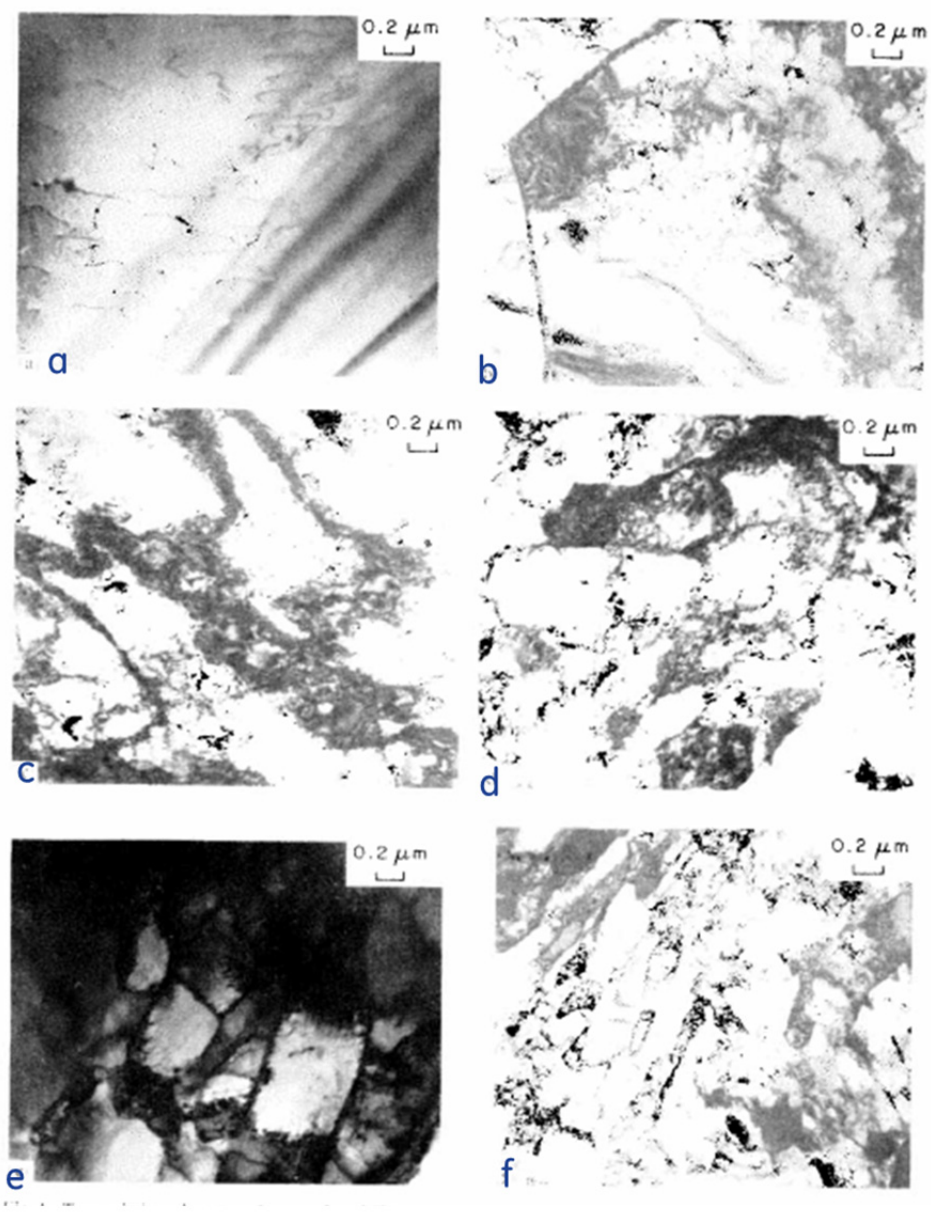

Fig 2.14 Dislocation substructure in uniaxial tension of 4340 steel as a function of true strain: a) ε=0.0, b) ε=0.12, c) ε=0.18, d) ε=0.3, e) ε=0.4, f) ε=0.7 [43] ***By Permission of Elsevier Ltd., July 1, 1989***

At high strains (ε=0.4-0.7), near the onset of fracture, Dense Dislocation Walls (DDWs) form, which appear as sharp boundaries, Fig 2.14e. At ε=0.7, subgrains delineated by such walls appear elongated as well as get arranged in groups of similar orientation termed as "microbands" as shown in Fig 2.14f . The transition from cells to subgrains is related to "recovery / softening"

during which annihilation of dislocation in the cell walls takes place at higher strains, which leads to very low work hardening. The appearance of a mixed dislocation cell-microband structure indicates the hardening behavior transition from Stage 3 to Stage 4, which eventually leads to onset of instability and fracture at large tensile strains [43].

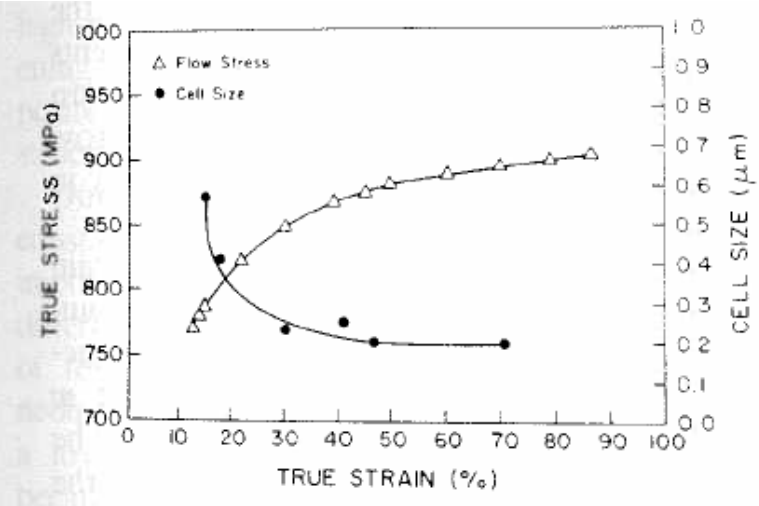

Fig 2.15 Variation of dislocation cell size, true stress, true strain for AISI 4340 steel [43]

By Permission of Elsevier Ltd., July 1, 1989

Fig 2.15 shows the relation of cell size and true stress and true strain. With increase in true stress and true strain, the cell size decreases and eventually reaches a constant value of 0.2.

Similarly, Rigney et al. [44, 41] studied the near surface layers of AISI 52100 steel and Bronze and observed a very thin fragmented layer near the surface (0.1-1um) that composed of cells, subgrains and recrystallized grains. Dislocation cells are defined as structures containing dimensions of less than or equal to 1um which consist of an enclosed space relatively free of dislocations, separated by highly tangled regions of dislocations which serve as cell boundaries or walls. On the other hand, subgrains are larger with small misorientations and well defined low energy boundaries. In their view, materials with higher Stacking fault Energy (SFE), form cells

easily and tend to have a higher wear rate. The regions with the higher energy cell boundaries are inherently prone to void formation and crack nucleation. These cell walls additionally provide paths for diffusion which could lead to composition changes near the surface during wear [44].

As mentioned earlier, subgrains were also observed by Waterhouse [17] near the slip region. Garbar et al. [46] also studied the near surface layers in a low carbon steel (C-0.08%, Mn-0.12%, Si-0.15%, Cr-0.02%, S-0.023%) under sliding conditions and observed the annihilation of grain structure to a cellular structure progressively as a function of reducing depth towards surface as shown in Fig 2.16.

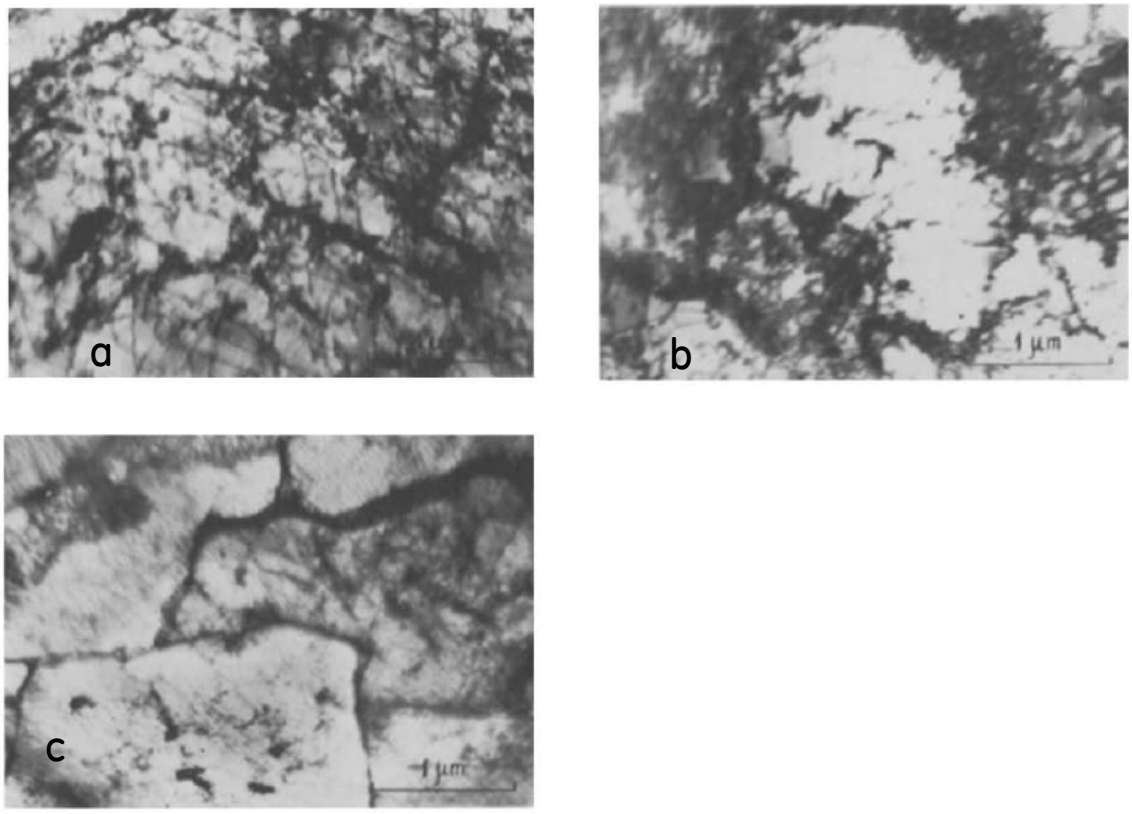

Fig 2.16 Dislocation structure a) 15 microns below surface b) 8-10microns below surface c) 5microns below surface [46] ***By Permission of Elsevier Ltd., December, 1978***

Furthermore they also observed the morphological evolution of the dislocation cell structure in sliding wear in the following progressive stages of - Equiaxial, Directional, Mutually disoriented

and Elongated streamlined as a function of reducing depth, from 5microns to the surface as shown in Fig 2.17 a, b, c, d respectively.

They also noted that the cells in the surface layer (<5 microns from the surface) are smaller and have higher dislocation densities at the cell walls compared to cell structure at higher depths (> 5microns). With increasing load, the cell size reduces to the minimum value beyond which the material experiences severe wear with no reduction in cell size. Evidence of fragmentation of cell boundaries oriented perpendicular to the sliding direction, leading to particle formation was distinctly observed [46].

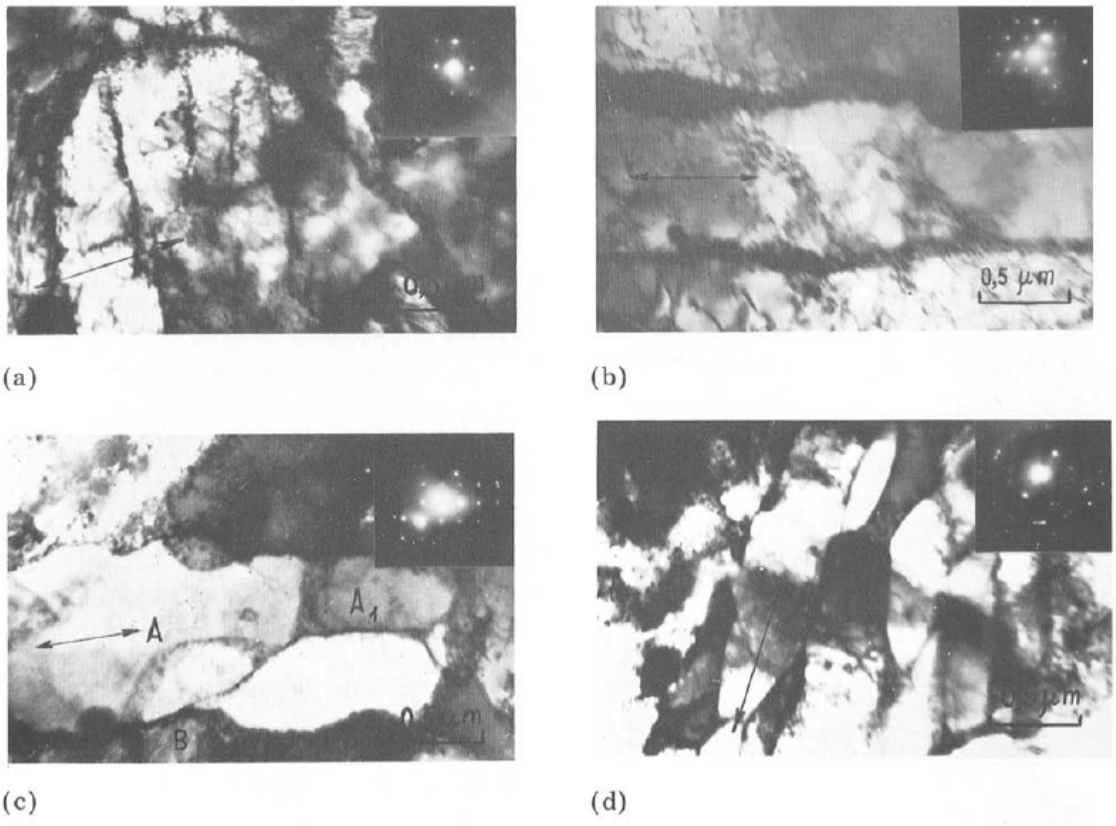

Fig 2.17 Dislocation structure (a, b, c, d) – Change in cellular structure from 5microns below surface to surface [46] ***By Permission of Elsevier Ltd., December, 1978***

Since valuable information can be obtained through study of microstructures at the submicron level, microstructure based studies as well as modeling approaches to predict fretting damage is

of interest. Fretting modelling using crystal plasticity has been carried out with emphasis on the need to capture the anisotropic behavior of fretting damage at the microstructural level. Dick et al. [14] modeled fretting of Ti-6Al-4V using crystal plasticity which included parameters representing microstructure and crystallographic texture and studied the anisotropic influence of polycrystal material on fretting fatigue. Zhang et al. [20] observed that the crystallographic texture and average grain size have a greater influence on plastic deformation and fretting fatigue behavior compared to grain size distribution. An increase in low angle misorientations due to plastic deformation near the slip regions is reported by Waterhouse [17]. The magnitude of misorientation depends on the relative slip amplitude and number of cycles [32].

Given the influence of microstructure in fretting damage, the classification of various regimes of fretting through subsurface damage features especially for regions of stick, slip and stick-slip interface would enhance the understanding on damage mechanisms that occur in the material during fretting**.** Additionally, the different regimes of the MRFM can be further validated with corresponding subsurface damage features.

CHAPTER 3

FRETTING EXPERIMENTAL PROCEDURES

To have a better understanding of rotational fretting subsurface microstructural developments, it is necessary to conduct a parametric experimental study of factors that influence fretting. In the current study the number of cycles was varied with other test parameters kept fixed. The intent was to obtain an understanding of the effect of fretting cycles on damage progression in the material subsurface.

AISI 4340 in the quenched and tempered condition was studied in the self-mated test condition. Tempering was carried out at 700°C to achieve a hardness of ~57HRA (equivalent to 15-17HRC) with an underlying assumption that low hardness material would enable a better capture of damage events / stages occurring during fretting.

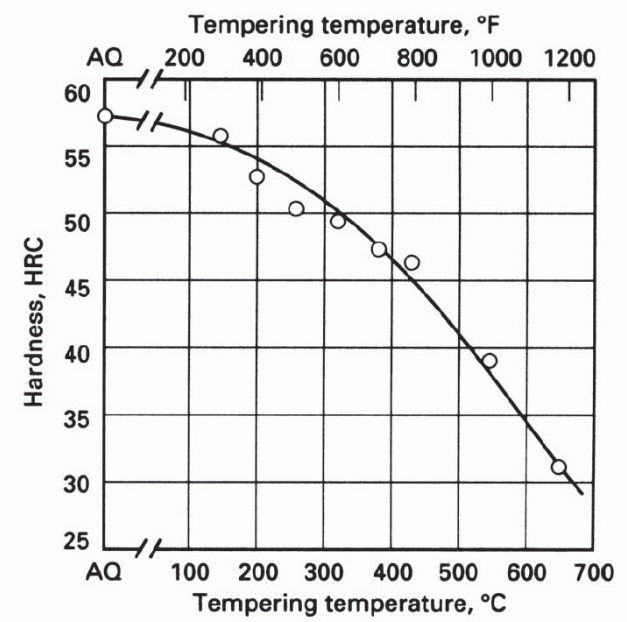

Variation for hardness with tempering temperature for 4340 steel. All specimens oil quenched from 845°C (1550°F) and tempered 2 h at temperature. AQ = as quenched.
Source: *ASM Handbook, Vol. 4, Heat Treating,* ASM International, 1991, p 211

Fig 3.1 Tempering Treatment of 4340 steel. ***By Permission of ASTM, June 30, 2002***

Fig 3.1 gives the general tempering temperature and corresponding hardness values that can be achieved for 4340 steel, which was used to identify the tempering temperature to achieve a low final hardness.

3.1 Rotational Fretting Machine

A custom built rotational fretting machine was used in this study. Fig 3.2 shows the various components of the test set-up. It consists of an arrangement to hold a specimen pair at 90° to each other. A radial load was applied using a dead weight assembly. The minimum and maximum load capacities for the machine are 1lb and 400lbs, respectively.

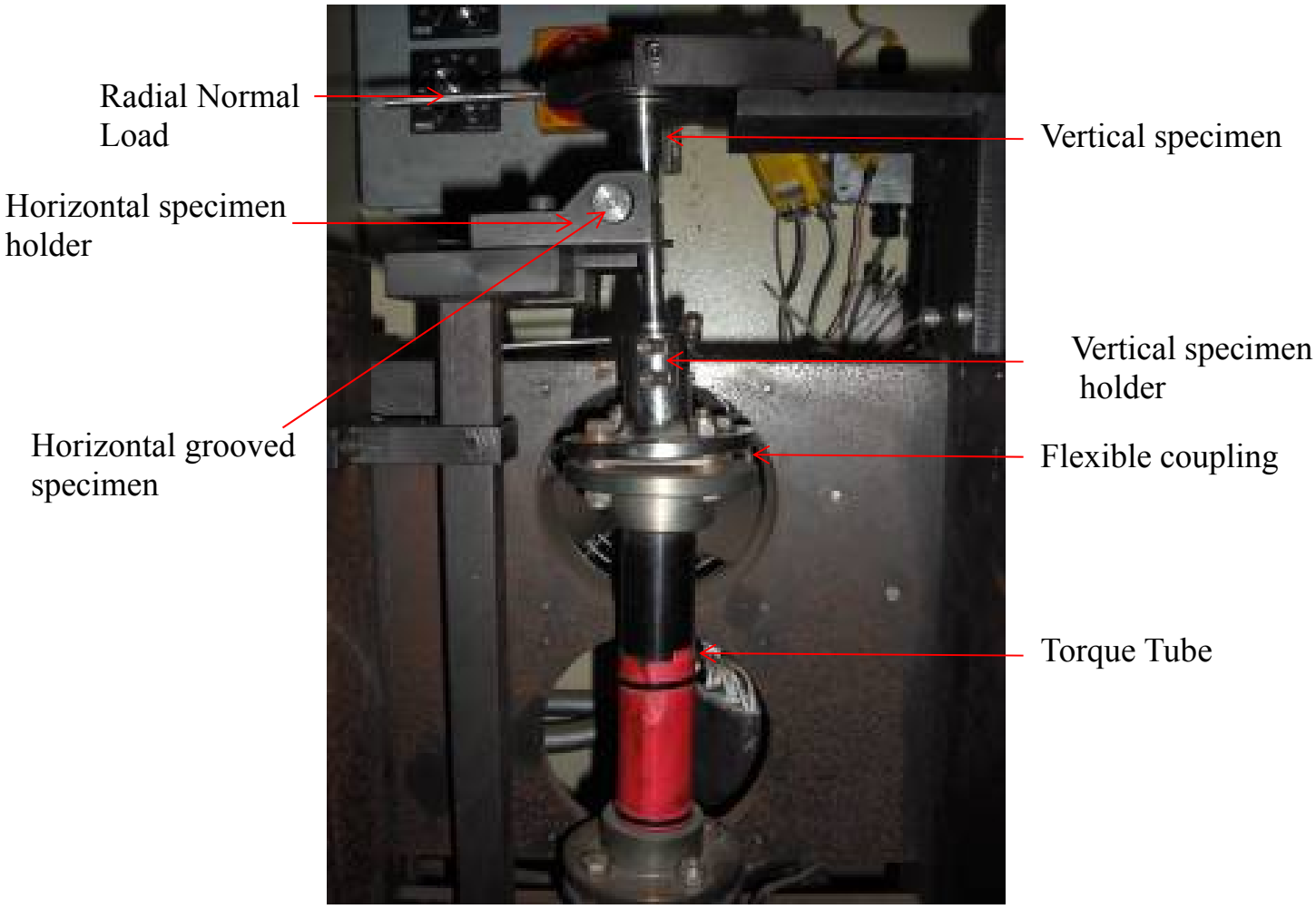

Fig 3.2 Rotational fretting test set up

A dead weight loading arrangement system was used for load application. The flexible couplings below the specimen holding assembly, provide flexibility for the vertical specimen to make contact with the grooved horizontal specimen. The torque actuation was provided to the vertical specimen. The minimum and maximum limits of actuation were +/-0.5 deg and +/-20 deg, respectively. The lower and upper limits of frequency of actuation were 1Hz and 100Hz, respectively. The torque is measured using a torque tube which consists of strain gages to measure the torque response of the specimens. The angular displacement is measured using an encoder that is placed around the shaft which holds the torque tube.

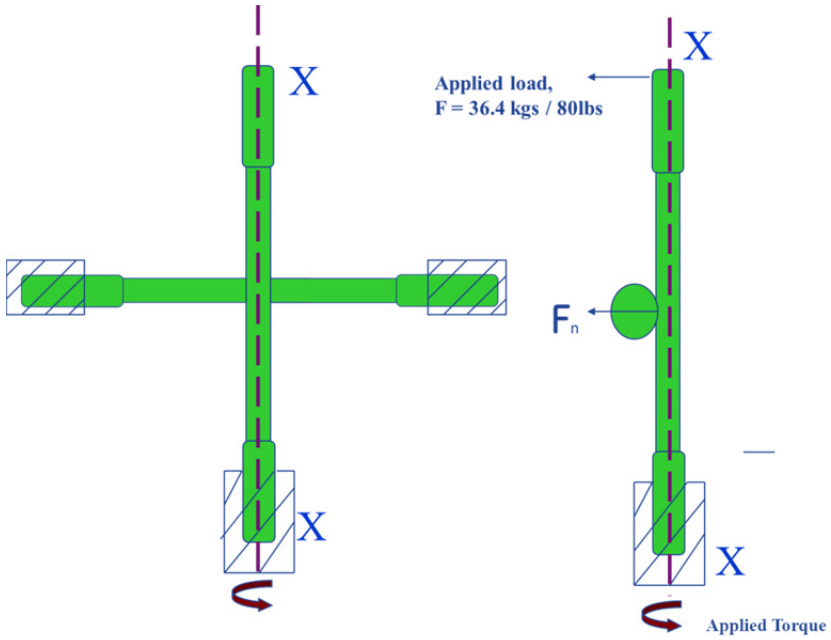

Fig 3.3 Schematic of specimen pair in the test set up

The output of the machine is a hysteresis plot of torque Vs angular displacement. The changing shapes and the magnitude of the hysteresis plots are indicative of fretting response at the specimen contact regions. Other capabilities of the machine like axial loading of the vertical specimen and heating of specimen contact to 800°F maximum were not employed in this study.

Fig 3.3 shows a schematic of the specimen pair. The hatched regions show the locations that are fixed with no relative movement with the specimen holder. The vertical specimen is actuated about its own axis.

3.2 Fretting Specimen Details

Cylindrical dog bone shaped specimens were chosen for the study, as shown in Fig 3.4. Surface roughness of the specimen was maintained to 0.8 microns Ra through machining. A specimen pair consists of a grooved and an ungrooved specimen that made contact under a specified load. The grooved specimen was held horizontal and fixed while the ungrooved specimen was held vertical and actuated to provide the relative fretting motion. The specimen pair was cleaned in acetone to remove any contaminant layers on the surface before start of test.

Fig 3.4 Test Specimens

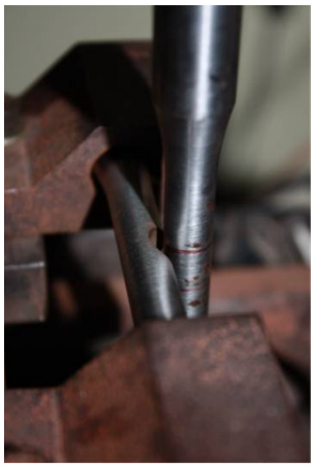

Fig 3.5 Specimens within holder at preload condition

On the application of load, the ungrooved specimen made contact with the grooved specimen inside the curved grooved region, as shown in Fig 3.5. Specimen dimensions are given in Fig 3.6.

Two separate specimen pairs were exposed to test time durations of 10K cycles and 89K cycles. In order to understand the effect of number of cycles on fretting damage, a low and high value of number of cycles was chosen to get distinct scenarios of subsurface rotational fretting damage. In

subsequent sections, the specimen pair exposed to 10K cycles is designated as "10K_A" while the specimen pair exposed to 89K cycles is designated as "89K_B". A third specimen pair "1.16MM C" was tested at 25Hz for 1.16MM cycles to primarily understand the friction and surface related differences from the specimen pairs tested at 10Hz.

Table 3.1- Specimen nomenclature and respective test details

Specimen Pair	No. of fretting cycles	Test Frequency (Hz)
10K_A	10273	10
89K_B	89582	10
1.16MM_C	116000	25

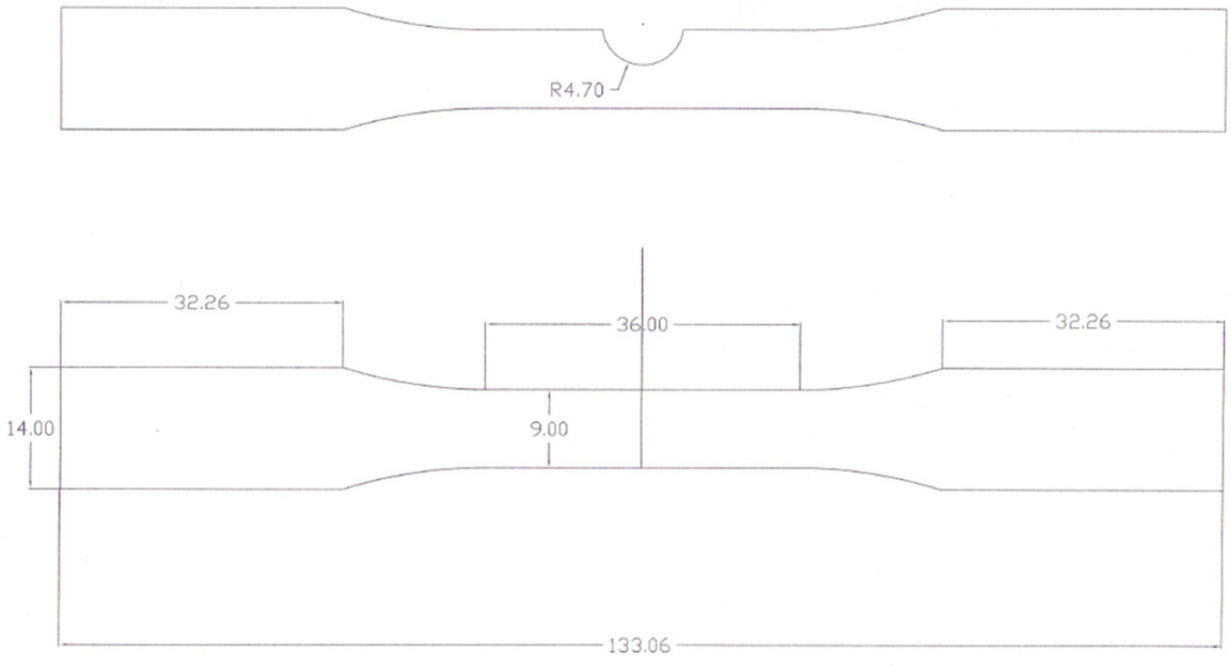

Fig 3.6 Test Specimen Dimensions

3.3 Fretting Specimen Holder Assembly

The holder for the vertical specimen consisted of a split bottom hub, inside which the specimen was placed and tightened by screws. The hub was connected to the torque tube through the flexible couplings. This allowed flexibility for the vertical specimen to bend in the direction of loading to make contact inside the groove. The horizontal specimen was held inside an adjustable C shaped holder with provision for adjustments of locational height. Angular rotation of the horizontal specimen about its own axis was possible to ensure proper contact between the two mating surfaces.

3.4 Contact Analysis

Contact analysis was primarily carried out to calculate the maximum initial contact stress that is experienced by the specimens at the application of load. Contact was analyzed using Abaqus 6.8-1. As part of the simulation, boundary conditions were applied to both specimens to represent the loading in the rotational test rig as shown in Fig 3.7. The horizontal grooved specimen was free to rotate but constrained from horizontal displacement / translation.

The lower end of the vertical specimen is fixed to the holder and is restricted to slip or displace, relative to the holder during rotation. The top end of the vertical specimen is free to move without any restrictions. Rotational displacement of the vertical specimen holder assembly was assumed constant throughout the specimen. The parameters of displacement and load were provided as inputs to the finite element (FE) analysis.

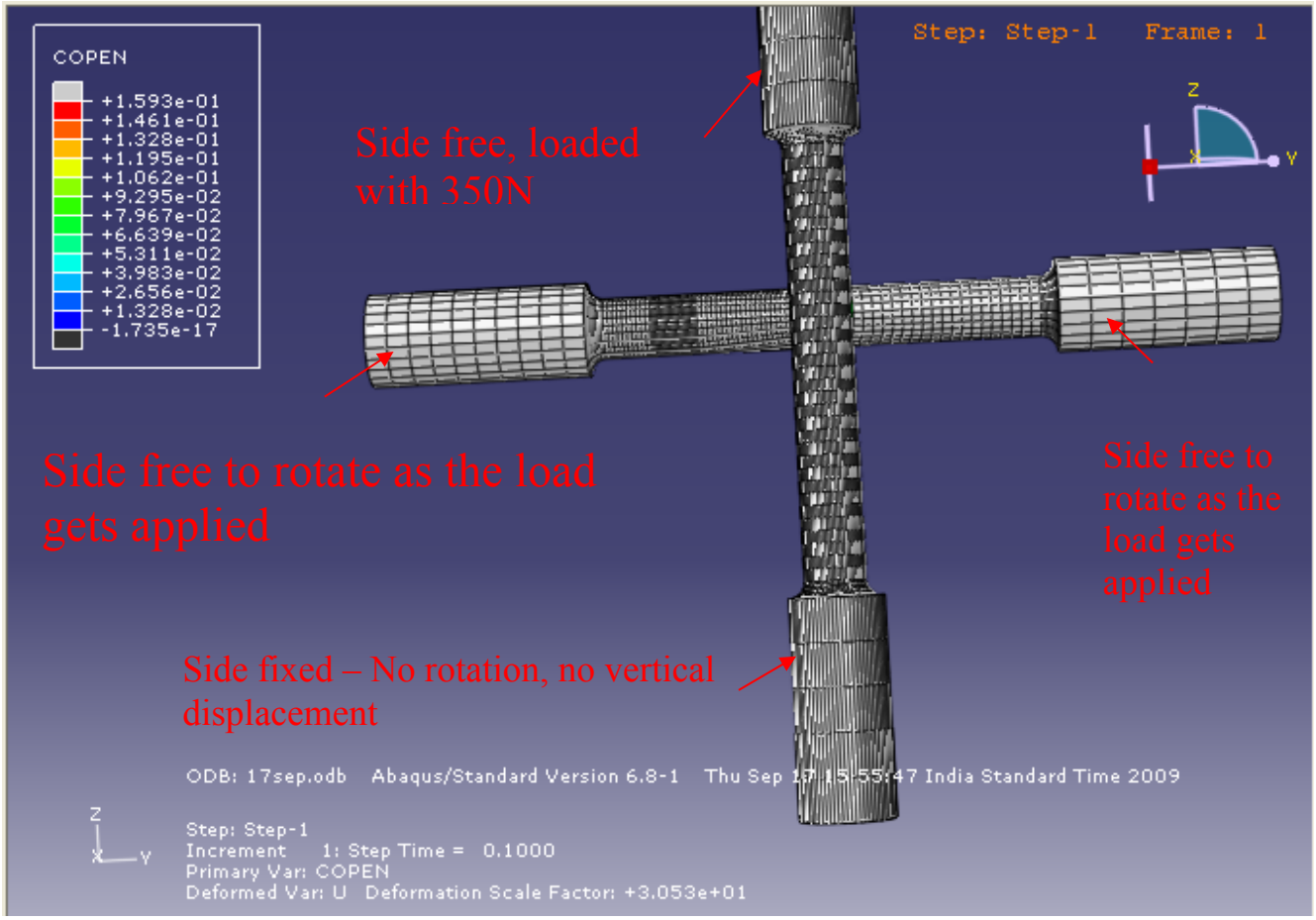

Fig 3.7 Cylindrical Specimens Meshed

The specimens were meshed using a C3D8R hex element. C3D8R is a general purpose linear brick element with 8-nodes. It has reduced integration capabilities and hourglass-control. The regions adjoining the groove chamfer were meshed using a combination of C3D8R and C3D6 which is a 6-node linear triangular prism wedge element. The number of seed elements was set to 75 to achieve fine mesh size of 10-20 microns inside the groove, which was the region of interest. Progressively lower number of seed elements such as 70, 65 and 50 were selected as a function of distance away from the groove, which gave a relatively coarser mesh size for the remaining cylindrical surface portion of the specimen. A 200 micron thick, 45° chamfer was provided at the groove edge to avoid sharp edges. This input was crucial to arrive at a converged

solution.

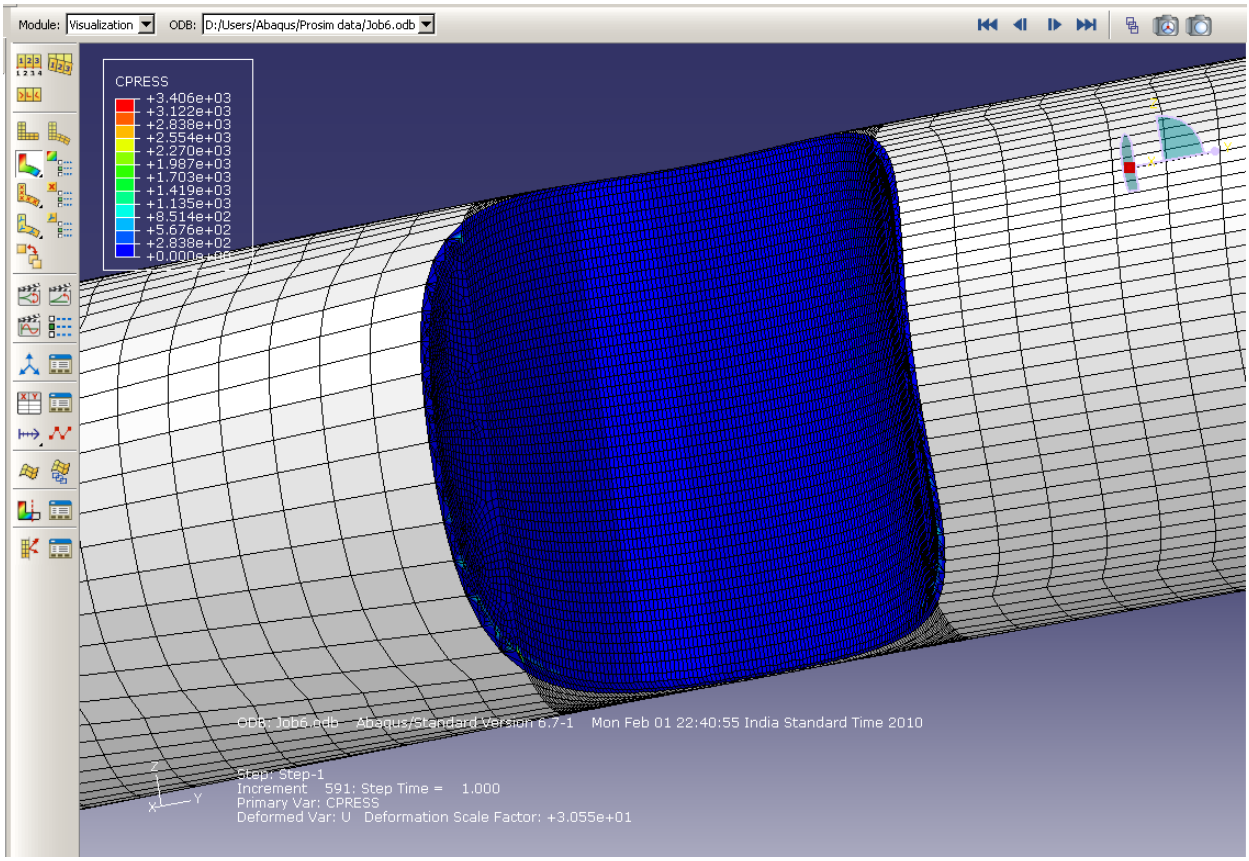

Fig 3.8a Pressure values of Initial Contact region

At the application of load, a maximum initial contact pressure of 3.41GPa was observed at the groove chamfer edges (red color, Fig 3.8b) while no initial contact was made at any other location inside the groove at the start of test (blue color). Figs 3.8b, 3.8c, 3.8d show the various locations on the chamfer edge of the grooved sample where the specimens make initial contact.

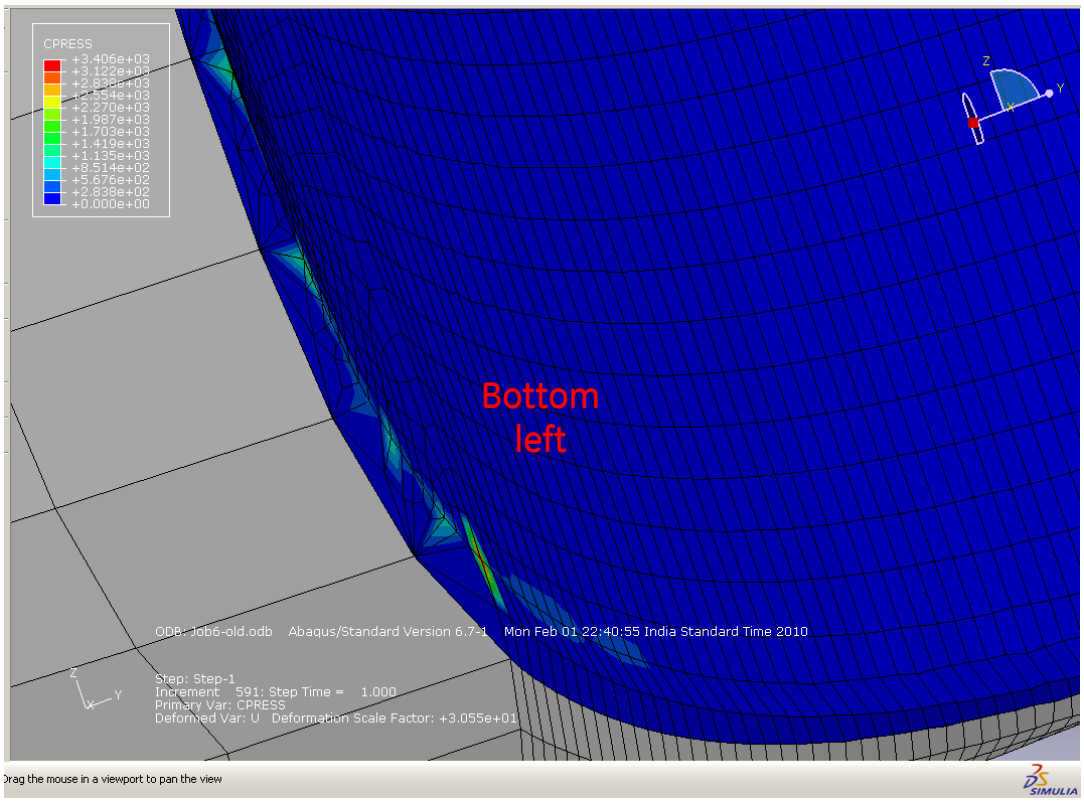

Fig 3.8b Contact pressure at the groove edges

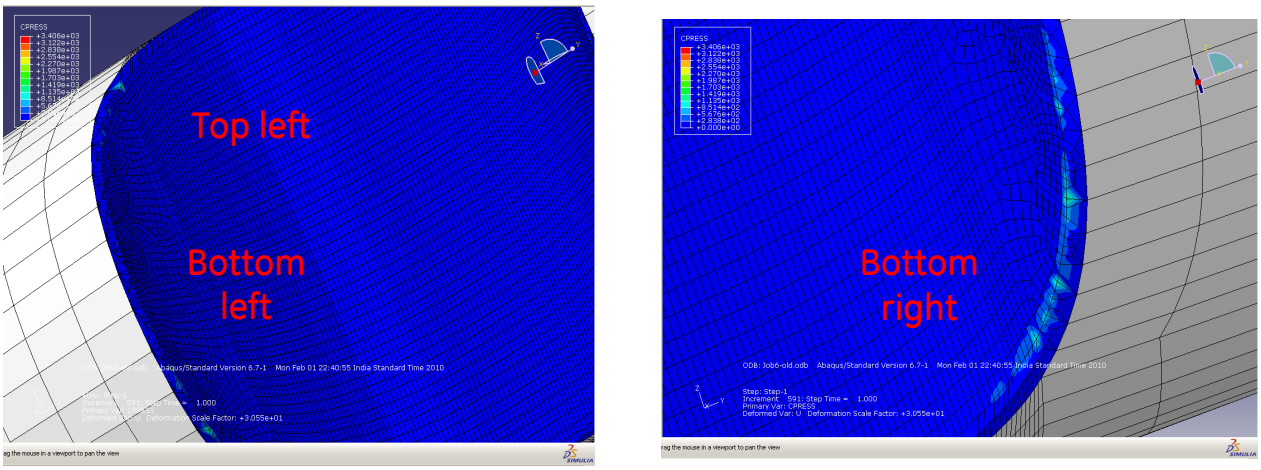

Fig 3.8c Contact pressure at the groove edges

The contact is non-symmetric and is observed only on the top left, bottom left and bottom right sections of the groove chamfer. This is primarily due to the bending of the vertical specimen

(Fig 3.9a) at an angle to the vertical axis as well as the axis of load application along with the simultaneous bending ("thrust out") of the horizontal sample about the vertical axis (Fig 3.9b). In the process, the groove also becomes elongated as shown in Fig 3.9c which "pinches" the vertical sample at the contact locations.

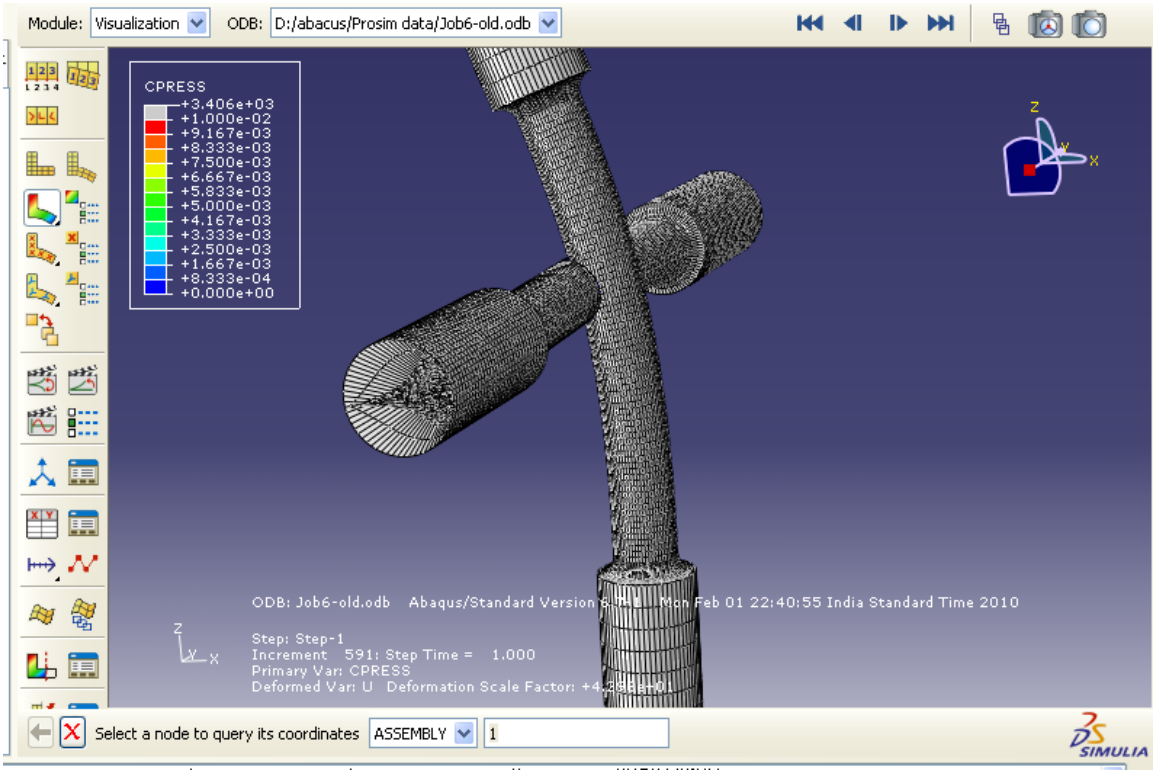

Fig 3.9a Specimen pair after the application of radial load

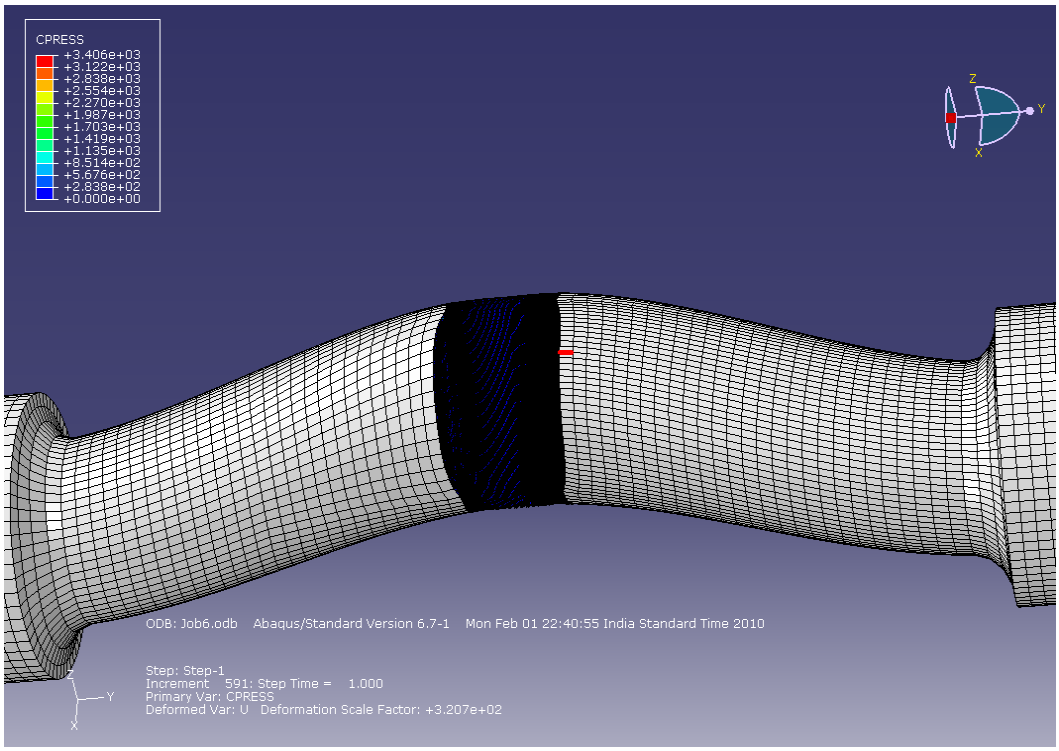

Fig 3.9b Horizontal specimen bending after application of normal load

Given the complexity of the loading condition as well as the contact geometry of the specimens only a very small portion of the chamfer edge makes contact initially. Hence the analysis is approximate and is expected to differ from the real contact pressure value obtained as a function of many cycles and a larger contact area.

To verify the FE results, Hertzian contact stress value was calculated. The specimens were approximated to a standard geometry. The groove was assumed to be a flat surface on which the vertical cylinder made line contact.

Following equations were used to arrive at a Hertzian solution for the problem.

Max contact pressure, $p_o = \left(\frac{PE^*}{\pi R}\right)^{\frac{1}{2}}$ - Eq. 3.1

Where Effective elastic moduli, $E^* \equiv \left(\frac{1-v_1^2}{E_1} + \frac{1-v_2^2}{E_2}\right)^{-1}$ - Eq. 3.2

Effective Radius, $R \equiv \left(\frac{1}{R_1} - \frac{1}{R_2}\right)^{-1}$ - Eq. 3.3

The input values used in these equations are given in the table below.

Table 3.2 Input Values for Hertzian Equation

Parameter	**Values**	**Units**
Load per unit length, P	99904.8	N/m
Elastic modulus, E_1, E_2	210000	MPa
Radius, R_1	0.0045	m
Radius, R_2	0.0047	m
Poisson's Ratio, ν_1, ν_2	0.33	

The Hertzian contact stress was calculated to be 0.362GPa which is lower compared to the stress obtained through FE analysis. This difference is attributed to the reduced contact area, occurring only on the groove edges (no contact at the center) in the FE analysis. This is caused by the bending of the vertical specimen (as shown in Fig 3.10). Additionally, the real normal force acting would be much larger than 3316.2N calculated analytically, ref section 3.4.1. In the real test, the contact patch forms at an angle to the vertical axis of the test assembly as shown in subsequent sections. This occurs because the bottom of the vertical specimen is fixed and the top end is free to move. When load gets applied to the top end of the specimen, the resultant is formed at an angle to the vertical axis of the test assembly. The contact further evolves as the test

progresses. Hence the FE and Hertzian analysis only provide a perspective and its direct application for assessment of real contact stress value for this case is limited.

3.4.1 Calculation of normal force acting on the groove.

The normal load acting on the groove was calculated as described here. The vertical specimen was considered as a cantilever beam that is radially loaded at the top with 80lbs (355N). From a mechanics point of view, this is regarded as a statically indeterminate problem and the moment-area method was used to determine the solution [42]. The free body diagram of the specimen is given in Fig 3.10 and the equations (3.4) - (3.6) were used to determine the normal load.

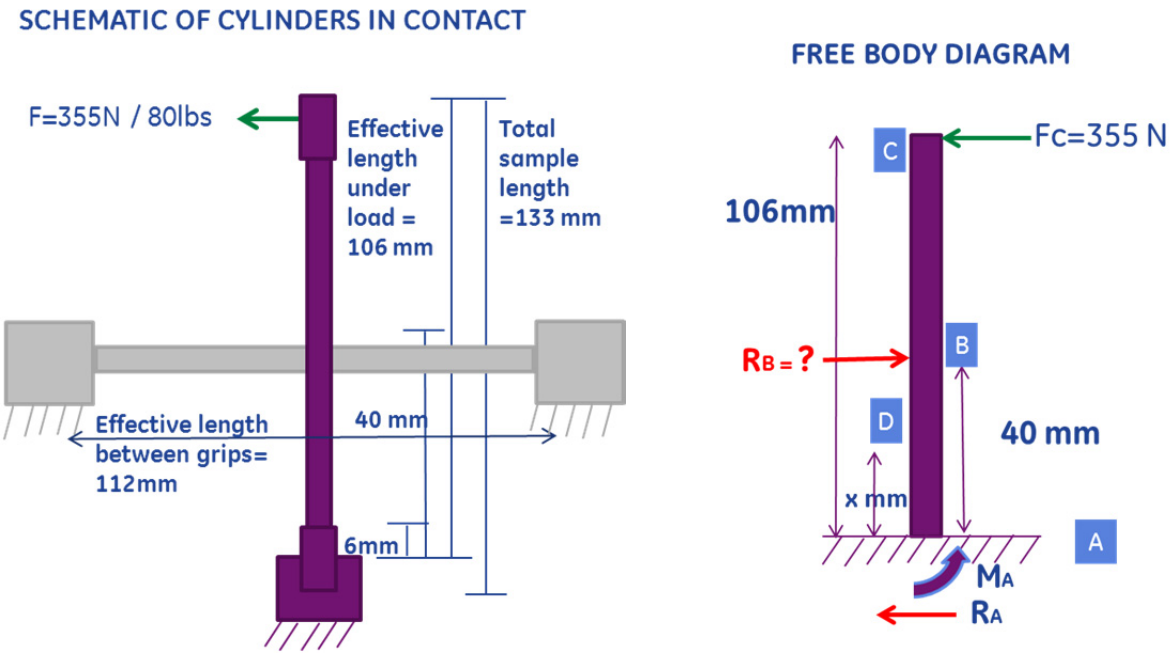

Fig 3.10 Free body diagram with specimen and loading details

Following equations can be used to solve this problem:

Summation of forces:

$$F_C - R_B + R_A = 0 \quad \text{- Eq 3.4}$$

Summation of moments at point A:

$$M_A - R_B \times 40mm + F_C \times 106mm = 0 \quad \text{-Eq 3.5}$$

Stiffness Equation using k and y as displacement:

$$\boldsymbol{R_B = -k(y)} \quad \text{-Eq 3.6}$$

Solving the above gives R_B = 3316.2 N=751.20lbs

(For a full work out of the solution, refer Appendix section)

The normal force acting at the contact was calculated to be 751.20 lbs (3316.20N).

3.5 Test Parameters

Specimens were subjected to a combination of normal load and rotational (angular) displacement. The specimens made contact on curved surfaces. The normal load, angular displacement and frequency were fixed. A radial /normal load of 80lbs (355N) at the top of the specimen and an actuation frequency of 10Hz were employed. The latter corresponds to a velocity of 1.57mm/s for a 9mm diameter specimen at +/-0.5 deg actuation. This corresponds to angular displacement amplitude of 39.2 microns. As per the Vingsbo, Soderberg classification [9] for tangential fretting given in Fig 2.2, this could be classified into Mixed Stick and Slip Regime. However such an approach without considering normal force and tangential stiffness at the contact may not be appropriate and needs to be established still for rotational fretting.

CHAPTER 4

RESULTS AND DISCUSSION

4.1 Typical Fretting Loop

Schematic of a typical fretting loop as obtained from the set-up used in this particular study is shown in Fig 4.1. The angular displacement is displayed on the X-axis, while the corresponding torque is displayed on the Y-axis.

.

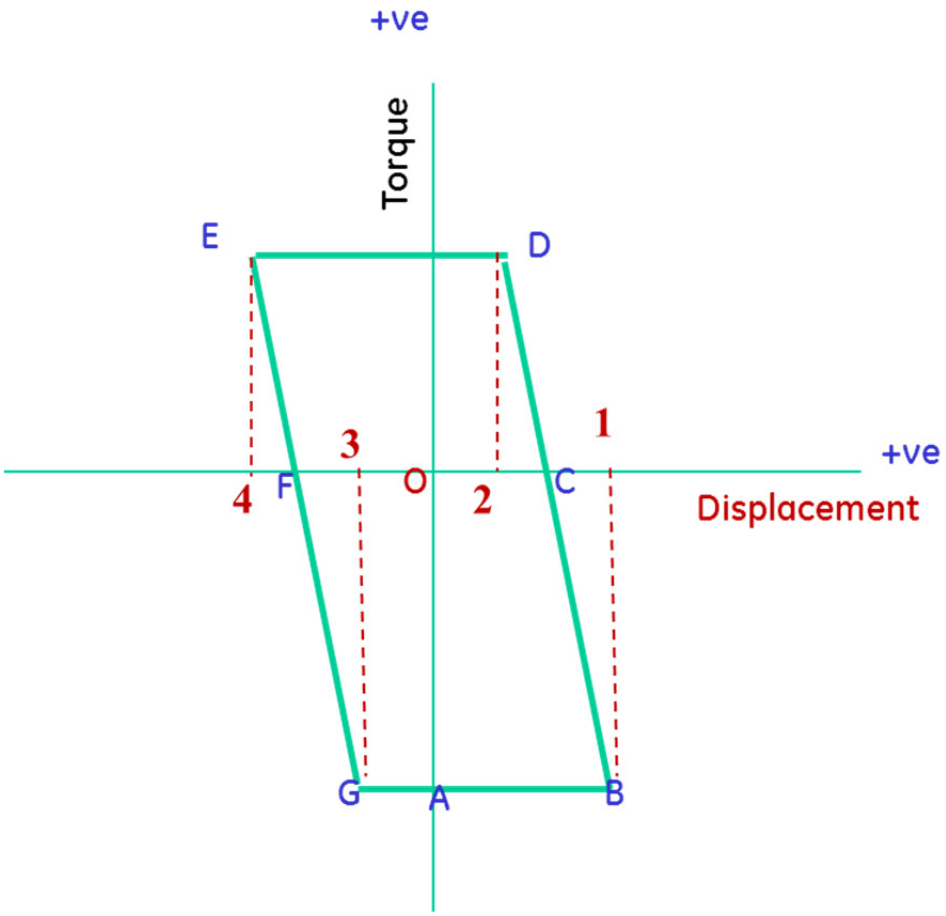

Fig 4.1 Typical Gross Slip Torque Displacement curve obtained from this test set-up

For this test the angular displacement is prescribed and the corresponding torque variation is recorded. Once the torque is applied, the loop gets traced over points shown as B-C-D-E-F-G-A-B, with corresponding displacement of the vertical specimen as 1-C-2-O-3-F-4-F-3-O-2-C-1. This completes the fretting loop and one fretting cycle.

Such a loop evolves dynamically over time. The horizontal sides of the hysteresis loop represent the constant torque and the related full sliding or slip experienced by the contact. Full slip occurs as the specimen rotationally displaces from one end of the contact to the other, with no region of the contact experiencing stick. The inclined sides represent a changing torque value and indicate the partial slip condition experienced by the contact. Partial slip occurs at the ends of the stroke, where some portion of the contact is in stick and the rest in slip. Hence during gross slip fretting regime, the specimens are subjected to an alternating sequence of full slip and partial slip. The constant slope of the inclined sides represents combined tangential stiffness of the contact, associated with formation of stick and slip regions and the stiffness of the machine [19]. Changes in the length of the horizontal sides of the loop and in the shape of the inclined portion of the loop are indicative of fretting regime transition [12].

4.2. Fretting Loop and Frictional Graphs for various test conditions

Fig 4.2 shows the torque vs. angle plot for the 10K cycle test. Fretting loop for cycle 15 is wider and shorter compared to cycle 407. Fretting loops for cycle 1065 and beyond are similar and can be grouped together since they are relatively narrower and have higher torque values compared to previous loops.

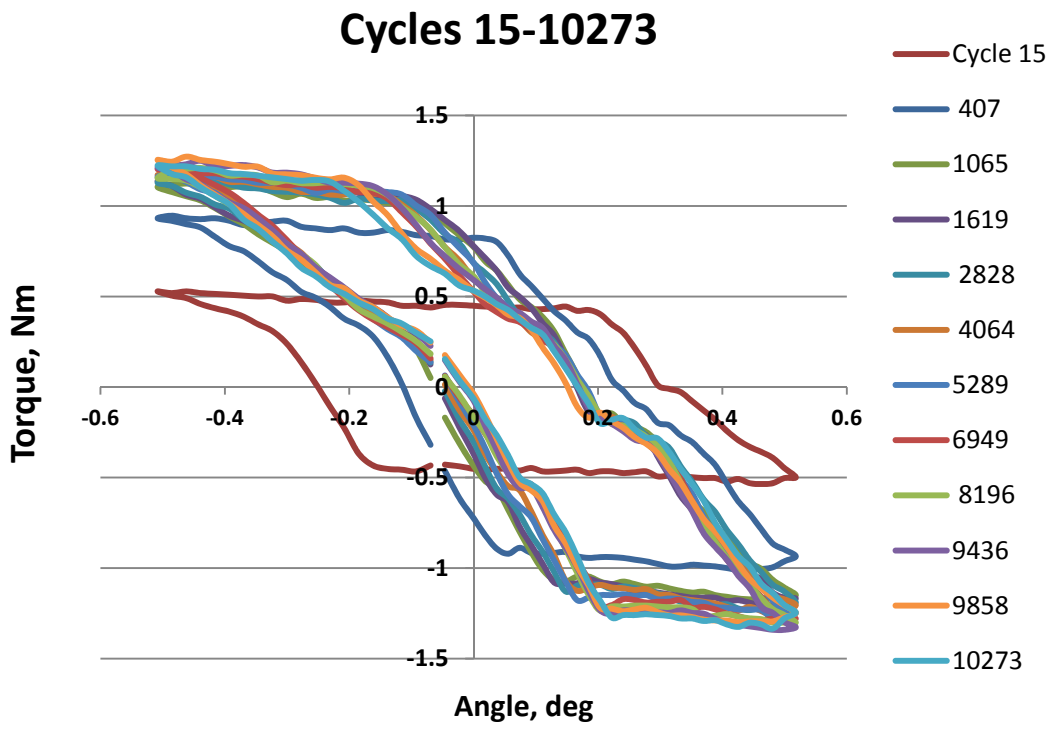

Fig 4.2 Torque -Angle plot for specimen 10K_A

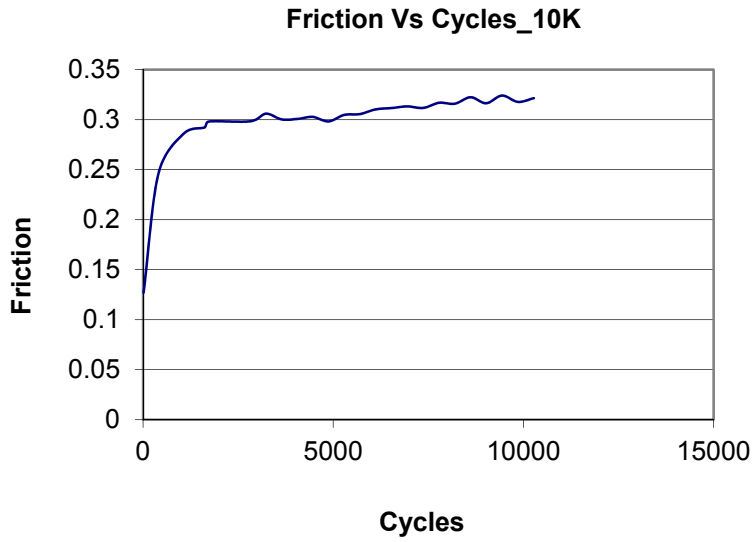

.

Fig 4.3 Friction - Cycles plot, 10K_A specimen.

A corresponding increase in friction from 0.126 to 0.321 with increase in number of cycles takes place as shown in Fig 4.3. Friction is calculated by dividing the tangential force with normal

force acting on the contact. Normal force was calculated using a mechanics based approach and found to be 899N (refer appendix section). The value of tangential force is the measured tangential torque divided by the radius of the cylindrical specimen.

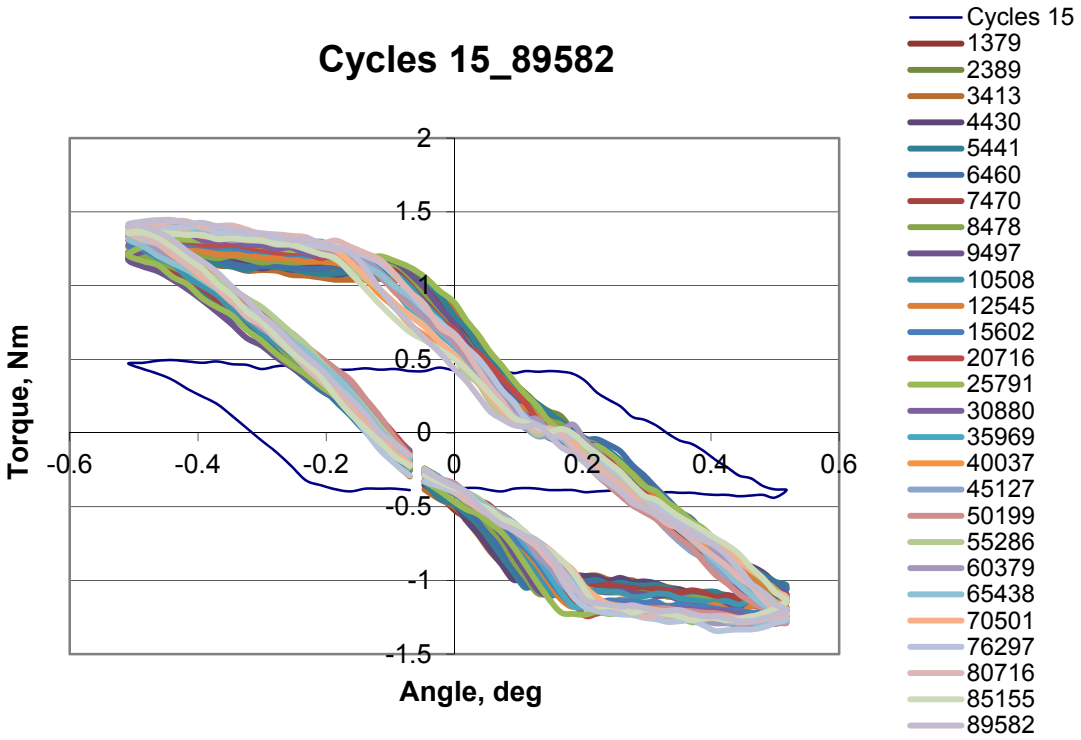

Fig 4.4 Torque -Angle plot, 89K_B specimen.

Fig 4.4 shows the Torque angle plot for the 89K_B specimen that was subjected to 89582 cycles of fretting. The discontinuity of the plot in this test near -0.05 deg was due to a glitch in the data recorder.

For the 89K_B specimen we obtain a torque vs. angle plot similar to the 10K_A specimen. The data capture rate frequency was set to one for every thousand cycles in the initial stages. The loops for the initial cycle number 15 is broad and short compared to the rest. This observation for 89K_B specimen is consistent with the 10K_A specimen. The friction evolution for 89K_ B

specimen is shown in Fig 4.5, which shows an increasing trend with number of cycles. Friction increased from 0.12 to 0.35.

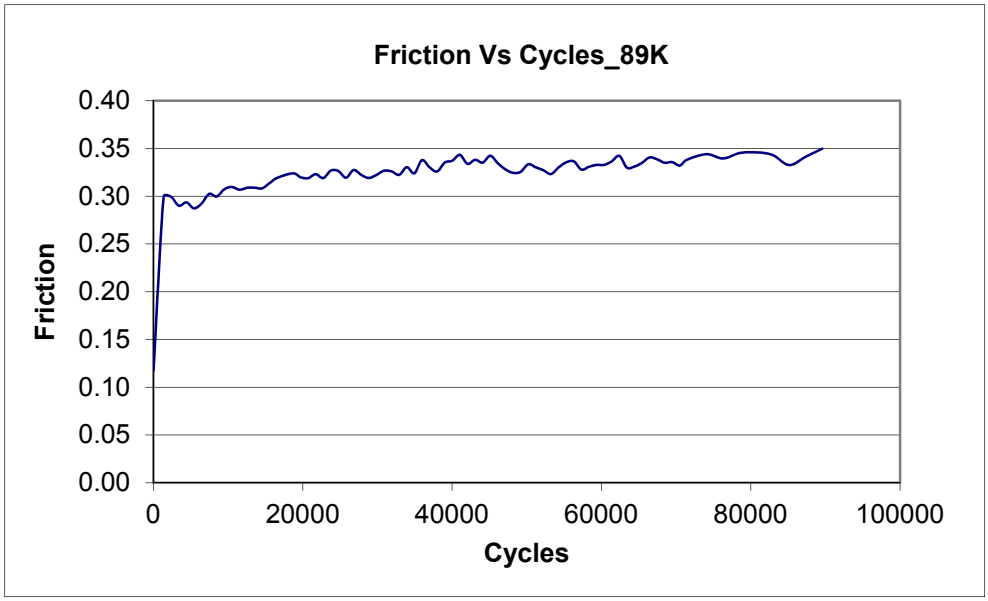

Fig 4.5 Friction-Cycles plot, 89K_B pair.

When compared against the same set of test parameters, a considerable level of consistency is observed in the data trends for the two test cases. Fig 4.6 shows similar number of fretting loops superimposed from 10K_A and 89K_B specimens.

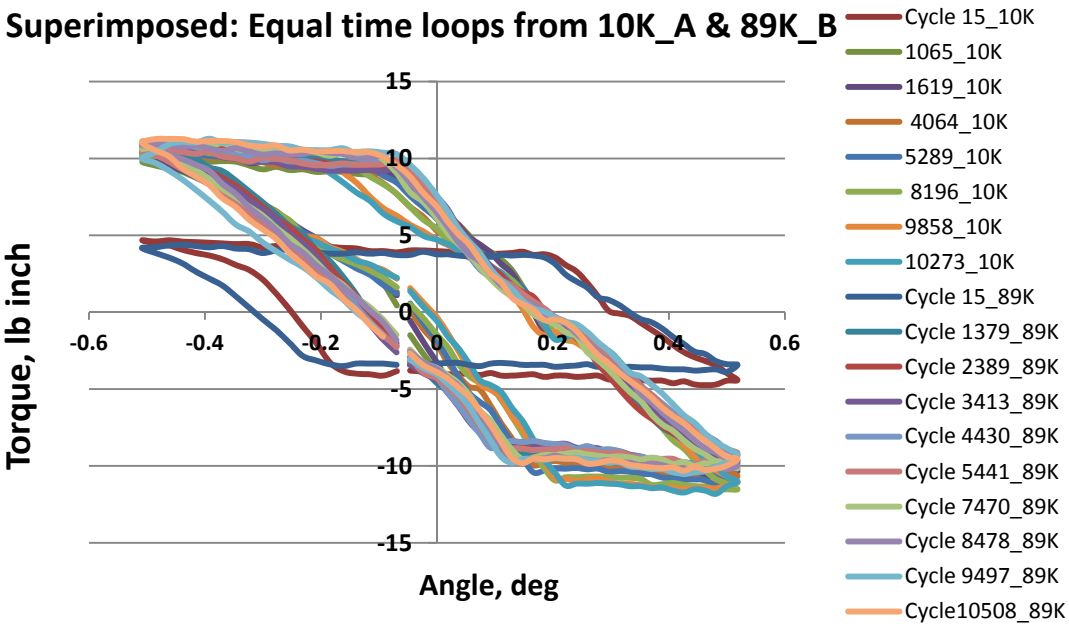

Fig 4.6 Superimposed loops, 10K & 89K.

The close conformity of torque and displacement values builds confidence on the test data, even though the loop shapes are not identical.

Another test at higher frequency of 25 Hz, Load- 80lbs and 1.16MM cycles gave a different friction trend, although the steady state friction values are not very different. The initial friction coefficient was higher which then stabilized to a lower value as shown in Fig 4.7.

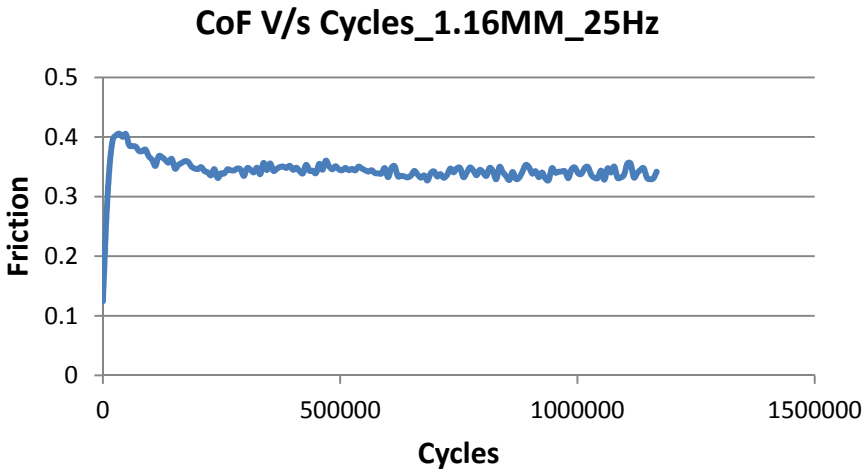

Fig 4.7 Friction- 1.16MM, 25Hz.

4.3 Nature of fretting loops

From Fig 4.2 and Fig 4.4, which correspond to 10K_A and 89K_B specimens, it is observed that the initial cycles are wider with a relatively small max. torque value which is characteristic of gross slip. With increase in number of cycles, the loops become relatively narrower with a corresponding increase in the torque value. This is consistently seen for both the 10K_A and 89K_B specimens. This can be attributed in varying degrees to three different phenomena occurring at the contact. Firstly, the partial slip contribution, depicted by the inclined flanks of the loop, increases progressively, for a given fixed energy input per cycle, until steady state. This means that the time spent and the corresponding energy dissipation at the end of each stroke during reversals increases progressively, until reaching of steady state. Secondly, wear debris piled at the ends of the stroke, also increase the frictional force experienced during the sliding portion of the loop, as reported in literature [15]. Thirdly, the increase in conformity of contact as the test progresses also leads to increase in torque. The specimens in this test initially make contact on diagonally opposite corners of the groove region where the pressure is maximum (as learnt from SEM images presented in chapter 5). Subsequently, the adjacent areas viz. the central inner regions also begin to make contact and develop relatively lower contact pressure. This results in a non-uniform pressure profile at the contact region, which can result in higher frictional force

4.4 Friction Trend

For the 10K_A and 89K_B specimens, the friction keeps increasing until it reaches a steady value. During the initial cycles, any loosely adherent surface film would be removed through the rubbing action between surfaces, followed by a metal to metal contact at the interface, which causes an increase in friction. Additionally, in the current case, the area of specimen in contact

also keeps increasing as the number of cycles increase, since the specimens become more conformal in contact. This would result in a decrease in normal pressure which coupled with an increase in interaction with surface asperities increases the tangential force thereby causing an initial rise in the friction coefficient [45]. However, formation of oxides at the interface due to rise in contact temperature after initial cycles would result in lowering of friction coefficient. Such a trend was observed only for 1.16MM_C specimens and not for 10K_A or 89K_B. On examination of 1.16MM_C specimens, a thick oxide layer was present at the interface. This provides evidence that the formation and presence of oxides at the interface influences the interface contact behavior and its effect on friction and wear rate needs to be studied more carefully. If the oxides are harder than the base material, friction and fretting damage can increase, on the other hand if the oxides are soft relative to the base material, it lowers friction and fretting damage reduces significantly [1][24][28].More details on the oxide characterization at the contact interface will be outlined in the next chapter.

4.5 Fretting Regime

The steady state loops are narrow compared to the initial fretting cycle loops. Correspondingly, there is a rise in friction with increase in number of cycles. Since the steady state loops are quasi rectangular in shape and not elliptic, this behavior is categorized as Gross Slip Fretting.

4.6 Fretting Wear

During the gross slip regime, fretting wear takes place. Table 4.1 provides details of the wear occurring in the specimens. It is clear that with increase in number of cycles, wear also increases. The ungrooved specimen showed higher wear, in case of 10K_A specimen pair whereas the grooved specimen showed higher wear in the 89K_B specimen pair. This may be partially influenced by the initial specimen geometry at contact and the development of the contact zone as a function of fretting cycles.

Table 4.1 Wear Values of 10K_A and 89K_B specimens

Specimen	Initial mass (gms)	Final mass(gms)	Mass loss (gms)
Ungrooved 10K_A	118.6788	118.6684	0.0104
Grooved, 10K_A	117.1529	117.146	0.007
Ungrooved,89K_B	118.5796	118.5249	0.0547
Grooved, 89K_B	117.1083	117.0172	0.0911

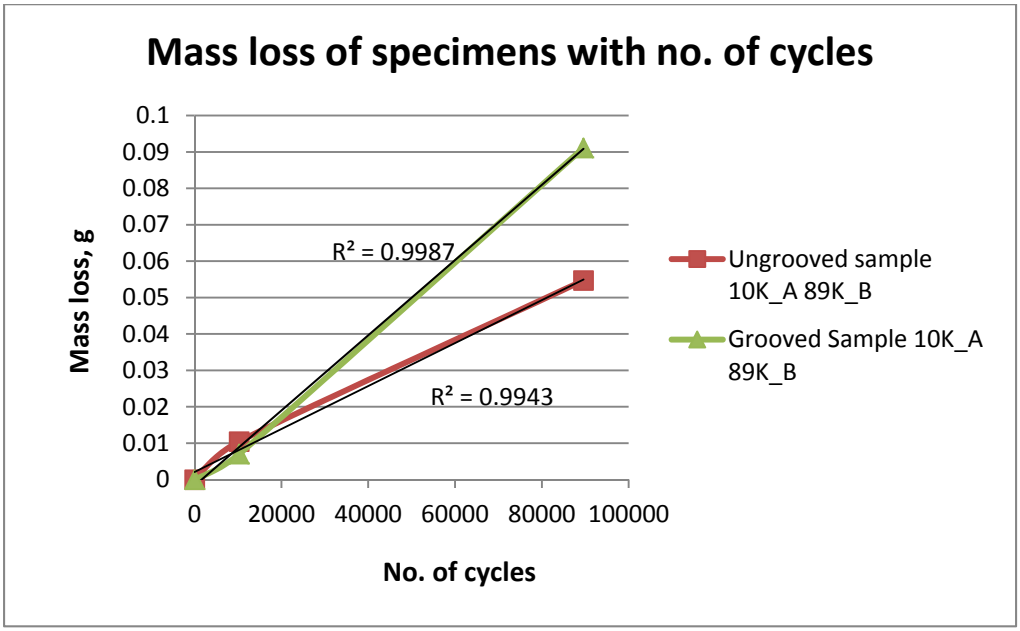

Fig 4.8 Mass loss vs. Number of fretting cycles

Fig 4.8 shows the change in mass loss of specimens with increase in number of cycles. A linear wear trend is observed. More experiments are required to confirm this trend.

CHAPTER 5

MICROSTRUCTURAL RESULTS & DISCUSSIONS

Microstructural characterization of the specimens was carried out to gain a better understanding of the material deformation response due to rotational fretting.

5.1 Macro pictures, Optical microscopy and SEM results

Fig 5.1 shows the pre-test bainitic microstructure of the 4340 specimen.

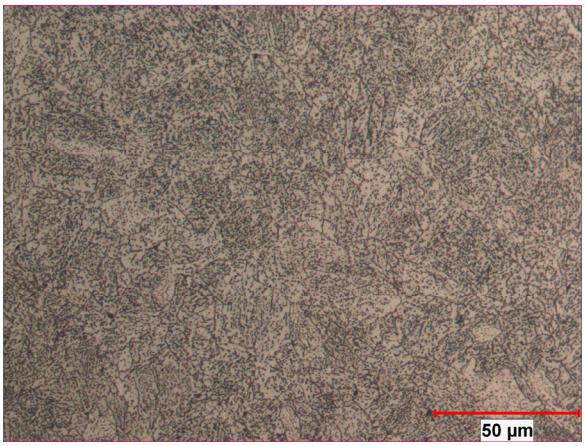

Fig 5.1 Pre-Test Bainitic microstructure, 500X

Fig 5.2 shows macro images of the fretted region of the 89K_B specimen pair. Two distinct regions, region1 and region2 are seen on the grooved horizontal specimen as well as on the ungrooved vertical specimen. This provides evidence of full contact occurring between specimens, as the test progresses. Similar observations were also found for the 10K_A specimen pair, although the extent of damage was much less and the contact patch discontinuous compared to 89K_B specimen, shown in Fig 5.3. For the 10K_A, the contact has taken place only at the diagonally opposite corners of the grooved region. The contact region is non-orthogonal to the horizontal axis of the groove. This is due to a certain extent of tilting and bending that occurs on the vertical specimen once the load is applied.

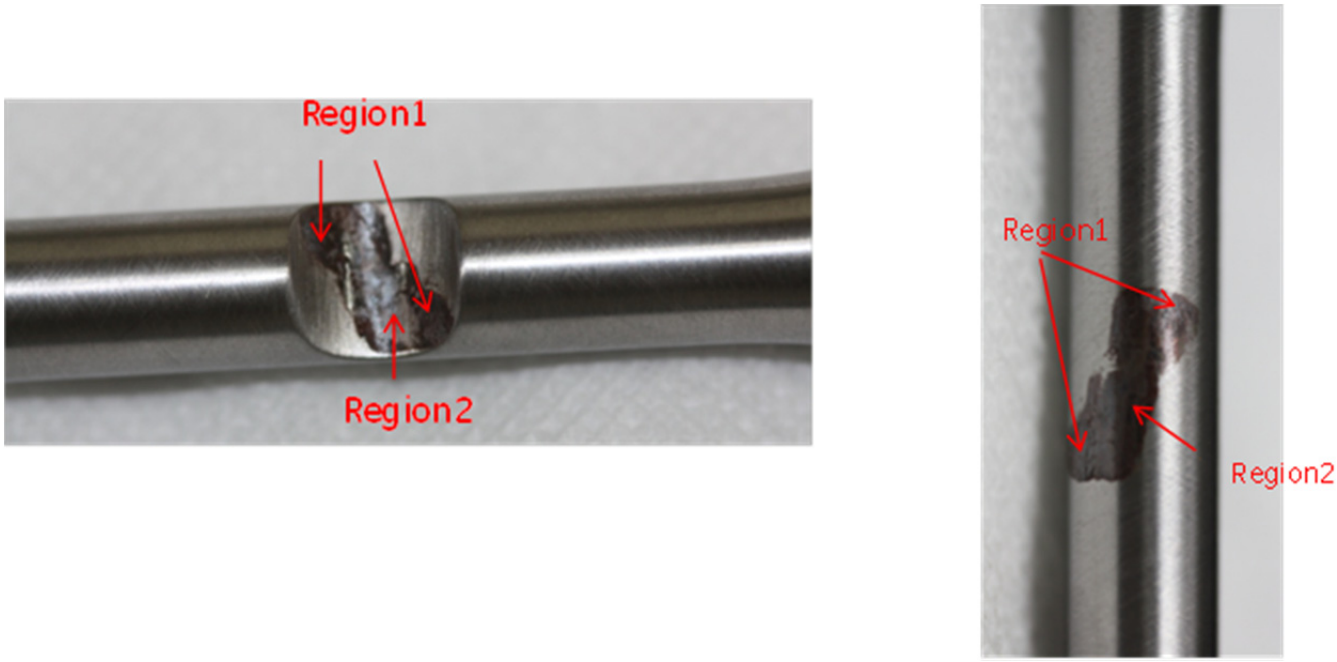

Fig 5.2 Distinct regions of fretting on the 89K_B specimen pair

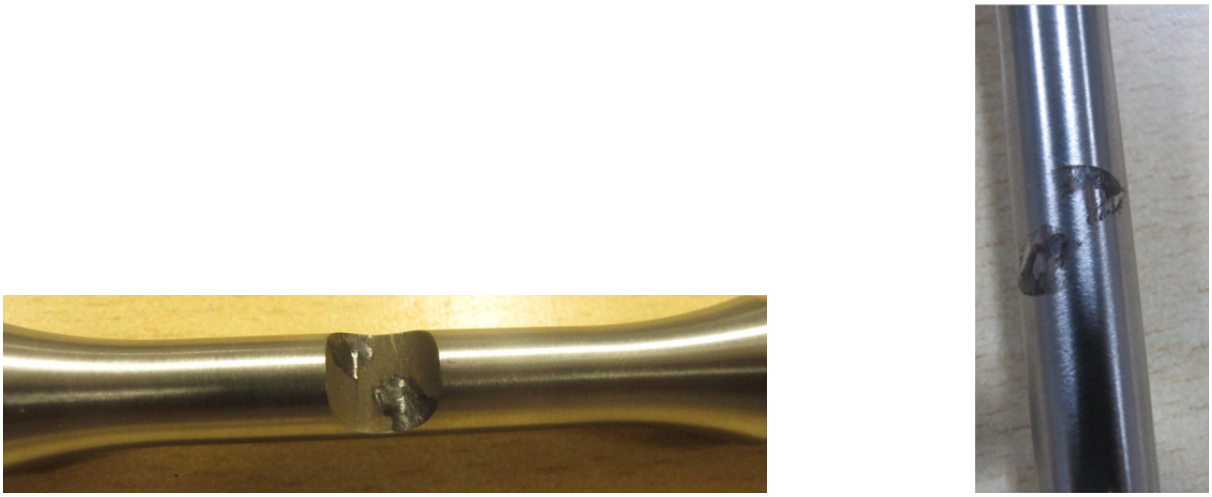

Fig 5.3 Fretted 10K_A specimen after 10K cycles of fretting

Fig 5.4a shows an SEM image of the fretted region of the grooved 10K_A specimen. Region 2 has large ripple features compared to region 1, which has a finer ripple structure. Fig 5.4b shows a schematic of the micrograph.

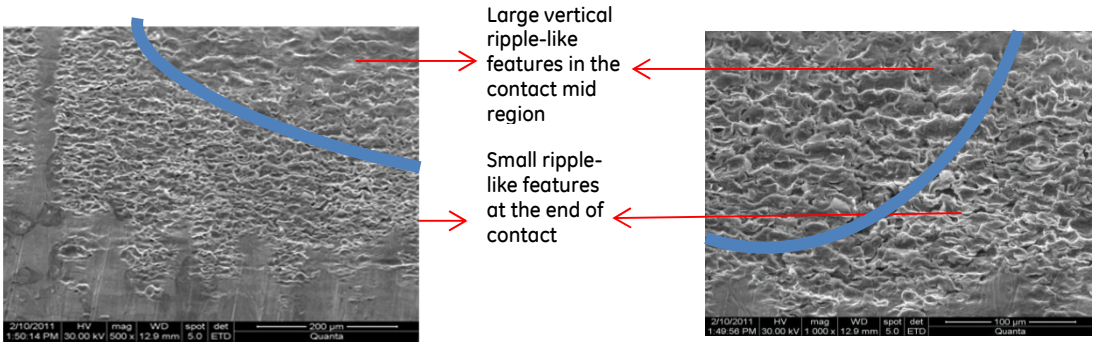

Fig 5.4a Distinct regions of 10K_A specimen

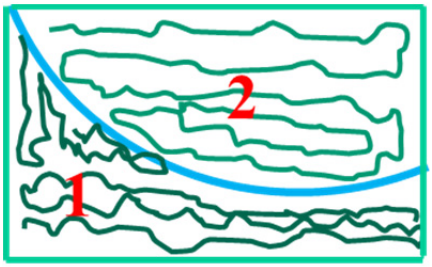

Fig 5.4b Schematic of Regions, 10K_A Specimen

Element	Weight%	Atomic%
O K	2.72	8.87
Cr K	3.48	3.49
Mn K	0.91	0.86
Fe K	91.69	85.70
Ni K	1.20	1.07
Totals	100.00	

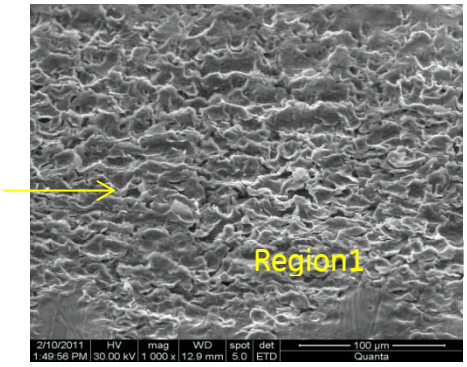

Fig 5.4c EDX of Region 1, 10K_A Specimen

Difference in surface roughness in the contact region within the fretted zone has been reported. Nicolaou et al. [38] studied partial slip condition and observed a rougher surface in the slip region, compared to the stick or non-contact areas. Pape et al. [51] observed ripples, bearing resemblance to fatigue crack striations, at the leading and trailing edge of fretting zone, within 200 fretting cycles. These regions also had smaller cracks traversing the surface.

Ripple feature on slip annulus was also reported by Yan [11] for a SS 304 vs. SS 304 combination, which belonged to regime II - fretting fatigue behavior. In their studies, they observed ripples as a well-developed thin adherent oxide film that has the property of a viscous thixotropic liquid. Ripples are hypothesized to be formed when oxidized metal particle debris flow out under continual shearing. Interestingly, ripple features are consistently observed in the slip region and not in the stick region. It points to the fact that besides normal load, some amount of movement is necessary for the ripple to form which is in agreement with the explanation provided by Yan [11].

Briscoe et al. [58] reported the formation of ripple at the fretted region, leading to wear in PMMA. They observed all debris accumulating in a single ripple. The ripple formed due to folding and consolidation of flakes created during early stages of tests.

In the present study, ripples formed on samples subjected to 10Hz fretting frequency, had a composition closer to the 4340 substrate material as shown in Fig 5.4c. Additionally, cracks were also observed on the ripple surface. The fact that ripples occur both in regions 1 and 2, which represent outer and inner / central regions of contact respectively for 10K_A, although with varying morphology, indicates that there is relative movement between the specimens throughout the contact region. The wavelength of the ripples suggests that the outer regions represented by 1 are subjected to a different combination of force and slip amplitude compared to region 2. This difference in contact conditions is possible, since the initial contact of the two specimens takes place initially in region1, which is consistent with the FE analysis shown in Fig 3.8, followed by region2.

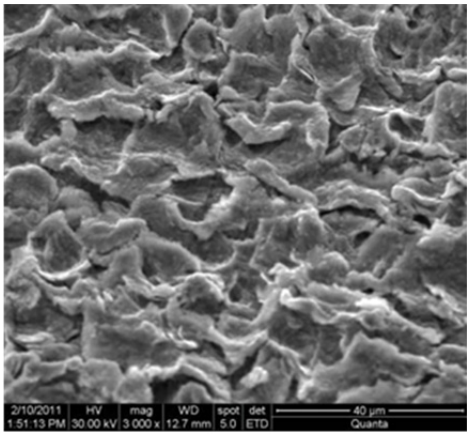

Fig 5.5 A higher mag image of the outer region 1, 10K_A specimen

Element	Weight%	Atomic%
O K	18.33	43.93
Fe K	81.67	56.07
Totals	100.00	

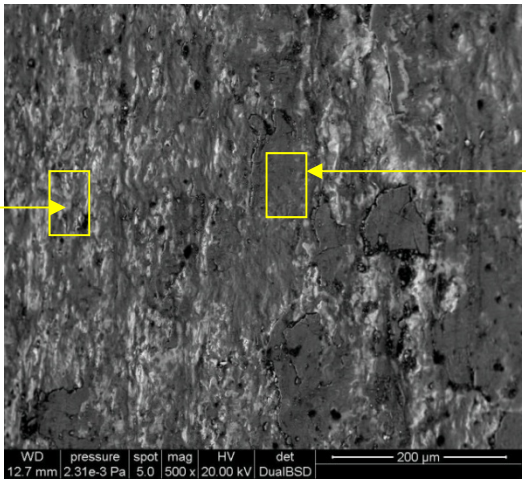

Element	Weight%	Atomic%
C K	6.57	14.96
O K	32.18	55.03
Fe K	61.26	30.01
Totals	100.00	

Fig 5.6 a Inner / Central region of the grooved, 89K_B specimen

Similar observations are made for the 89K_B specimen. The inner (central) and outer regions of the grooved specimen after 89K fretting cycles show significant difference. This is to be expected since the non-uniform pressure across these regions would also cause a different effect of slip in these two regions for the same slip amplitude, as observed with 10K_A specimen. In Fig 5.6a, the inner region of the grooved specimen shows a relatively smooth region consisting of dark patches interspersed with lighter regions. The dark layer has relatively higher concentration of oxygen, diffused from the atmosphere into the transferred layers. This is

indicative of elevated temperature in the inner region due to continuous exposure to high number of fretting cycles, although no direct temperature measurements were made. The presence of a smooth flat layer in the inner region of 89K_B grooved specimen, in place of the long wavelength ripple like feature as seen in 10K_A, could likely be the next stage in the evolution of surface fretting damage with increasing cycles.

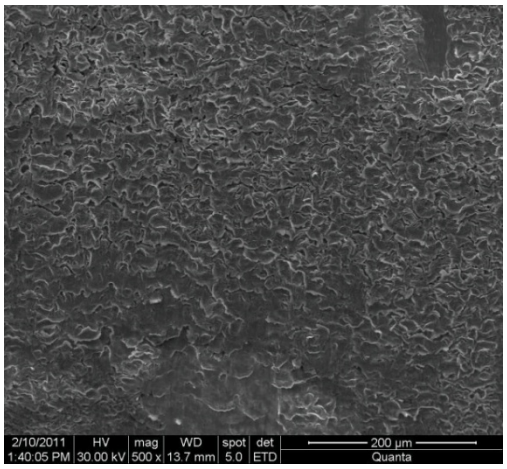

Fig 5.6 b Outer region of the grooved, 89K_B specimen

Considering the outer region of contact, region1 of the grooved 89K_B shown in Fig 5.6b, the region shows finer ripples with delamination cracks occurring at the top of most of these ripple features.

The region 2 (inner region of contact) of the ungrooved 89K_B specimen shown in Fig 5.7a also shows ripple-like features that look continuous unlike the grooved specimen. Cracks were also observed in the same region, Fig 5.7b.

Hence it is evident that the contact regions of 10K_A and 89K_B samples, subjected to 10Hz fretting frequency, showed ripples of distinct wavelengths, whose composition was closer to the base substrate 4340 material. These ripples would have formed due to the repeated cyclic shear strains experienced by the contact surfaces. The formation of ripples and the presence of cracks

indicate that the material removal is through a ductile failure mechanism at the 10Hz fretting condition.

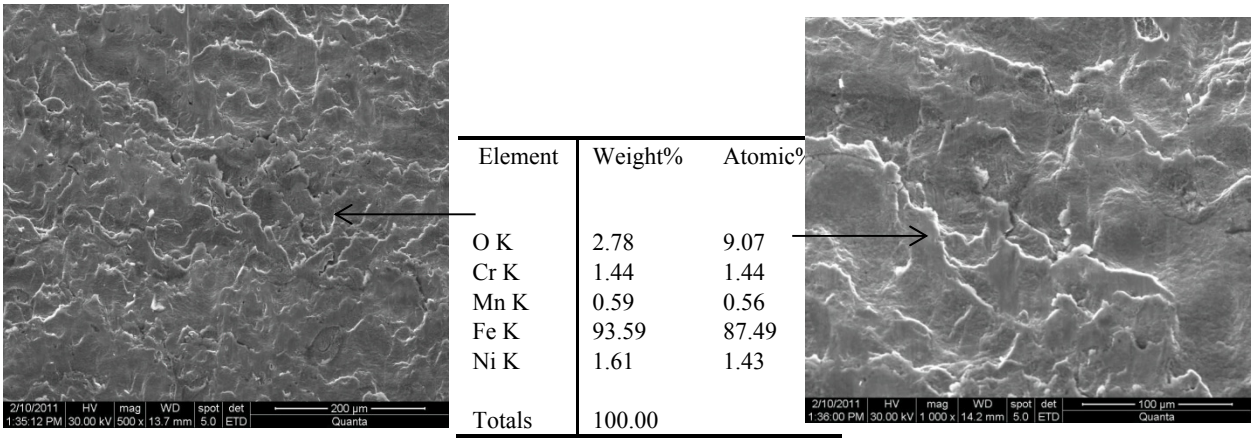

Element	Weight%	Atomic%
O K	2.78	9.07
Cr K	1.44	1.44
Mn K	0.59	0.56
Fe K	93.59	87.49
Ni K	1.61	1.43
Totals	100.00	

Fig 5.7a SEM image of inner region (region2), ungrooved 89K_B specimen

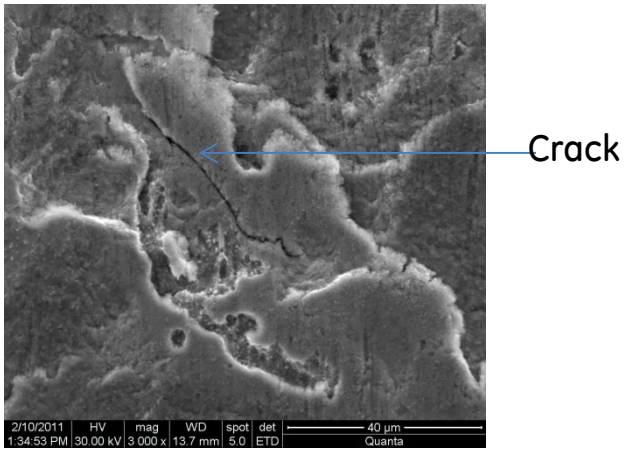

Fig 5.7b Cracks in the ripple surface (region2), ungrooved 89K_B specimen

5.2 High Frequency Test Response

1.16MM_C specimens were tested at 25 Hz. The worn regions showed a flaky appearance at the interface as shown in Fig 5.8. These flakes are oxides of the base material which indicate presence of high temperatures at the contact interface. The desired temperature measurements could not be made.

Such thick oxide flakes were absent for the 10K_A and the 89K _B specimens run at 10Hz. This can be explained on the basis of higher frequency of 25 Hz that corresponds to a higher velocity of 1.9mm/s which leads to higher interface temperatures, resulting in oxidation and buildup of flakes. Cracks in the subsurface flaky region leads to delamination wear [32].

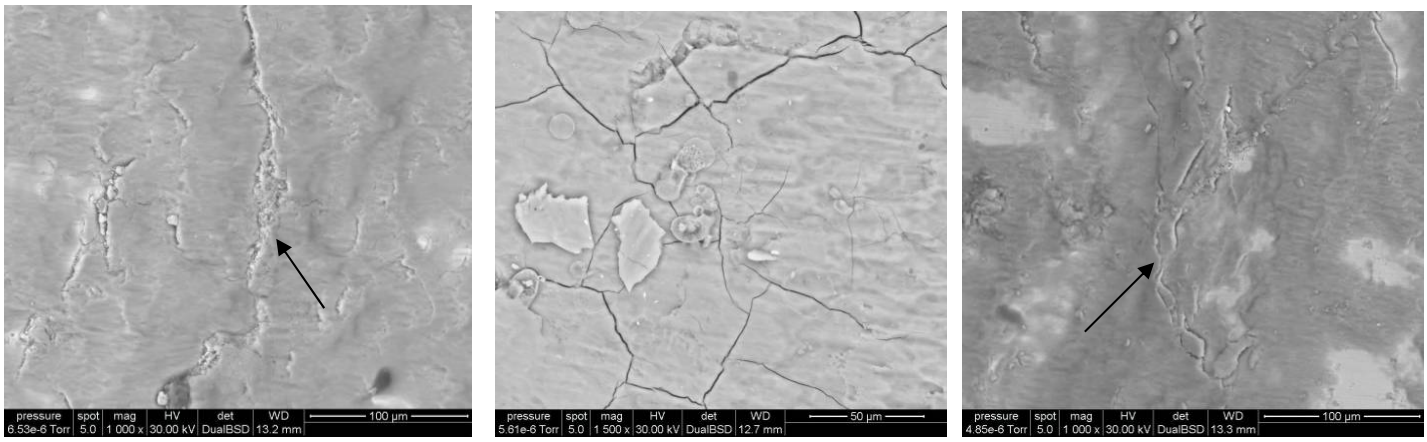

Fig 5.8 a) SEM of center and either side regions of the <u>grooved</u> specimen -25Hz, 80lbs, 1.16MM

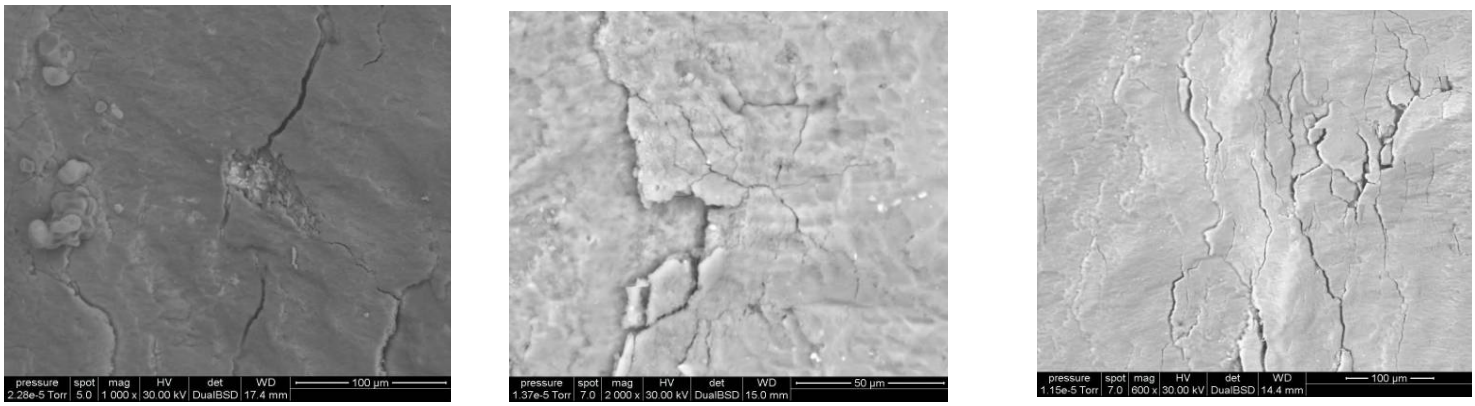

Short cracks (Center) Longitudinal s/f cracks Longitudinal s/f cracks

Fig 5.8 b) Center & both side regions of the <u>ungrooved</u> vertical specimen-25Hz, 80lbs, 1.16MM

The correlation between interface temperature and velocity was also reported by Gaul et al. [24]. Higher temperatures aid the formation of glaze oxides which lowers the friction and increases fretting life [1] [28].

Nicolaou et al. [38] reported the diffusion of oxygen into the material at higher contact interface temperatures. Additionally, the transformation to finer sized microstructure also showed increased hardness below the slip regions as compared to stick region.

5.3 Transmission electron microscopy (TEM)

The distinct regions of contact namely region1 and region2, in the 10K_A and 89K_B specimens were further analyzed by TEM, to understand the fretting damage progression in the subsurface with increase in number of fretting cycles.

5.3.1 Specimen Preparation:

In order to study the underlying dislocation structure in fretted region and to identify features that distinguish region1 and region2, TEM foils were prepared from these regions. The following procedure was adopted in order to obtain foils that were representative of region 1 and region 2.

Fig 5.9 Representation of Central Region2 and outer Regions 1 for TEM specimen

As shown in Fig. 5.9, region1 and region2 was demarcated initially through naked eye observation. Region 1 (Outer regions) also had fine striation like surface features which made it easy to distinguish it from region 2. The TEM specimen preparation steps are illustrated in Fig 5.10.A 250 microns thick specimen slice was cut from the region of interest using a Buehler slow speed CBN cutting blade. The use of a slow speed blade is important to preserve the

microstructural features and to avoid introduction of defects due to cutting. In the general procedure, either side of such a slice is polished using a disc grinder, which ensures 75 microns of material removal from either side of the slice. That would remove defects, if any that were introduced due to the cutting process as well as yield a final slice thickness of 100 microns. However in the present case, in order to preserve the fretted side of the sliced specimen, a transparent nail polish was applied to the fretted surface and the opposite side was then polished using the disc grinder on emery paper of Grit size 400, 800, 1200 until the thickness reduced to 100microns. A 3mm diameter piece was then punched out of the sliced specimen. This 3mm diameter, 100 micron thick slice was then placed in an electrolytic twin jet polisher that sprays a twin jet from either side of the specimen at the center of the specimen. A Struers Tenupol-5 twin jet electropolishing system having an electrolyte of 950ml Methanol +50 ml Perchloric Acid, was used. Once a hole was formed on the specimen, the infra-red light sensors got activated to effect an end of the polishing process. Standard operating settings of the polisher viz. current 25 - 30mA, voltage 15V and temperature at -45°C were used to produce a hole of 30-40 micron diameter at the center of the specimen. The specimens were then dipped in methanol for 15 min to get rid of the nail polish and further cleaned with acetone. The cleaning process was repeated again to ensure no traces of nail polish remain on the final specimen. The electron transparent thin region surrounding the hole was used for TEM studies. A schematic of the TEM specimen preparation steps is shown in Fig 5.10.

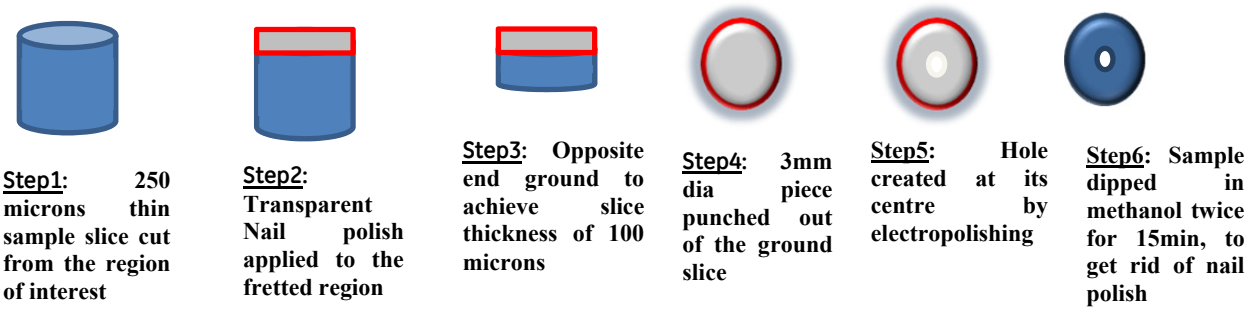

Fig 5.10 Steps for TEM specimen preparation

5.4 Baseline Specimen

Fig 5.11 shows the untested Bainitic structure with fine carbides in a ferritic matrix. Fig 5.12a shows the lamellar pearlitic structure which constitutes of ferrite (gray phase) and carbides (dark long phase). The formation of these long carbides is influenced by the prior lath martensitic structures which get converted to carbide during tempering. Fig 5.12b shows discontinuous carbides in ferritic matrix. The ferrite region from the untested specimens shows very little dislocation activity as shown in Fig 5.12b and is taken as the baseline reference against which fretting damage in exposed specimens are compared.

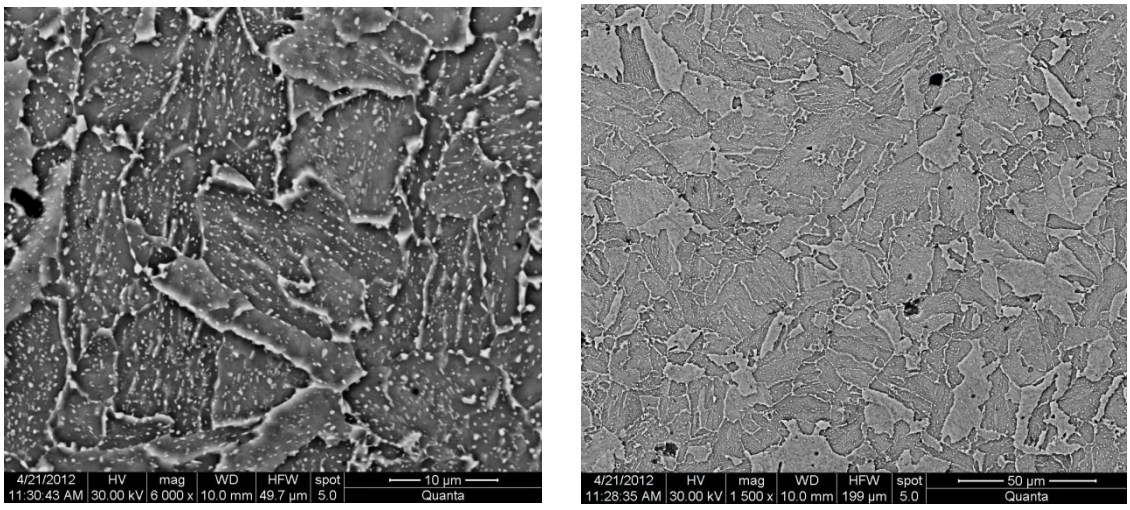

Fig 5.11 SEM image of 4340 pretest microstructure

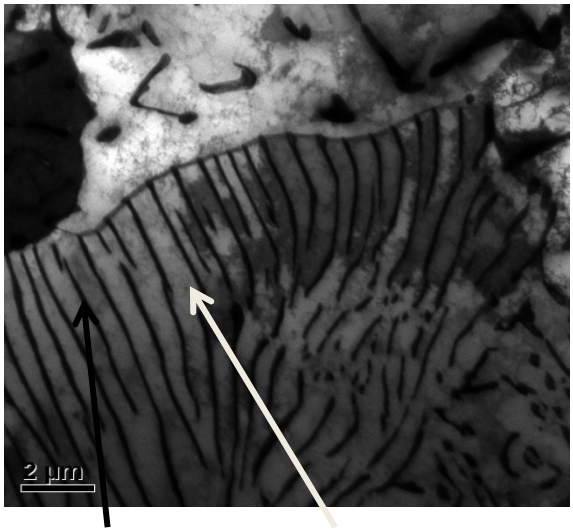

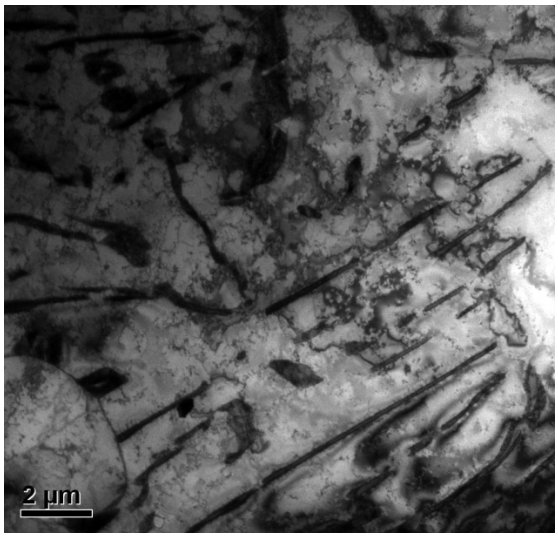

Fig 5.12a **Fig 5.12b**

TEM images of Heat treated untested specimen. a) Lamellar structure b) Discontinuous carbides

5.5 Dislocation structures in Fretted Specimens

Dislocations in fretted regions show an increased activity due to the introduction of localized plastic deformation that ultimately leads to fretting damage.

5.5.1 10K_A Specimen- Region 2

Fig 5.13 is a TEM image of the inner or central region of contact termed as region 2 of the 10K_A specimen. This specimen is marked by distinct prior austenitic grain boundaries (GB) lined with dislocations and tiny black spots which may be presence of dislocation dipoles that are formed inside the ferrite grain. Carbides (Cementite) are seen as dark spherical /elliptic/cylindrical features measuring 150-200nm in length approximately.

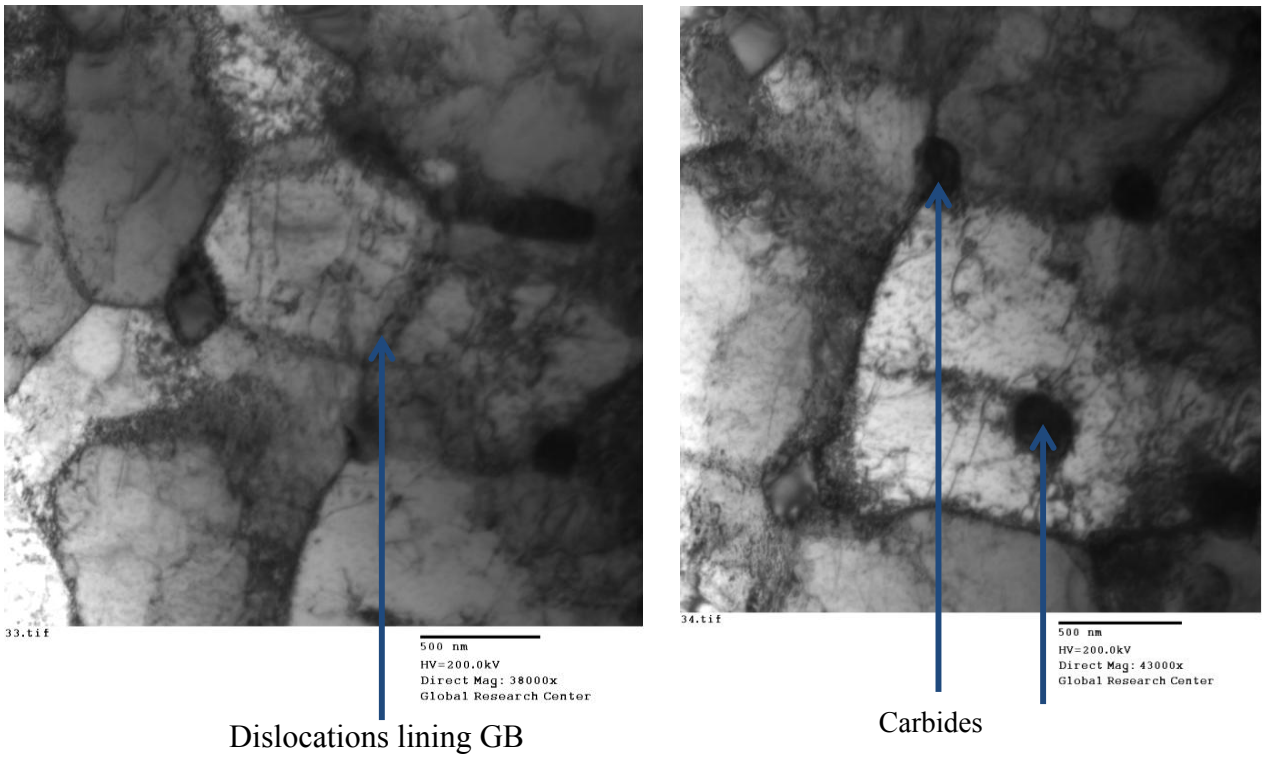

Fig 5.13 TEM image of a 10K_A Specimen _Region 2

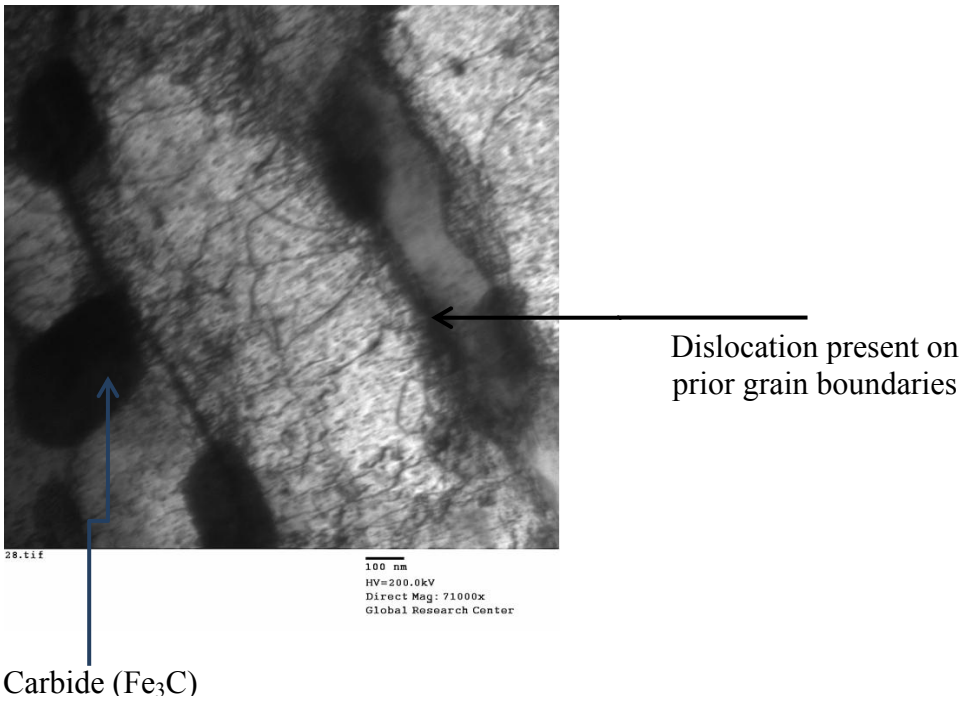

Fig 5.14 Dislocation activity within a ferritic structure, 10K_A _Region 2

Fig 5.14 shows significant dislocation activity inside the ferrite region. Overall, the dislocations are randomly distributed. In some regions the dislocations are sparse while in others clustering of dislocations is observed (see Fig 5.15).

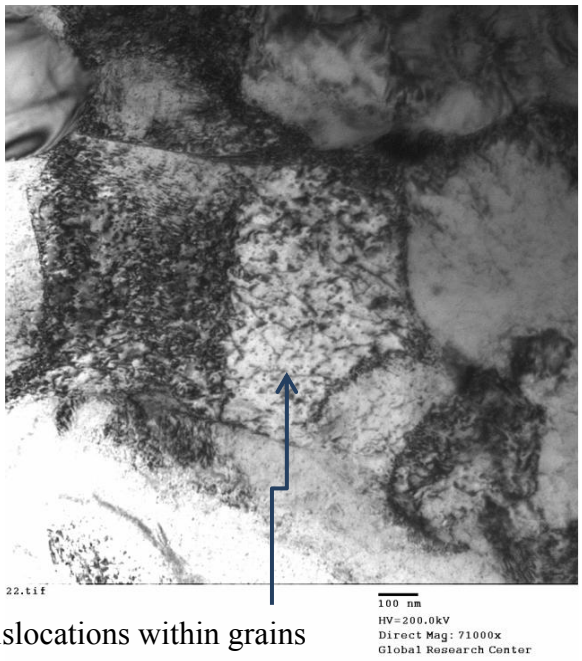

Fig 5.15 Grains with differing levels of dislocation activity, 10K_A Region 2

5.5.2 10K_A specimen. Region 1

The 10K_A outer region of contact, termed as region 1 could not be characterized for dislocation activity. This was because the region on the surface being small and irregular in shape, an attempt to obtain a representative TEM specimen was not successful.

5.5.3 89K_B specimen. Region 2

Figs 5.16, 5.17 and 5.18 show high dislocation density within ferritic regions, on grain boundaries and on carbides respectively. These microstructural features act as barriers causing dislocation pile-ups or as sources for dislocation generation.

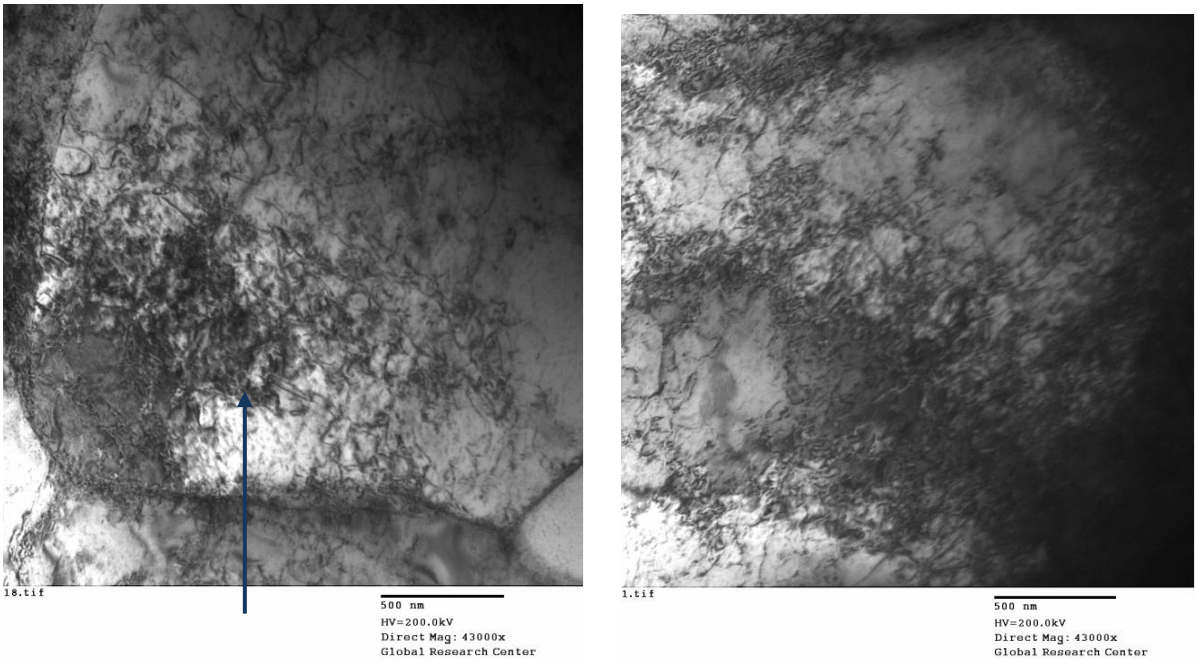

Dislocation activity inside a ferritic structure

Fig 5.16 Dislocation present within the grains, 89K_B.

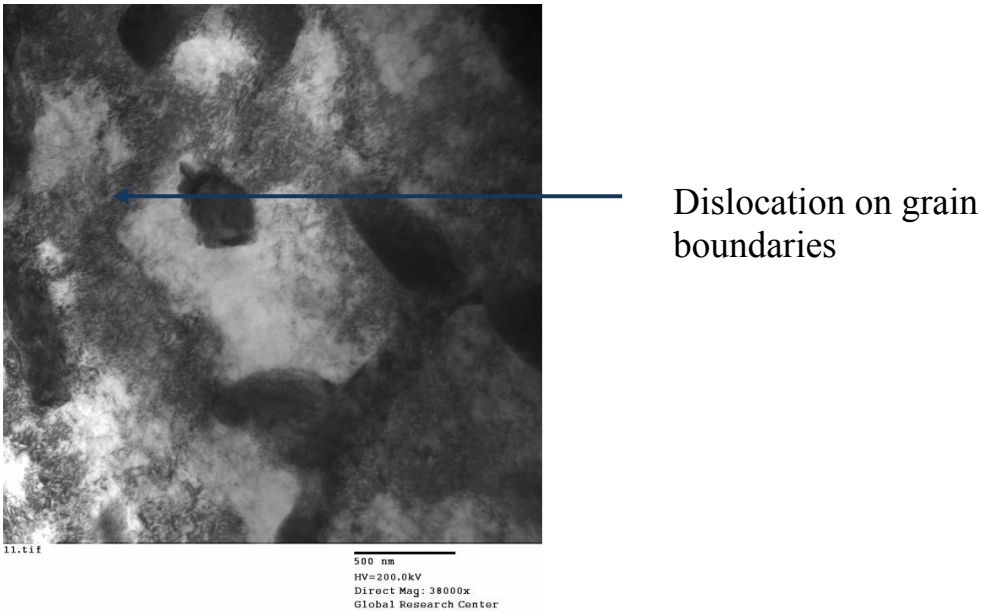

Fig 5.17 Dislocation present on the grain boundary, 89K_B

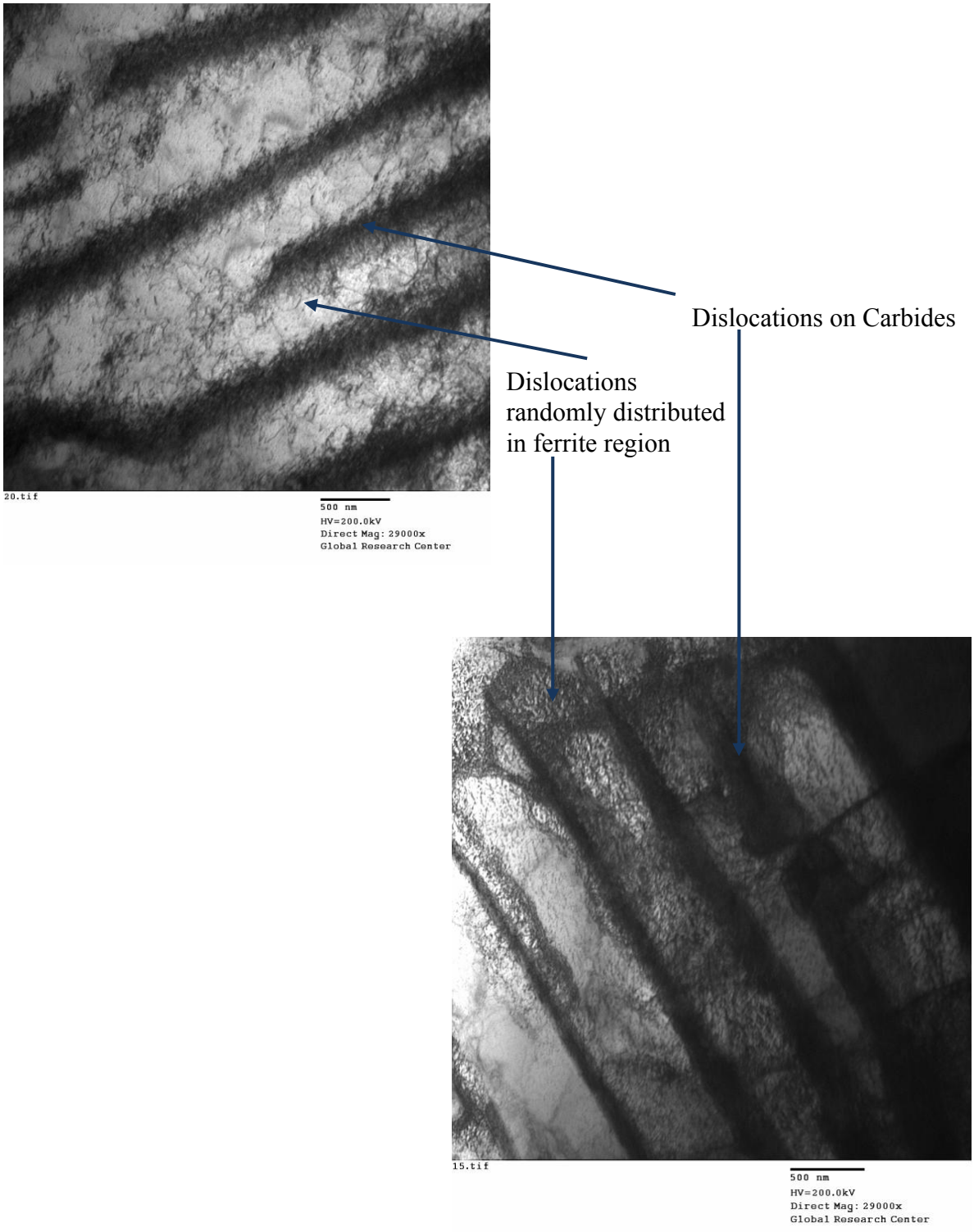

Fig 5.18 High density of dislocation on the carbide laths and high activity of dislocation inside the ferrite regions

89K_B's region 2 shows tangles of high dislocation density lining the prior grain boundaries as well as carbide structures. This shows a clear evidence of very high density of dislocations, compared to region 2 of 10K_A.

5.5.4 89K_B specimen. Region 1

Besides the random arrangement of dislocations and lining of grain boundaries and carbides, dislocations move and rearrange to form dislocation cells, within the prior grain boundaries of 89K_B's region1, as shown in Fig 5.19 to 5.21. In comparison with the micrograph results examined in this study so far, dislocation cell structures are characteristically unique of region1 of 89K_B specimen. In some locations of region1, dislocation cells are in the early stages of formation while in other locations, fully formed cells are found. The cell walls can be regarded as a cluster of dense tangled structures as seen in Fig 5.19.

The dislocation cell diameter, d or maximum internal distance of the cell in case of non-circular cells is approximately within 250-500nm. Fig 5.21 also shows various other regions which have formed similar dislocation cells.

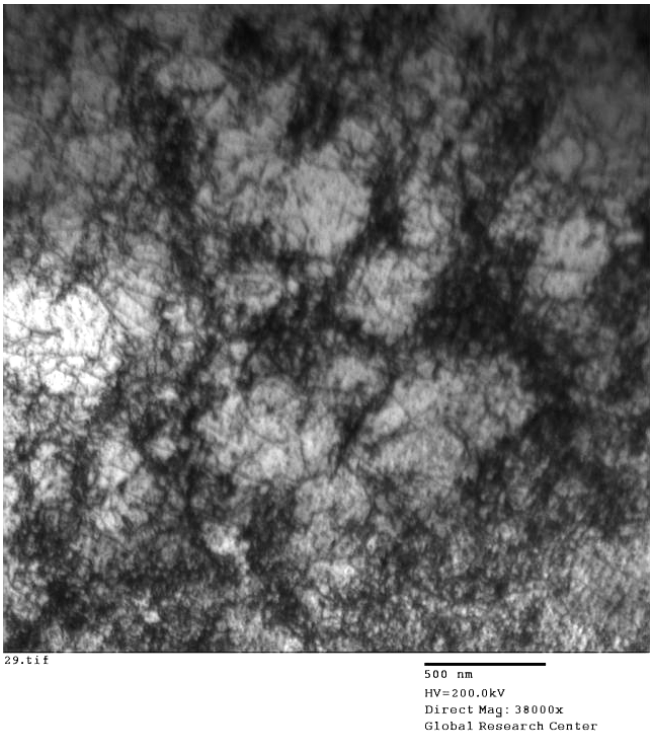

Fig 5.19 Cluster of dislocation cells.

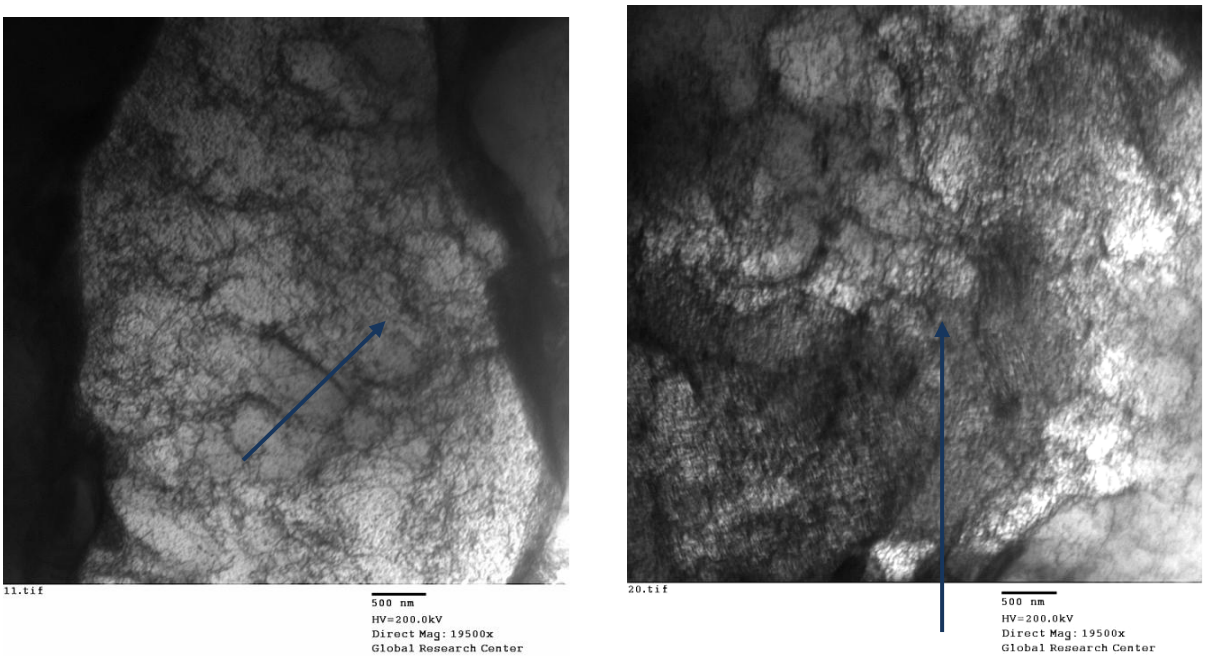

High density dislocations forming cells

Fig 5.20 Dislocations rearrange to form cells and dislocations present within cells

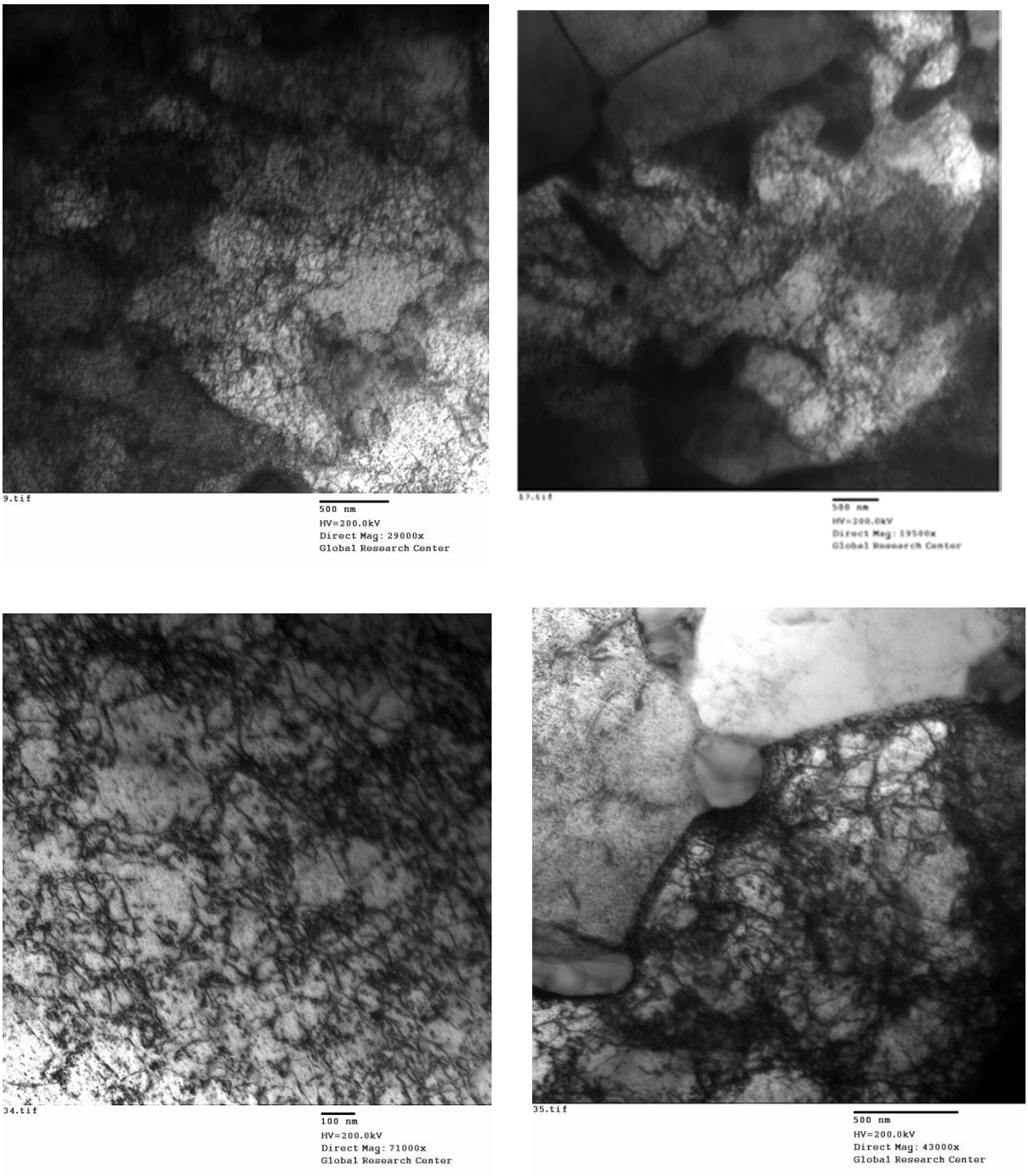

Fig 5.21 Regions with dislocation cells

5.6 Relationship of fretting characteristics to dislocation structures

Various techniques to understand fretting characteristics and to characterize fretting related surface and subsurface damage characteristics are reported in literature. For example microscopy techniques like SEM, TEM, OIM were used for assessment and quantification of fretting damage in the near surface layers.

However there aren't any detailed studies on dislocation and dislocation interactions to explain fretting damage. Such studies would be useful to validate or explain the mechanisms of fretting damage. It is clear from the preceding sections that the nature of dislocation arrangements may have strong correlations to subsurface deformation behavior in the fretting contact regions. The following sections discuss the nature of dislocation and dislocation related structures in the fretted regions, their interaction with test parameters and test environment and its ultimate effect on fretting behavior.

5.6.1 Distinction between Region 1 and Region 2

89K_B specimen had very high density of dislocations present both in regions 1 and 2 compared to 10K_A. The considerably high level of dislocation activity for 89K_B specimen can be explained by the exposure to a higher number of fretting cycle. However the distinct evidence of dislocation cell formation was unique to region1 and absent in region2 of 89K_B. These cell structures have most likely formed under the influence of higher pressure and strains caused as a result of non-uniform contact of specimens - inherent to the loading and specimen geometry at the contact interface. Under the combined influence of high pressure and strain, dislocation tangles align themselves into arrays of parallel dislocations that form cell boundaries. Such cellular structures have also been reported in literature for materials subjected to high strains

during compression [33], uniaxial tensile [43] as well as in contact sliding wear conditions in near surface layers of materials subjected to heavy plastic deformation[44][41].

Incidentally, Fig 2.15 a) obtained from a depth of 15 microns from the surface observed by Garbar et al. [46] is very similar to images from the current study shown in Fig 5.19 and Fig 5.21 from region 1, which pertains to a depth of 100 microns from the fretted surface. Besides, in both cases, dislocations are present within dislocation cells indicating a non-equilibrium dislocation cell structure formation. This non-equilibrium state is governed by balance of rates of input of external strain energy into the system and its reduction through clustering of dislocations into a cell pattern [46]. The occurrence of dislocation cells exclusively in region 1 also renders it prone to cracking and void formation which would ultimately lead to higher wear rates as compared to region 2.

The formation of dislocation cells under high strain and its role in wear particle formation and removal is affirmed through literature studies. A similar comparison of regions could not be made for 10K_A specimen due to unavailability of TEM specimen for region 1.

5.6.2 Effect of increase in fretting cycles

A comparison between 10K_A and 89K_B specimen pair clearly reveals that with increase in number of fretting cycles, the dislocation activity increases. Higher energy input to the fretted region results in greater dissipation of energy from higher strain accumulation and higher damage. With increase in number of cycles, the different contact regions of the specimen would also likely be more clearly distinguished by their characteristic features.

5.6.3 Hardening Effect

Since the fretted regions were curved and the depth of damage is typically localized to a few microns below surface, conventional techniques cannot be used for hardness measurement. Cross

section specimens of curved regions would be required to determine the hardness profile and estimate the depth of damage. It is well known in literature that the presence of high density of dislocations causes extensive interaction between dislocations, which increases the hardness of the subsurface. The hardening occurs due to interaction of the dislocation stress field, formation of sessile locks and dislocation jogs [36] [37]. Hardening of fretted subsurface layers is reported by Nicolaou [38] for Ti-6Al-4V and Pape et al. [51] for PH13-8Mo. Work hardening has also been reported by Cuddy et al. [43] in substructures consisting of dislocation cells when subjected to increasing strain in uniaxial tension [43]. Comparing the images of regions 1&2, region 1 has higher dislocation density and tangle networks compared to region2. This would suggest a relatively higher hardness for region1 compared to region2 and can provide an explanation for hardening phenomenon occurring in fretted regions [38]. Since no increase in hardness was observed for hardened 4340 steel HRC subjected to fretting [49] a nano-hardness measurement of these two regions is required to confirm the hardening behavior of this low hardness 4340 steel specimens used in this study.

With the techniques employed in the study, no direct evidence of fretting induced martensitic transformation was observed in the 4340 specimen contact region. Occurrence of plastic deformation leading to wear at the contact clearly indicated that the contact stress experienced by the material was much higher than 67% of YS of austenite, exceeding the stress limit for martensitic transformation in 4340 steel [55]. Hence it is very unlikely that fretting induced martensitic transformation would have occurred at the contact regions.

Similarly, no direct evidence of dynamic recrystallization was observed. Literature suggests that dynamic recrystallization in 4340 steel would occur during hot deformation (900-1200°C) [56]. Additionally, dynamic recrystallization occurs in progressive stages of a) Multiplication of

dislocations dispersed randomly b) Arrangement of dislocations in the form of elongated dislocation cells c) Generation of sub-grains d) Breakdown of sub-grains into equi-axed submicron size grains and grain rotation [57]. In this fretting study, it is very unlikely that the contact temperatures would rise to 900°C at 10Hz test condition. Even though there was evidence of dislocations arranging into cells, the further stages of subgrain formation evolving into equi-axed submicron size grains was not observed. This makes the occurrence of dynamic recrystallization very unlikely under these fretting conditions.

5.6.4 Temperature Effect

Friction induced temperature rise can have a significant effect on the fretting behavior. As shown in Fig 5.6b, this can lead to formation of oxides at the contact interface which can influence fretting behavior. Exposures to high temperatures in a no load condition can have a different effect on deformed microstructures. Fig 5.22 shows the microstructure of deformed and annealed 3.5% Si Iron.

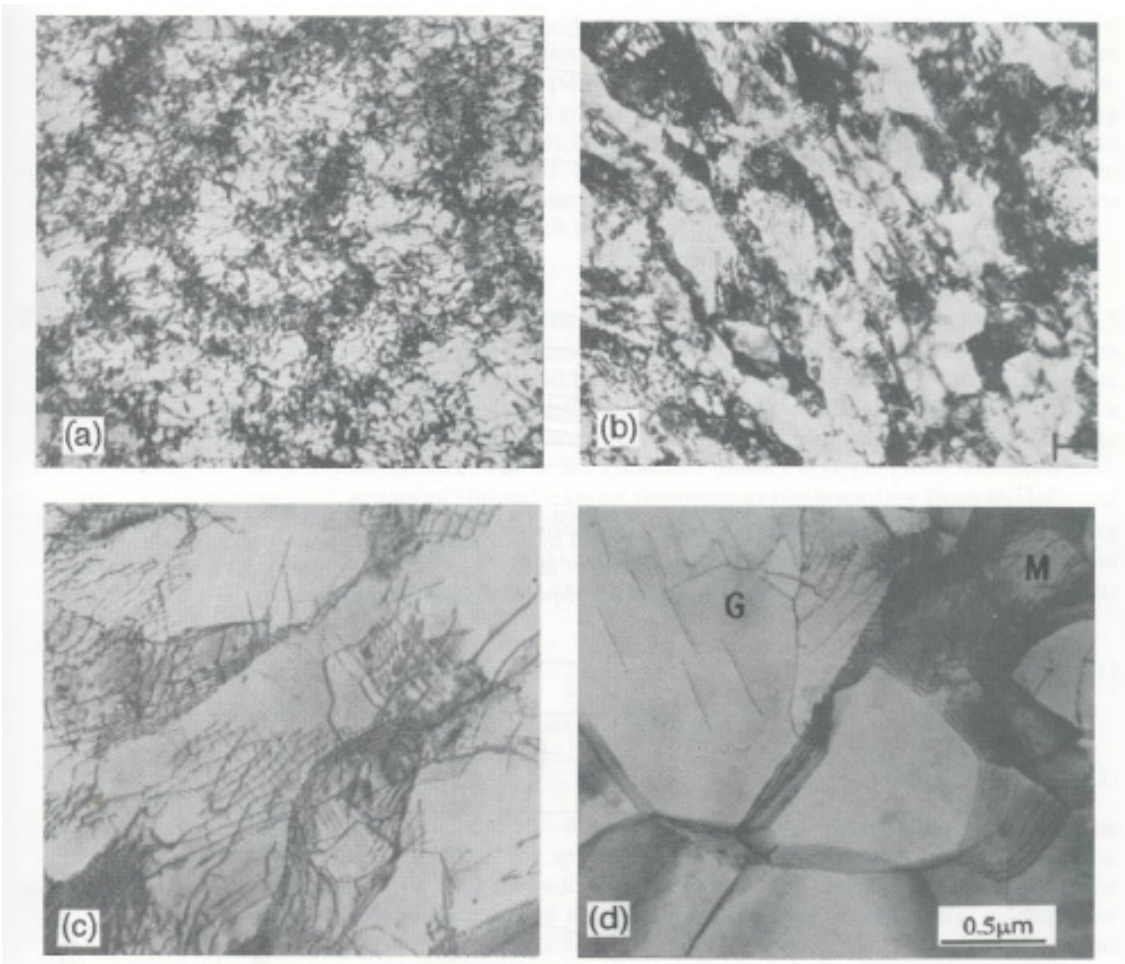

Figure 9.2 Transmission electron micrographs illustrating the structure of deformed and annealed 3.25 per cent silicon iron. (a) Approximately uniform distribution of dislocations in a crystal rolled 20 per cent. (b) Formation of small sub-grains in rolled material annealed 15 min at 500 °C. (c) As for (b) annealed 15 min at 600 °C. (d) As for (b) annealed 30 min at 600 °C. (From Hu, *Trans. Met. Soc. AIME* **230**, 572, 1964.)

Fig 5.22 TEM images of Fe-3.5Si [37] ***By Permissions of Elsevier Ltd., 2001***

Fig 5.22 a) shows the microstructure of a 20% rolling in Si Fe material which represents a heavily deformed structure with a uniform distribution of tangled dislocations and is similar to the microstructure reported in Fig 5.18. At 500°C, the cell structure of the deformed and annealed 3.5% Si Iron progressively changes and goes into recrystallized state forming smaller sub-grains as shown in Fig 5.22 b). These sub-grains further grow progressively into larger grains (grain growth) causing a reduction in energy due to lesser grain boundary area. This leads

to reduction in overall defect densities. In a similar manner, fretted areas which exhibit high dislocation activity can be potentially exposed to high temperatures for material recovery.

5.6.5 Damage assessment

One of the methods to accurately quantify damage of fretted region is dislocation density measurement. An easy indirect approach to quantify dislocation density is through dislocation cell structure dimensions. In general, the dislocation cell diameter of the equilibrium state, d is inversely proportional to the square root of dislocation density, ρ. This is given by $d \alpha \rho^{-1/2}$ [40]. The proportionality constant, K is approximately equal to 1. By this approach using d=0.25microns, the calculated average dislocation density from Fig 5.19, would be approximately 1.6 x 10^13 /m^2. However this value is much lower than what can be observed from Fig 5.19. Since the dislocation cell microstructure is not in equilibrium condition, with dislocations present within the cell, this easy to use approach is not valid for the current case. Hence an easy and accurate method to measure dislocation density especially in non-equilibrium states is much required to quantify damage. The evidence of dislocation density increase for rotational fretting reported in this work may also be applicable to other forms of fretting.

However, from Fig 2.14, the size of the cell can be used to quantify the strain level. This translates to strain of ~40% for d = 0.25microns and lies in the flat region of the curve, which indicates a regime of constant cell size and occurrence of material wear. Although this is an easy method to measure strain damage evolution, more studies are needed to prove the invariance of dislocation cell size to strain as a function of heat treatment to establish this method.

CHAPTER 6

CONCLUSIONS AND SUGGESTIONS FOR FUTURE WORK

Rotational fretting is a key damage mode for industrial applications such as cable ropes under tension for support in construction industry and Variable Stator Vanes (VSVs) in compressors of turbines. In such cases, the damage leads to dimensional variations which lead to significant loss of performance and even reliability issues. In spite of this, not much work has been reported in literature to understand this damage mode in detail. The current study attempted to fill this gap by studying rotational fretting in 4340 steel which is an important engineering material. The study focused on understanding the underlying subsurface damage and its relation to fretting damage.

To achieve this, a unique, custom built rotational fretting machine was used which is capable of operating under various test loads, frequencies, displacement amplitudes and temperatures to simulate field conditions. Fretted regions were characterized initially using SEM and TEM. This is one of the few TEM based studies employed to understand fretted substructures and fretting damage.

SEM revealed the presence of two distinct regions within the fretted zone – the outer and inner region of the fretting scar. The presence of two distinct regions, non-characteristic of any gross slip conditions were formed due to uneven contact of surfaces under load and displacement for the given geometry. TEM studies further revealed the distinct microstructures present in these two regions. The outer region of fretting scar showed early stages of formation of dislocation cell structures, consisting of dense network of tangles while the inner region of the fretting scar,

showed dislocation pile-ups at former grain boundaries and microstructural features like carbides.

As noted from literature, these features could lead to different wear behavior. The cell structures are more likely to undergo wear compared to substructures consisting of tangled pile-ups of dislocations. The cell walls formed potential sites for generation of voids and crack formation. It was from such a point of view that subsurface regions of fretted areas were analyzed. A close match between dislocation cell structures from a depth of 100micron from the fretted surface and from a depth of 15microns from the surface subjected to sliding wear, as noted in literature, presents evidence that similarities in wear mechanisms between sliding and fretting wear may exist. Hence the evidence of dislocation cell formation and its presence as an indicative tool to distinguish regions that contribute to wear in gross slip fretting is brought forth in this study. A further systematic study in this direction is required to clearly explain the mechanism of fretting wear. This could also lead to prediction of wear rates and wear life.

Another useful learning is the potential of assessing strain values on the basis of fretted subsurface dislocation structure. The fact that predominantly two different microstructures were generated in the contact region in a single test, due to differences in applied stress values and cumulative strains, is consistent with the idea of a threshold strain value for dislocation cell formation. The decrease in cell size relates to increase in strain until a minimum cell size characteristic of the material is reached, beyond which material undergoes severe wear. More systematic studies need to be carried out to identify the threshold strain level for dislocation cell formation in fretting for a given material. In summary, the appearance of dislocation cell structure and the size of dislocation cells can be used to distinguish regions that experience wear, assess severity of wear and quantify local stress and strain levels at the subsurface regions. This

can lead to design inputs on load and material selection for components operating in the gross slip fretting conditions.

Dislocation cells, density and size of the cells can also serve as useful microstructural parameters to validate fretting map conditions (MRFM) that predict wear in gross slip condition. Such an approach can lead to material specific fretting wear maps and thereby corroborate or complement existing RCFM and MRFM maps.

Suggestions towards test methodology includes application of normal load directly at the point of contact between specimens to eliminate bending and non-uniform contact of specimens associated with the current configuration and enable better control of experiments in fretting regime of interest. Active temperature measurement and wear debris analysis can provide valuable information on contact temperature experienced by the material which can be useful in investigating material damage recovery, if any, as well as nature of stress existing at the interface. A post-test cross section hardness profile would provide valuable information on depth of fretting damage and identification of subsurface microstructure that leads to hardening and better wear resistance. Future tests should also involve assessment of effect of heat treatments on subsurface fretting damage of AISI 4340 relevant to engineering applications.

Finally, this preliminary study also provides useful pointers to avoid or delay fretting wear damage in applications. For instance it appears that methods to delay cell formation, accommodation of smaller cell sizes, localized annealing of fretted zones are potentially useful microstructure related approaches that can be explored for solutions. This can help maintain right geometrical tolerances and enable better performance and life in industrial components undergoing fretting.

APPENDIX

A) Calculation of normal force at the contact region of two cylindrical specimens

The force diagram of the system is given in Fig 6.1. The applied force of 80lbs (355N) is applied radially on the top of the specimen. At 40mm from the fixed bottom end, the normal force acting at the point of contact needs to be calculated.

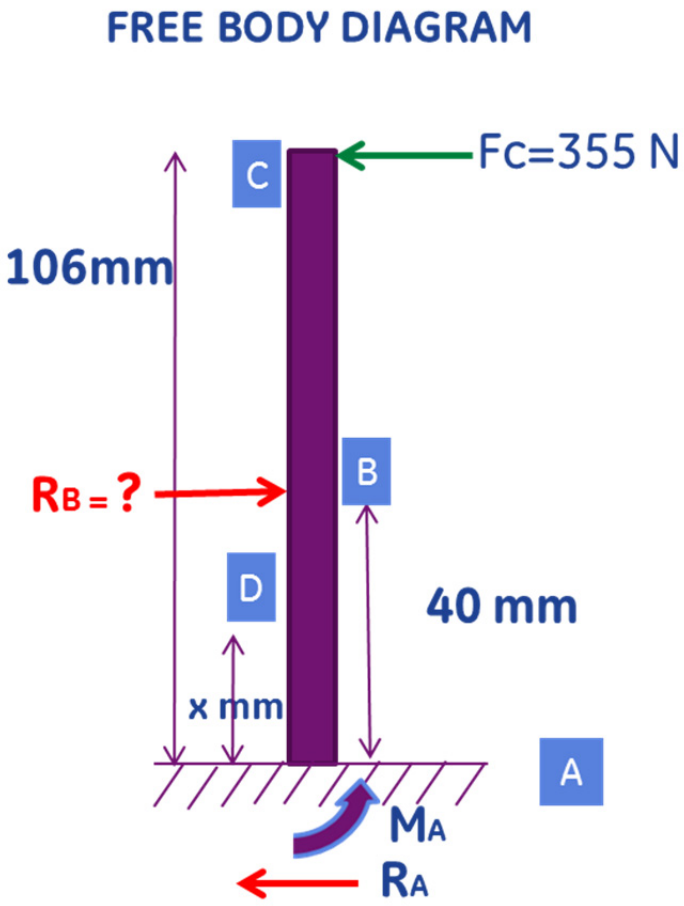

Fig 6.1 Free Body diagram of the test specimens

Following equations can be used to solve this problem:

Summation of forces:

$$F_C - R_B + R_A = 0 \quad \text{- Eq.6.1}$$

Summation of moments at point A:

$$M_A - R_B \times 40mm + F_C \times 106mm = 0 \quad \text{-Eq 6.2}$$

Stiffness Equation using k and y as displacement:

$$\boldsymbol{R_B = -k(y)} \quad \text{-Eq. 6.3}$$

The governing differential equation for the deflection of an elastic beam is

$$\boldsymbol{\frac{d^2y}{dx^2} = \frac{M}{EI}} \quad \text{-Eq. 6.4}$$

Analytical expression for the moment M(x) at point D where AD = $\boldsymbol{x}$ mm

$$\boldsymbol{EI\frac{d^2y}{dx^2} = -M_A + R_A x} \quad \text{-Eq. 6.5}$$

Integrating the above equation we get,

$$\boldsymbol{EI\,Y' = -M_A x + \frac{R_A x^2}{2} + C_1} \quad \text{-Eq. 6.6}$$

(Y′ gives the slope of displacement)

Integrating the above equation we get,

$$\boldsymbol{EI\,Y = -\frac{M_A x^2}{2} + \frac{R_A x^3}{6} + C_1 x + C_2} \quad \text{-Eq. 6.7}$$

(Y gives the displacement)

To solve for constants C1 and C2, use boundary conditions and substitute x=0 in Eq. (6.6) and Eq. (6.7).

Since $Y(0) = 0$ and $Y'(0) = 0$, we get C1= C2=0.

Substituting x= 40mm and using Eq. (6.2), Eq. (6.7) reduces to

$$\boldsymbol{EI\, Y_{40} = -\frac{M_A \times (40^2)}{2} + \frac{R_A \times (40^3)}{6}} \qquad \text{-Eq. 6.8}$$

By introducing $\mathbf{k = \frac{48EI}{L^3}}$ in Eq. (6.3) where L =112mm, length of the horizontal rod and substituting for Y_{40} in Eq (6.8), we get,

R_B = -3316.2N

REFERENCES

1) Waterhouse, R.B., Wear 100 (1984) 107-118

2) Waterhouse, R.B., "Fretting in Steel Ropes and Cables- A review" Fretting Fatigue: Advances in Basic understanding and applications, STP 1425, Muthoh, Kinyon, Hoeppner, ASTM International, PA, 2003

3) Urchegui, M.A., Hartelt, M., Klaffke, D., Gomez, X., "Laboratory fretting tests with thin wire specimens", Tribotest 2007; 13; 67-81

4) Hesbur,M.G., "Recent attempts of improving the mechanical properties of AISI 4340 steel by control of microstructure – A Brief Review", Journal of Materials for Energy Systems Volume 4, Number 1, 28-37

5) Mo, J.L., Zhu, M.H., Zheng, J.F., Luo, J., Zhou, Z.R., "Study on rotational fretting wear of 7075 aluminum alloy", Tribology International 43 (2010) 912–917

6) Zhu, M.H., and Zhou, Z.R., "An Experimental study on radial fretting behavior" Tribology International 34 (2001) 321-326

7) Zhu, M.H., Zhou, Z.R., Kapsa, Ph., and Vincent, L., " Radial fretting fatigue damage of surface coatings" Wear 250 (2001) 650-657

8) Hoeppner, D.W., "Mechanisms of fretting fatigue and their impact on test methods development" ASTM- STP 1159 (1992) 23-32.

9) Vingsbo,O., Soderberg,S.,"On Fretting Maps", Wear,126 (1988) 131-147

10) Fouvry, S., Kapsa, Ph., Vincent, L., "Analysis of Sliding Behaviour for fretting loadings: Determination of transition criteria" Wear 185 (1995) 35-46.

11) Yan, P., "The effect of number of cycles on the critical transition boundary between fretting fatigue and fretting wear" Wear 160 (1993) 279-289.

12) Fouvry S.,Kapsa P., and Vincent, L.," A Global Methodology to Quantify Fretting Damages," Fretting Fatigue: Advances, 2003,pg 17-32

13) Varenberg, M., Etsion, I., and Halperin,G., "Slip Index: A New Unified Approach to Fretting", Tribology Letters, Vol 17, No. 3, Oct 2004

14) Dick, T., and Cailletaud,G., "Fretting modeling with a crystal plasticity model of Ti6Al4V" Computational Material Science 38 (2006) 113-125

15) Fouvry,S., Duo,P., Perruchaut, Ph., "A quantitative approach of Ti-6Al-4V fretting damage: friction, wear and crack nucleation,"Wear 257(2004) 916-929.

16) Neu, R.W. "The Fretting fatigue behaviour of Ti-6Al-4V" Key Engineering Materials, Vo,l. 378-379 (2008) pp 147-162

17) Waterhouse, R.B.,: Fretting Fatigue: Current Technology and Practices, ASTM STP 1367, edited by D.W. Hoeppner, V. Chandrasekaran and C.B. Elliott, American Society for Testing and Materials, West Conshohocken, PA (2000), p. 3.

18) Sauger, E., Fouvry,S., Ponsonnet , L., Kapsa, Ph., Martin, J.M., Vincent, L., "Tribologically Transformed Structure in Fretting," Wear 245 (2000) 39-52

19) Fouvry, S., " Shakedown analysis and fretting wear response under gross slip condition," Wear 251 (2001) 1320-1331

20) Zhang, M., Dowell, D.L., Neu, R.W., "Microstructure sensitivity of fretting fatigue based on computational crystal plasticity" Tribology International 42(2009) 1286-1296

21) Mall,S., Namjoshi, S.A., Porter, W.J., "Effects of microstructure on fretting fatigue crack initiation behavior of Ti-6Al-4V" Materials Science and Engineering A 383 (2004) 334-340

22) Hines, J.A., Lutjering, G., “Propagation of microcracks at stress amplitudes below the conventional fatigue limit in Ti–6Al–4V” Fatigue Fracture Engineering Mater Structure, 22, 657-665

23) Kovalevskii, V.V., “ The mechanism of fretting fatigue in metals” Wear, 67 (1981) 271-285

24) Gaul, D.J., Duquette, D.J., “Cyclic Wear Behaviour (Fretting) of Tempered Martensite Steel” American Society for metals and metallurgical society of AIME, Volume 11A, Sep 1980-1581.

25) Woei- Shyan Lee, Tzay- Tian Su, “ Mechanical properties and microstructural features of AISI 4340 high strength alloy steel under quenched and tempered conditions” Journal of Materials Processing Technology 87 (1999) 198–206

26) Panda, B., Balasubramaniam, R.,Mahapatra, S.,Dwivedi, G.,, “Fretting and fretting corrosion behavior of novel micro alloyed rail steels” Wear 267 (2009) 1702–1708

27) Waterhouse, R.B., Fretting Corrosion, Pergamon Press, Oxford, 1972

28) Waterhouse,R.B.,“ Fretting at high temperatures”, Tribology International, Vol 14, No.4, 1981, pp 203-207

29) Zhou, Z.R., Nakazawa,K., Zhu,M.H., Maruyama,N., Kapsa, Ph.,Vincent,L., “Progress in Fretting Maps” Tribology International 39 (2006) 1068-1073

30) Fouvry, S., Kapsa,P.,Vincent,L., “Fretting Wear and Fretting Fatigue: Relation through a mapping concept” Fretting Fatigue, Current technology and Practices, ASTM STP 1367, p167.

31) Gao Husheng, Gu Haicheng, Zhou Huijiu, "The effect of hardness on the fretting fatigue of alloy steels" Fatigue and fracture of Engineering Materials & Structures, Vol 14, No. 7, pp 789-796

32) Suh, N.P. "Delamination Theory of Wear," Wear, Vol 25, 1973, pp111-124.

33) Landau , P., Shneck, R.Z., Makov, G., Venkert,A., " Evolution of dislocation patterns in fcc metals," Dislocation 2008, Material Science and Engineering 3 (2009) 012004

34) John Pape "Fretting Fatigue Damage Accumulation and Crack Nucleation in High Strength Steels", PhD Thesis

35) Dana R. Swalla , Richard W. Neu," Fretting damage assessment of titanium alloys using orientation imaging microscopy", Tribology International 39(2006) 1016-1027

36) George E Dieter "Mechanical Metallurgy" McGraw Hill Publications (Book, 3rd Edition) p 232

37) Hull, D., Bacon, D.J., "Introduction to Dislocations" Butterworth Heinemann (Book,4th Edition) p 159

38) Nicolaou, P.D., Shell, E.B., Matikas, T.E., "Microstructure and surface characterization of Ti-6Al-4V alloys after fretting fatigue" Material Science and Engineering A269 (1999) 98-103

39) Rohatgi, A., Vecchio, K.S., " The variation of dislocation density as a function of stacking fault energy in shock-deformed FCC materials" Material Science and Engineering A328 (2002) 256-266

40) David L Holt, "Dislocation cell formation in Metals", Journal of applied Physics Volume 41, Number 8, July 1970.

41) Ambrico, J.M., Begley, M.R., " Plasticity in fretting Contact" Journal of the mechanics and Physics of Solids 48(2000) 2391-2417

42) Egor P. Popov, " Introduction to mechanics of solids" Prentice- Hall, Inc, Engle Wood Cliffs, New Jeresy, pg 385

43) Cuddy, J., Bassim, M.N., " Study of dislocation cell structures from Uniaxial deformation of AISI 4340 Steel," Material Science and Engineering, A113(1989) 421-429

44) Rigney, D.A., Glaeser,W.A., " The significance of near microstructure in the wear process", Wear, 46 (1978) 241-250

45) Rigney, D.A., and Hirth,J.P., " Plastic Deformation and Sliding friction of metals", Wear 53 (1979) 345-370

46) Garbar, I.I., Skorinin, J.V., "Metal surface layer structure formation under sliding friction", Wear, 51 (1978) 327-336

47) Shaffer, S.J.,Glaeser, W.A., "Fretting Fatigue Testing, Mechanical Testing and Evaluation", Vol 8, ASM Handbook, ASM International, 2000, p 730-739 (Can be included as 12a)

48) Hirsch, M.R., Neu, R.W., "Fretting damage in thin sheets: Analysis of experimental configuration" Tribology International 44 (2011) 1503-1510

49) Pape, J.A., Neu, R.W., "A comparative behavior of the fretting fatigue behavior of 4340 steel and PH 13-8 Mo stainless steel", International Journal of Fatigue 29 (2007) 2219-2229

50) Pape, J.A., Neu, R.W., "Subsurface damage development during fretting fatigue of high strength steel", Tribology International 40 (2007) 1111-1119

51) Pape, J.A., Neu, R.W., "Fretting Fatigue damage accumulation in PH 13-8 Mo stainless steel", International Journal of Fatigue 23 (2001) S437-S444

52) Ginter, T.,Bouvay, T., "Uprate Options for the MS7001 Heavy Duty Gas Turbine ," GE Energy, Atlanta, GA, pg 12-13

53) Chan, P.C., Thomley, J.C., "Common features of fretting fatigue cracking in steels," Practial Failure Analysis, Volume 2(6) December 2002

54) Bill, R.C., Rohn, D.A., "Influence of fretting on flexural fatigue of 304 stainless steel and Mild Steel," NASA Technical Paper 1193, April 1978.

55) Hong- Zhuang, Z., Lee, S., Lee, Y.,Xiang Hua, L.,Guo-dong, W.,"Effects of applied stresses on martensitic transformation in AISI 4340 Steel," Journal of Iron and Steel Research, International, 2007, 14(6), 63-67

56) Sajadifar, S.V., Ketabchi, M.,Bemanizadeh, B., " Dynamic recrystallization behavior and hot deformation characteristics in 4340 Steel," Metallurgist, Vol 56, Nos 3-4, July 2012.

57) Owolabi,G.,Odoh,D.,Odeshi,A.,Whitworth,H., "Occurrence of Dynamic Shear Bands in AISI 4340 Steel under Impact Loads", World Journal of Mechanics, 2013,3,139-145

58) Briscoe, B.J.,Chateauminois, A.,Lindley,T.C.,Parsonage,D., "Fretting wear behavior of polymethylmethacrylate under linear motions and torsional contact conditions", Tribology International, Vol. 31, No. 11, pp. 701–711, 1998